UNIVERSITY OF CALIFORNIA,
IRVINE

Mechano-Responsive Stem Cells for Cancer Metastasis Diagnostics and Therapeutics Through Biophysical Cues

DISSERTATION

submitted in partial satisfaction of the requirements for the degree of

DOCTOR OF PHILOSOPHY

in Pharmaceutical Sciences

by

Linan Liu

Dissertation Committee:
Associate Professor Weian Zhao, Chair
Associate Professor Lisa A. Flanagan
Associate Professor Andrej Lupták

2017

DEDICATION

To:

the memory of my Grandmother Huang Mei-Ying (1934-2013)

And to:

my mother, Xiaojing Li, and my father, Zhoujun Liu,

for your never-ending support and for the unlimited sacrifice and selflessness you have presented in providing for my life.

Table of Contents

List of Figures

List of Tables

ACKNOWLEDGMENTS

Firstly, I would like to thank Dr. Weian Zhao for giving me the opportunity to work in his laboratory over the past five years. I met with you for the first time in a luncheon after your presentation in the Stem Cell Research Center knowing that we had not only mutual research interests but also shared philosophy. I am extremely thankful for your mentorship, guidance, and friendship over the years and for all the collaborative opportunities that you have provided for me. I sincerely believe you possess a grounded and deep understanding of how science should be properly executed in terms of research, mentorship, leadership and lifelong learning. I would also like to thank Dr. Lisa A. Flanagan and Dr. Andraj Lupták for serving on my committee and being excellent collaborators over the years. I thank Dr. Michelle A. Digman and Dr. Jennifer A. Prescher for serving on my qualifying exam committee and finally would like to thank Dr. Michael G. Cumsky and Dr. Taosheng Huang for offering a starting point of my graduate research career.

Although there are many members in the Zhao laboratory as well as our collaborating laboratories that I must thank for their assistance in completing these studies, I must acknowledge Dr. Wenbin "Vincent" Liao and Dr. Mark A. Eckert, who both served as alternate mentors for me. Vincent opened a door for me on mesenchymal stem cells and taught me a spectrum of techniques that I used throughout the years in the lab, which was and will be passed to junior mentees year by year. Mark served as my first supervisor in the lab and enlightened me to the wonderful world of mechanotransduction and cancer biology. I must thank the members of the team, Shirley X. Zhang who is the most senior team member, for her diligent work and friendship and George Polovin who is the first-ever member, for his support both technically and

mentally during my hardest time of graduate study. Henry P. Farhoodi has been a great friend, teammate, and fellow graduate student in the lab and Rangoli Aeran, who graduated from the same Biotechnology Master program as Henry and I was, was a hard worker and a great teammate. Claire C. Chen was not only a great scientist but also a tough life-fighter, who has been always inspiring me and Mengrou "Mary" Lu was the "Artist of Science". Lily P. Nguyen has been dedicated to multiple sophisticated assays with overqualified potential as an undergraduate researcher and Chi Wut "William" Wong was absolutely a "graduate level" undergraduate mentee that robustly contributed to the projects. I also learned a lot from William and was always inspired from the discussions with him.

I must also thank the other members of the Zhao lab, Dr. Egest J. Pone for his comradeship and sharing of both science and life experience, Dr. Aude I. Ségaliny for her friendship, excellent sense of science and high standard of work quality and Dr. Jan Zimak for being a great friend equipped with constant/instant tech support, as a "honey badger", – "Don't Care!" I must also thank Dr. Xuning "Emily" Guo for being a great lab manager all the time as well as a big sister. I would also like to thank Dr. Zhiqing Zhang and Dr. Fengxia Ma, who were both visiting scholars, for their hard work, their humble outlook to both other team members and their serious attitude to science as senior professors. I would also like to thank Dr. Dong-Ku Kang, Dr. M. Monsur Ali, Dr. Hongzhang "Simon" He and Kaixiang "Kai" Zhang for kind support and friendship. Dr. Feng Li was an excellent collaborator and friend during my initial years in the lab. I must also thank Dr. Yongjun "Andy" Liu, Dr. Guangyang "Tony" Liu and Dr. Jingxia Yu for their introduction of stem cell in industry and being excellent collaborators on the mesenchymal stem cell manufacturing and standardization. I would like to thank Christina H. Tu for teaching me about the tissue culture skills. I would also like to Dr. Michelle A. Digman and

Dr. Jenu V. Chacko for their constructive collaboration and technical support on imaging. I must thank Dr. Devon A. Lawson for being great collaborator and the help on establishing the patient-derived xenograft model and Dr. Timothy L. Downing for constructive input on mechanotransduction. I must thank Dr. Felix Grun, the director of the UCI Mass Spectrometry Facility for his precious advice and help with the mass spectrometry training and analysis. I would also like to thank Tao Peng, Dr. Adam L. MacLean and Dr. Qing Nie for being great colleagues and collaborators on developing a mathematic model mimicking the mechanotransduction in mesenchymal stem cells. I must also thank Dr. Shivani Sharma from the California NanoSystems Institute (CNSI) at University of California-Los Angeles for her kind help on AFM. I would also like to thank Dr. Karen Aboody for sharing the method of LC-MS/MS assay. As I am the first student in the Zhao lab, I must thank Dr. Janahan Arulmoli and Dr. Shirley Y. Wong for the mentoring as senior graduate students and friendship.

Lastly, I must thank my family. Most of my family members live in China and I am appreciative of the continuous support I have received from them. My parents have always been there providing endless encouragement both mentally and physically, and showing their unlimited selflessness backing me up. I must thank my grandparents for their mercy and understanding for my away from home, little accompanying with them.

CURRICULUM VITAE

Linan Liu

Education:

Ph.D. Pharmaceutical Sciences,
University of California, Irvine (2017)

M.S. Biotechnology,
University of California, Irvine (2012)

B.S. Bio-Pharmaceutical Engineering,
Zhejiang University of Technology, China (2010)

B.B.A. Business Administration and Management,
Zhejiang University of Technology, China (2010)

Executive Summary:

- Pharmaceutical Sciences PhD with expertise including stem cell therapy, stem cell engineering, cancer therapy, *in vivo* cell imaging and mechano-sensing
- Leading projects through design, troubleshooting, and optimization
- Managing an independent research team and mentoring junior graduate researchers

Research and Industry Experience:

2012 - Present Graduate Student Researcher, Department of Pharmaceutical Sciences, University of California, Irvine

Mentor: Dr. Weian Zhao

- Developing a mesenchymal stem cell (MSC) based system that responds specifically to mechano-environmental cues at the breast cancer metastatic niche;
- Engineering cells including stem cells and immune cells to detect and treat diseases including cancer, fibrosis, stroke and multiple sclerosis;
- Leading and managing preclinical studies using umbilical cord-derived MSCs to treat autoimmune diseases including Rheumatoid Arthritis and Crohn's Disease;
- Leading the designing and cloning of constructs for cell engineering system including lenti-viral vectors;
- Leading the *in vivo* bioluminescence and fluorescence imaging of cells (e.g., stem cells and cancer cells) and extracellular vesicles (EVs);
- Leading the establishment of *in vivo* animal models including cancers (breast, colon, melanoma, *etc*. both primary tumor and metastasis) and fibrosis. Participating in the establishment of stroke and multiple sclerosis models;
- Leading a project using a high throughput detection system Integrated Comprehensive Droplet Digital Detection (IC3D) for early stage cancer detection and metastasis monitoring;
- Supervising and trouble-shooting the *in vitro*, *ex vivo* and *in vivo* assays for junior researchers in the lab.

2011(Summer) Internship, Department of Biological Science, Allergan, Inc.

Supervisor: Dr. Huajun Yan

- Developed standard *in vitro* assays to test drugs for wound healing and glaucoma treatment.

2010 - 2012 Graduate Student Researcher, Biotechnology, University of California, Irvine

Mentor: Dr. Taosheng Huang

- Studied a mutant gene called *NAA10* associated with Lenz Microphthalmia Syndrome using PCR and next generation sequencing techniques.

2009 - 2010 Undergraduate Student Researcher, Department of Bio-pharmaceutical

Sciences, Zhejiang University of Technology, China

Mentor: Dr. Wen Zhang

- Worked on the identification of chemical compounds that bind to G-rich DNA of telomere to block telomerase functions as potential cancer therapeutics.

Management Experience:

2013 - Present

Group leader and supervisor of an independent research team, Zhao Laboratory, University of California, Irvine

- Groups of 6-7, including junior graduate students, undergraduate students, interns and visit scholars
- Making experimental plans and assigning tasks
- Performing technique training to group members
- Trouble-shooting and optimizing assays
- Mentoring personal development of group members
- Coordinating with other research teams within the lab and with collaborators

2013 - Present

Manager of IACUC animal protocols, Zhao Laboratory, University of California, Irvine

- Modifying experimental procedures
- Managing protocol personnel
- Filing related paperwork for reports, renewal, etc.
- Animal ordering and managing
- Coordinating with animal facilities

Publications:

1. Chen C.C.*, **Liu L.***, Ma F., Wong C.W., Guo X.E., Chacko J.V., Farhoodi H.P., Zhang S.X., Zimak J., Ségaliny A.I., Riazifar M., Pham V., Digman M.A., Pone E.J. & Zhao W. Elucidation of Exosome Migration across the Blood-Brain Barrier Model *In Vitro*. *Cellular and Molecular Bioengineering*. **2016**. 9: 509-29. * = Equal contribution. **Selected as Featured paper** (Journal cover for the December 2016 issue). (Research article)
2. **Liu L.**, Zhang S.X., Aeran R., Liao W., Lu M., Polovin G., Pone E.J. & Zhao W. Exogenous Marker-engineered Mesenchymal Stem Cells Detect Cancer and Metastases

in A Simple Blood Assay. *Stem Cell Research & Therapy*. **2015**. 6(1): 181. (Research article)

3. **Liu L.**, Eckert M.A., Riazifar H., Kang D.-K., Agalliu D. & Zhao W. From Blood to the Brain: Can Systemically Transplanted Mesenchymal Stem Cells Cross the Blood-Brain Barrier? *Stem Cells International*. **2013**. 2013: 435093. (Review article)
4. **Liu L.**, Wu Y., Jiang S., Qiu T., Zhang H. & Zhang W. Targeting Human Telomeric G-quadruplex with Perfluoroalkyl Metal Phthalocyanine Derivatives. *Advanced Materials Research*. **2012**. 365: 382-88. (Research article)
5. Liao W., Pham V., **Liu L.**, Riazifar M., Pone E.J., Zhang S.X., Ma F., Lu M., Walsh C.M. & Zhao W. Mesenchymal Stem Cells Engineered to Express Selectin Ligands and IL-10 Exert Enhanced Therapeutic Efficacy in Murine EAE. *Biomaterials*. **2015**. 17: 87-97. (Research article)
6. Zhang K., Kang D.-K., Ali M.M., **Liu L.**, Labanieh L., Lu M., Riazifar H., Nguyen T.N., Zell J.A., Digman M.A., Gratton E., Li J., & Zhao W. Digital Quantification of miRNAs Directly in Plasma Using Integrated Comprehensive Droplet Digital Detection. *Lab on Chip*. **2015**. 15(21): 4217-26. (Research article)
7. Tang Y., Wang Z., Yang X., Chen J., **Liu L.**, Zhao W., Le X.C. & Li F. Construct Real-Time, Wash-Free, and Reiterative Sensors for Cell Surface Proteins Using Binding-Induced Dynamic DNA Assembly. *Chemical Science.* **2015**. 6: 5729-33. (Research article)
8. Chang E., Eckert M.A., Ali M.M., Riazifar H., Pone E.J., **Liu L.** & Zhao W. Facile Super-molecular Aptamer Inhibitors of L-selectin. *PLoS One*, **2015**. 10(3): e0123034. (Research article)
9. Zhang Z., Eckert M.A., Ali M.M., **Liu L.**, Kang D.-K., Chang E., Pone E.J., Sender L.S., Fruman D.A., & Zhao W. DNA-Scaffolded Multivalent Ligands to Modulate Cell Function. *ChemBioChem*, **2014**. 15(9): 1268-73. (Research article)
10. Esmailpour T., Riazifar H., **Liu L.**, Donkervoort S., Huang V.H., Madaan S., Shoucri B.M., Busch A., Wu J., Towbin A., Chadwick R.B., Sequeira A., Vawter M.P., Sun G., Johnston J.J., Biesecker L.G., Kawaguchi R., Sun H., Kimonis V. & Huang T. A Splice Donor Mutation in *NAA10* Results in the Dysregulation of the Retinoic Acid Signaling Pathway and Causes Lenz Microphthalmia Syndrome. *Journal of Medical Genetics*. **2014**. 51(3): 185-96. (Research article)
11. Li F., Aeran R., Pone E.J., Kang D.-K., **Liu L.**, Le X.C. & Zhao W. Probe and Control of Cell-cell Interactions Using Bioengineered Tools. *In "Micro and Nanoengineering of the Cell Surface"*, edited by Weian Zhao and Jeffery M. Karp, Elsevier. **2014**. (Book chapter)
12. **Liu L.***, Zhang S.X.*, Liao W., Wong C.W., Chen C.C., Farhoodi H.P., Ségaliny A.I., Chacko J.V., Nguyen L.P., Lu M., Polovin G., Pone E.J., Downing T.L., Lawson D.A., Digman M.A. & Zhao W. Mechano-Responsive Stem Cells to Target Cancer Metastases Through Biophysical Cues. *Science Translational Medicine.* Under revision. * = Equal contribution. (Research article)
13. Peng T.*, **Liu L.***, MacLean A.L., Wong C.W., Zhao W. & Nie Q. A Mathematical Model of Mechanotransduction Reveals How Mechanical Memory Regulates Mesenchymal Stem Cell Fate Decisions. *BMC Systems Biology.* Under revision. * = Equal contribution. (Research article)

14. Wong C.W.*, **Liu L.***, Pone E.J., Han M., Gao S., Liao W. & Zhao W. Meta-analysis of Preclinical Studies of Mesenchymal Stromal Cells for Rheumatoid Arthritis. Manuscript in preparation. * = Equal contribution. (Meta-analysis review)

Patents:

- **Liu L.**, Zhao W., Eckert M.A., Liao W., Kang D.-K., Pone E.J., Zhang S.X., Lu M. & Zimak J. **2015**. Systems for Detecting, Monitoring or Treating Diseases or Conditions Using Engineered Cells and Methods for Making and Using Them. US2016/028675.

Presentations:
Presenter underlined

1. **Liu L.** & Zhao W. Next Generation Stem Cell-Based Therapeutics and Miniaturized Diagnostics. ZJUT Year-End Symposium, Department of Pharmaceutical Sciences, Zhejiang University of Technology, Hangzhou, Zhejiang, China, December 26, **2015**. (Invited talk)
2. **Liu L.**, Peng T., Polovin G., Kang D.-K., Zhao W. & Nie Q. Measuring Tissue Stiffness of Cancer Metastases *In Vivo* Using Sensor Engineered Stem Cells. CCBS Retreat 2013 Opportunity Award Winners Talk, Pasadena, CA, March 29, **2014**. (Oral presentation)
3. **Liu L.** & Huang T. Lenz Microphthalmia Syndrome and *NAA10* gene. Biotechnology Program Graduate Symposium, Department of Molecular Biology and Biochemistry, University of California, Irvine, CA, May 31, **2012**. (Oral presentation)
4. **Liu L.**, Farhoodi H.P. & Zhao W. Mechano-Responsive Stem Cells to Target Cancer Metastases Through Biophysical Cues. Departments of Pharmaceutical Sciences and Pharmacology Social Mixer Poster Session, University of California, Irvine, CA, May 23, **2016**. (Poster presentation)
5. **Liu L.**, Zhang S.X., Liao W., Pone E.J. & Zhao W. Mechano-Responsive Stem Cells to Target Cancer Metastases Through Biophysical Cues. 2nd UCI-Ewha International Symposium, University of California, Irvine, CA, January 25, **2016**. (Poster presentation)
6. **Liu L.**, Zhang S.X., Liao W., Pone E.J. & Zhao W. Mechano-Responsive Stem Cells to Target Cancer Metastases Through Biophysical Cues. Stem Cell Awareness Day, the Sue and Bill Gross Stem Cell Research Center, University of California, Irvine, CA, October 28, **2015**. (Poster presentation)
7. **Liu L.**, Zhang S.X., Liao W., Pone E.J. & Zhao W. Mechano-Responsive Stem Cells to Target Cancer Metastases Through Biophysical Cues. Chao Family Comprehensive Cancer Center 2015 Annual Retreat, Palm Springs, CA, September 18-19, **2015**. (Poster presentation)
8. **Liu L.** & Zhao W. Microencapsulated Aptamer Sensors for Digital Quantification of Blood Biomarkers. American Society of Gene & Cell Therapy (ASGCT) 18th Annual Meeting, New Orleans, LA, May 13-16, **2015**. (Poster presentation)
9. **Liu L.**, Zhang S.X., Aeran R., Liao W., Lu M., Polovin G., Pone E.J. & Zhao W. A Stem Cell Approach for Cancer Blood Test. American Society of Gene & Cell Therapy (ASGCT) 18th Annual Meeting, New Orleans, LA, May 13-16, **2015**. (Poster presentation)

10. **Liu L.**, Liao W., Pham V. & Zhao W. Targeted Therapeutic Delivery of Mesenchymal Stem Cells Using mRNA Engineering in Mouse EAE Model. 12th Stem Cell Research & Regenerative Medicine at GTCbio Stem Cell Summit 2015, Boston, MA, April 27-29, **2015**. (Poster presentation)
11. **Liu L.**, Polovin G. & Zhao W. Stem Cell-Based Therapeutics and Polyvalent Aptamer Platform for targeted drug delivery. Graduate Recruitment Symposium, Department of Pharmaceutical Sciences, University of California, Irvine, CA, March 13, **2014**. (Poster presentation)
12. **Liu L.** & Zhao W. Next Generation Stem Cell-Based Therapeutics and Miniaturized Diagnostics. Graduate Recruitment Symposium, Department of Pharmaceutical Sciences, University of California, Irvine, CA, March 1, **2013**. (Poster presentation)

Contributed Presentations:
Presenter underlined

1. Han M., Zhang S.X., **Liu L.** & Zhao W. Mechano-Responsive Stem Cells to Target Cancer Metastases Through Biophysical Cues. Graduate Recruitment Symposium, Department of Pharmaceutical Sciences, University of California, Irvine, CA, January 23, **2017**. (Poster presentation)
2. Farhoodi H.P., **Liu L.** & Zhao W. The Mechanosensation of Metastatic Cancer. Biotechnology Program Graduate Symposium, Department of Molecular Biology and Biochemistry, University of California, Irvine, CA, May 31, **2016**. (Oral presentation)
3. Wong C.W., **Liu L.** & Zhao W. Mechano-Responsive Stem Cells to Target Cancer Metastases Through Biophysical Cues. The 2016 UCI Campus-Wide Symposium on Basic Cancer Research, University of California, Irvine, CA, May 7, **2016**. (Poster presentation)
4. Chen C.C., **Liu L.**, Ma F., Wong C.W. & Zhao W. Elucidation of Exosome Migration across the Blood-Brain Barrier. 2nd UCI-Ewha International Symposium, University of California, Irvine, CA, January 25, **2016**. (Poster presentation)
5. Zhang S.X., **Liu L.** & Zhao W. Engineered Mesenchymal Stem Cells to Treat Tissue Fibrosis. Biomedical Engineering Society (BMES) Annual Meeting, Tampa, FL, October 7-10, **2015**. (Poster presentation)
6. Zhang S.X., **Liu L.**, Aeran R., Liao W., Lu M., Polovin G., Pone E.J. & Zhao W. A Stem Cell Approach for Cancer Blood Test. Chao Family Comprehensive Cancer Center 2015 Annual Retreat, Palm Springs, CA, September 18-19, **2015**. (Poster presentation)
7. **Liu L.**, Liao W., Pham V., & Zhao W. Targeted Therapeutic Delivery of Mesenchymal Stem Cells Using mRNA Engineering in Mouse EAE Model. MSC 2015, Cleveland, OH. August 17-19, **2015**. (Poster presentation)
8. Zhao W. & **Liu L.** Track the Fate of Single Transplanted Cells *In Vivo* Using Surrogate Blood Markers, UCI Cancer Center Heme Dot, Orange, CA, July 22, **2015**. (Invited talk)
9. Pham V., Liao W., **Liu L.**, Riazifar H., Zhang S.X., Ma F., Lu M., Pone E.J., Walsh C.M., & Zhao W. MSCs Engineered to Express Selectin Ligands and IL-10 Exert Therapeutic Efficacy in Murine EAE Model. CIRM Bridge Trainee Meeting, Burlingame, CA, July 15, **2015**. (Poster presentation)
10. Dooman, E., Zhang S.X., **Liu, L.** & Zhao W. Effect of Biophysical Cues of Tumor Microenvironment on Macrophage Phenotype. 2015 UCI Undergraduate Research

Opportunities Program (UROP) Symposium, Irvine, CA, May 16, **2015**. (Poster presentation)

11. Liao W., **Liu L**. & Zhao. W. Stem Cell Technology to Diagnose and Treat Breast Cancer. Shenzhen - Los Angeles Innovative and Entrepreneurial Environment Conference, Irvine, CA, May 13, **2015**. (Oral presentation)
12. Zhang S.X., **Liu L.**, Aeran R., Liao W., Lu M., Polovin G., Pone E.J. & Zhao W. A Stem Cell Approach for Cancer Blood Test. 12th Stem Cell Research & Regenerative Medicine at GTCbio Stem Cell Summit 2015, Boston, MA, April 27-29, **2015**. (Poster presentation)
13. Zhao W. & **Liu L**. Tumor Hunter: Mechano-Responsive Stem Cell System to Study, Detect and Treat Cancer Metastases" UCI Cancer Center Women's Dot, Orange, CA, August 29, **2014**. (Invited talk)
14. Polovin G., **Liu L.** & Zhao W. Stem Cell-Based Therapy to Treat Breast Cancer Metastases in the Lungs. CIRM Bridges Trainee Meeting 2014, Burlingame, CA, July 28, **2014**. (Poster presentation)
15. Aeran R., **Liu L.** & Zhao W. Mesenchymal Stem Cells as the Basis for A Selective Cancer-detecting Point-of-care Blood Test. Biotechnology Program Graduate Symposium, Department of Molecular Biology and Biochemistry, University of California, Irvine, CA, May 31, **2014**. (Oral presentation)
16. Polovin G., **Liu L.** & Zhao W. Next Generation Stem Cell-Based Therapeutics and Miniaturized Diagnostics. International Stem Cell Awareness Day, the Sue and Bill Gross Hall: A CIRM Institute, University of California, Irvine, CA, October 1, **2013**. (Poster presentation)

Abstracts:

1. **Liu L.**, Zhang S.X., Liao W., Pone E.J. & Zhao W. Mechano-Responsive Stem Cells to Target Cancer Metastases Through Biophysical Cues. 2nd UCI-Ewha International Symposium, University of California, Irvine, CA, January 25, **2016**.
2. **Liu L.**, Zhang S.X., Liao W., Pone E.J. & Zhao W. Mechano-Responsive Stem Cells to Target Cancer Metastases Through Biophysical Cues. Stem Cell Awareness Day, the Sue and Bill Gross Stem Cell Research Center, University of California, Irvine, CA, October 28, **2015**.
3. **Liu L.**, Zhang S.X., Liao W., Pone E.J. & Zhao W. Mechano-Responsive Stem Cells to Target Cancer Metastases Through Biophysical Cues. Chao Family Comprehensive Cancer Center 2015 Annual Retreat, Palm Springs, CA, September 18-19, **2015**.
4. **Liu L.**, Zhang S.X., Aeran R., Liao W., Lu M., Polovin G., Pone E.J. & Zhao W. A Stem Cell Approach for Cancer Blood Test. *Molecular Therapy*. **2015**. 23(S1): S91.
5. **Liu L.**, Liao W., Pham V. & Zhao W. Targeted Therapeutic Delivery of Mesenchymal Stem Cells Using mRNA Engineering in Mouse EAE Model. 12th Stem Cell Research & Regenerative Medicine at GTCbio Stem Cell Summit 2015, Boston, MA, April 27-29, **2015**.
6. Zhao W. & **Liu L.** Mechano-Responsive Stem Cells to Target Cancer Metastases Through Biophysical Cues. 2016 High-Risk, High-Reward Research Symposium in the Natcher Conference Center on the NIH Main Campus, Bethesda, MD, December 5-7, **2016**.

7. Chen C.C., **Liu L.**, Ma F., Wong C.W. & Zhao W. Elucidation of Exosome Migration across the Blood-Brain Barrier. 2nd UCI-Ewha International Symposium, University of California, Irvine, CA, January 25, **2016**.
8. Zhang S.X., **Liu L.** & Zhao W. Scar Eraser: Mechano-Responsive Cell System to Study, Detect and Treat Tissue Fibrosis. Biomedical Engineering Society (BMES) Annual Meeting, Tampa, FL, October 7-10, **2015**.
9. Zhang S.X., **Liu L.**, Aeran R., Liao W., Lu M., Polovin G., Pone E.J. & Zhao W. A Stem Cell Approach for Cancer Blood Test. Chao Family Comprehensive Cancer Center 2015 Annual Retreat, Palm Springs, CA, September 18-19, **2015**.
10. Dooman, E., Zhang S.X., **Liu, L.** & Zhao W. Effect of Biophysical Cues of Tumor Microenvironment on Macrophage Phenotype. 2015 UCI Undergraduate Research Opportunities Program (UROP) Symposium, Irvine, CA, May 16, **2015**.
11. Zhang S.X., **Liu L.**, Aeran R., Liao W., Lu M., Polovin G., Pone E.J. & Zhao W. A Stem Cell Approach for Cancer Blood Test. 12th Stem Cell Research & Regenerative Medicine at GTCbio Stem Cell Summit 2015, Boston, MA, April 27-29, **2015**.
12. Polovin G., **Liu L.** & Zhao W. Stem Cell-Based Therapy to Treat Breast Cancer Metastases in the Lungs. CIRM Bridges Trainee Meeting 2014, Burlingame, CA, July 28, **2014**. https://www.mosaicevents.com/cirmtrainee14/viewer/#anc103

Other Events:

1. **Liu L.**, Chacko J.V. Pham V., Digman M.A & Zhao W. Oblivion. 2nd Annual Pharm Sci Research Day, University of California, Irvine, CA, May 18-19, **2016**.
2. **Liu L.**, Chacko J.V., Digman M.A & Zhao W. Oblivion. Stem Cell Center Art Show, "Gross Hall Biennale 2015", University of California, Irvine, CA, December 16, **2015**.

Awards/Honors/Fellowships:

2016	Pharmacological Sciences Travel Award, University of California, Irvine
2012 - 2013	Graduate Fellowship, University of California, Irvine
2012	Institute for Cell and Molecular Biology (ICMB) doctoral fellowship, University of Texas, Austin (Declined)
2012	Recruitment Award, University of Texas, Austin (Declined)
2012	Pre-Doctoral Scholars of Excellence Fellowship from the Provosts, University of Georgia (Declined)
2012	Recruitment Award, University of Georgia (Declined)
2012	Biomedical Sciences Doctoral Fellowship, Institute of Biosciences and Technology (IBT) in Houston, at the Texas A&M University Health Science Center (TAMHSC) (Declined)
2010	Graduate Fellowship, University of California, Irvine
2010	Award for Outstanding Graduate (Top 5% students), Zhejiang University of Technology, China
2010	Award for Excellent Graduation Thesis (Top 5% students), Zhejiang University of Technology, China
2008	Scholarship for Excellent Social Work, Zhejiang University of Technology, China
2008	Second Prize (Team leader), Innovation Competition of Physics of Zhejiang

University of Technology, China

2007 First-class Scholarship (Top 2% students), Zhejiang University of Technology, China

Teaching Experience:

2014 - Present IVIS *In-Vivo* Imaging System Trainer, Stem Cell Research Center, University of California, Irvine

2014 (Fall) Lead Teaching Assistant, BIOPHARM & NANOMED (PHRMSCI 174), Department of Pharmaceutical Sciences, University of California, Irvine
- Led discussion sections weekly (180 students)
- Made and graded exams

2014 (Fall) Invited speaker, *Cell Based Drug Delivery,* BIOPHARM & NANOMED (PHRMSCI 174), Department of Pharmaceutical Sciences, University of California, Irvine

2013 (Fall) Lead Teaching Assistant, BIOPHARM & NANOMED (PHRMSCI 174), Department of Pharmaceutical Sciences, University of California, Irvine
- Led discussion sections weekly (120 students)
- Made and graded exams

Approved Grants:

- National Institutes of Health Director's New Innovator Award (among 50 investigators selected for the 2014 award).

NIH DP2 (PI: Zhao) 09/30/14-08/31/19

NIH $1,500,000 DC + $817,500 F&A

Mechano-sensing stem cells to study, detect and treat cancer metastases

Goals: The major goals of the project are to develop the first generation, stiffness-sensing stem cells to elucidate tumor mechano-niche biology and to develop new and effective cancer diagnostics and therapeutics using unique mechano-markers as a target.

Role: Assisted in grant writing, updated key components of project progression for resubmission, performed experiments and produced preliminary data.

Event Organization:

January 25 - 31, 2015 Zhejiang University of Technology Medical Program, at University of California, Irvine
- Invited speaker, *Graduate study in the United States*
- Organized and led a laboratory tour with oral presentation
- Coordinated with staff from UC Irvine Extension and professors from ZJUT international program

Professional Societies:

2013 - Present American Heart Association (AHA)

2015 - Present American Society of Gene & Cell Therapy (ASGCT)

ABSTRACT OF THE DISSERTATION

Mechano-Responsive Stem Cells for Cancer Metastasis Diagnostics and Therapeutics Through Biophysical Cues

By

Linan Liu

Doctor of Philosophy in Pharmaceutical Sciences

University of California, 2017

Professor Weian Zhao, Chair

Cancer metastases are responsible for more than 90% of cancer deaths, however no current effective therapeutics directly and specifically targets them. The exclusive mechanical properties of metastatic niche offer an intriguing target for the development of treatments selectively targeting metastases. Systemically infused mesenchymal stem cells (MSCs) preferentially home to tumors. Besides, it has been established that tissue mechanical properties regulate MSC differentiation by driving expression of certain genes. We hypothesize that increased matrix stiffness is an essential property of the metastatic niche that can be targeted with MSC-based, mechano-responsive therapies. Here we presented, by targeting the mechano-environment of the metastatic niche, a new methodology for the treatment of cancer metastases, using promoter-driven, MSC-based vectors, named as mechano-responsive cell system (MRCS).

Our data suggest that the MRCS homes to and targets cancer metastasis responding to specific mechanical microenvironment to deliver therapeutics, such as cytosine deaminase (CD) that locally activates the prodrug to kill cancer with minimal side-effects. Compared to MSCs expressing CD constitutively, MRCS not only treats metastatic breast cancer with reduced deleterious effects and more effective outcome, but may also serve as a platform technology for prospective application to therapies targeting abnormal tissue stiffness including fibrotic diseases.

CHAPTER 1

INTRODUCTION

Many disease states in the body, including cancer, diabetes, fibrosis, and autoimmune diseases, are difficult to detect especially at an early stage and even harder to treat using conventional methods. Current detection methods include imaging modalities such as positron emission tomography (PET), computed tomography (CT), and magnetic resonance imaging (MRI), and biological tests such as histology, polymerase chain reaction (PCR), flow cytometry and enzyme-linked immunoassay (ELISA). These have downsides such as limited sensitivity and specificity, lengthy detection times, the use of irritating or harmful contrast agents and ionizing radiation, limited to no functionality *in vivo*, invasive procedures required for tissue biopsies and the need for extensive sample preparation or modification. Current treatment methods such as systemic pharmacologic agents (*e.g.*, chemotherapy) have limited targeting and specificity, limited effectiveness, and harmful side effects. Another hurdle in cell therapy is the lack of tools and methods to monitor and manipulate the fate of transplanted cells including biodistribution, homing and engraftment, proliferation, differentiation, cell signaling, therapeutic efficacy and potential toxicity. A major challenge in the field of detection and targeted treatment is finding appropriate biomarkers to indicate the diseased state. Unfortunately, molecular biomarkers are generally unreliable due to heterogeneity between patients. This work highlights the platform technology of cell engineering for detecting and treating diseases such as metastatic cancer, by targeting novel biomarkers, for example, increased mechanical modulus, or stiffness. Thereby

this platform provides specific and localized detection assays and therapies for the abovementioned disease states.

1.1 BREAST CANCER METASTASIS

Cancer metastases, a process of the spread of cancer from the primary organ[1-3], are responsible for over 90% of cancer deaths, however no current treatments directly target metastatic cancer[4]. For breast cancer, in particular, about 1 in 8 American women will develop invasive breast cancer during their lifetime, leading to 40,000 deaths a year. Almost all breast cancer deaths are due to the spread of the cancer from the breast to other organs[1] which is essentially incurable with a median survival of only 2 to 3 years[5-7]. Resection of widespread metastases is often infeasible and chemotherapeutics, including taxanes and anti-metabolites, are discouragingly ineffective at treating disseminated disease and often associated with severe side effects[8, 9]. Current therapy for metastatic breast cancer therefore focuses on prolonging survival and palliation[1, 7].

An additional major challenge in treating cancer metastasis is that micrometastases (small numbers of cancer cells that have spread to distant organs) are often too small to be detected by traditional diagnostic tests such as CT and MRI. Indeed, only a small percentage of patients exhibit clinically detectable metastases at diagnosis. Importantly, micrometastases are known to be able to undergo a period of dormancy and escape chemotherapy. It is now thought that micrometastases, which may occur early during breast cancer progression, may account for cancer recurrence[7]. Therefore, the ability to detect micrometastases will allow us to identify patients who are at high risk for relapse at early stages when treatment is most effective. Unfortunately, current micrometastases detection techniques are either not sensitive (*i.e.*, CT and

MRI) or require invasive biopsy procedures (*e.g.,* sentinel lymph node, or lung biopsies), making them inappropriate for clinical application.

Therefore, there is clearly an enormous need for sensitive detection methods to identify metastases at early stages and for treatments specifically targeting breast cancer metastases to reduce mortality and side effects of current systemic therapies.

1.2 MECHANOBIOLOGY OF TUMOR AND PRE-METASTATIC NICHE

Cells constantly interact with their niche, which includes an array of complex biochemical and biophysical signals from the surrounding extracellular matrix (ECM). Although not appreciated historically, it has recently become evident that the physical and mechanical properties of cellular microenvironments (the so-called "mechano-niche") regulate important cell functions[10, 11]. Specifically, important roles for matrix stiffness (or elasticity) in driving breast cancer metastasis have been elucidated. Increased matrix stiffness, primarily driven by increased collagen deposition and crosslinking by lysyl oxidase (LOX) proteins, promotes breast cancer migration, invasion, cell plasticity, and eventual metastasis, primarily through regulation of integrin signaling[12, 13]. Interestingly, LOX accumulation spatially correlates with the presence of metastases in both mouse models of metastasis and human patients[10, 14, 15]. In mouse models of breast cancer metastasis, secretion of LOX by the primary breast tumor leads to collagen crosslinking in discrete areas of the lung that promote formation of metastases[11, 14, 16-18] (Figure 1.1). Deposition of LOX at the metastatic niche correlates with both collagen linearization and formation of collagen-collagen covalent bonds in the lung parenchyma, both of which dramatically increase matrix stiffness[12]. We reason that the unique physical properties of the

LOX-induced metastatic niche offer an intriguing target for the development of therapeutics specifically targeting lung metastases.

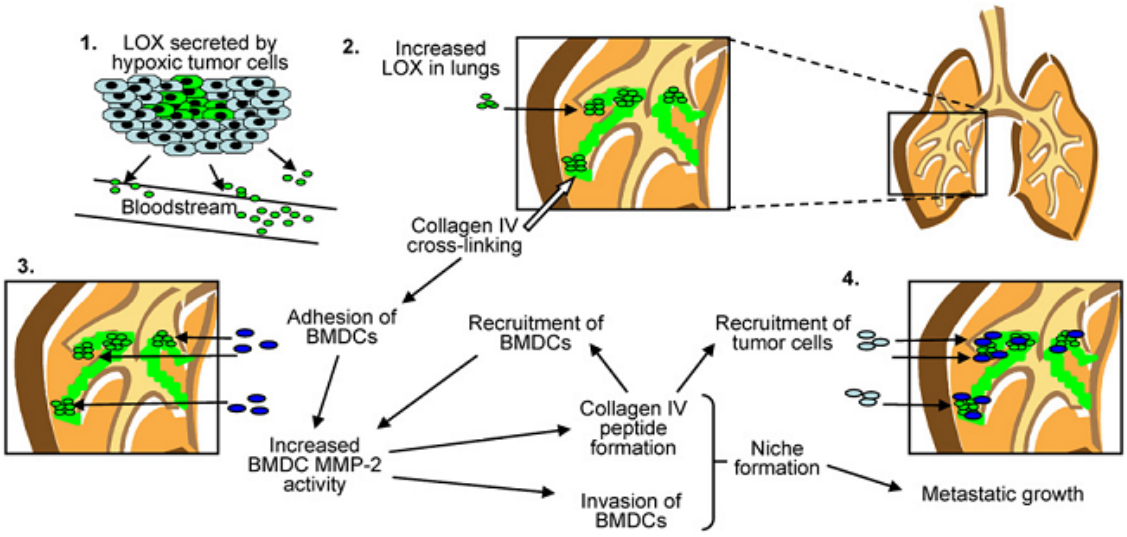

Figure 1.1. LOX is associated with metastases. (1) Hypoxic primary tumor cells secrete LOX into the bloodstream. (2) LOX accumulates in the lungs of tumor-bearing mice and cross-links collagen IV. (3) Adhesion of $CD11b^+$ cells to cross-linked matrix increases bone marrow derived cells (BMDC) matrix metallopeptidase 2 (MMP-2) activity. Collagen IV remodeling by LOX and MMP-2 leads to peptide formation, invasion of $CD11b^+$ cells, and increased recruitment of BMDCs. (4) LOX-dependent formation of the pre-metastatic niche enhances metastatic growth. Reprinted by permission from Elsevier: Cancer Cell[11], copyright 2009.

Therefore matrix stiffness could be an appealing therapeutic target due to its intimate connection with formation of lung metastases and its long half-life (measured in years). If the mechano-environmental cues at the metastatic niche could be used to target breast cancer metastases, this novel cancerous biomarker can make it refractory to development of resistance[19].

1.3 STEM CELL BASED ANTI-CANCER THERAPIES

Although they are a relatively new approach of therapeutics, stem cell-based therapies offer a huge potential in the practice of medicine. With the thorough understanding of stem cell biology and the advent of targeted therapeutics for cancer, stem cell-based therapeutic strategies

are being explored in the treatment of various cancer types[20]. Stem cells, which bear two main features: self-renewal and differentiation, are the natural sources of embriogenetic tissue generation and continuous regeneration throughout adult life. Tissue-specific stem cells, such as mesenchymal stem cells (MSCs, mesoderm), hematopoietic stem cells (HSCs, mesoderm), and neural stem cells (NSCs, ectoderm), have been identified as present and active for virtually every bodily tissue and are hierarchically situated between their germ layer progenitors and differentiated end-organ tissues[21]. Specifically adult stem cells (ASCs) have been studied extensively and are already a successful source of FDA-approved treatments for nine human diseases, such as Parkinson's disease and juvenile diabetes, currently applied in clinical centers[22]. Though not as highly pluripotent and self-renewing as their embryonic counterparts, ASCs are much safer with respect to postgrafting tumor formation[23].

In spite of lower totipotency and restricted life span, ASCs can avoid ethical constraints and their use for research and therapeutic purposes are less restricted[24]. In addition, the stem cells with higher totipotency have been shown to be more tumorogenic in mice[25]. Thus, for ease of availability and lesser constrained on ethical issue, ASCs are the stem cells most commonly used for research and therapeutic purposes. The other reason for the use of ASCs is their easy accessibility. According to literature, ASCs from bone marrow (HSCs & MSCs) are the most commonly studied stem cells[26].

Different stem cells have been modified with selected genes via, for example viral transduction, with different vectors. Besides the gene transfer performed to introduce a gene expressing a fluorescent protein to track the behavior of the cell *in vivo* or to correct a genetic defect (*i.e.* a gene mutation or deletion) or to make the target cell susceptible to the action of a selected drug (*i.e.* by expressing tymidine kinase)[27], the combination of stem cell and gene

therapy has been used to efficiently release a therapeutic agents. Among those studies, direct functioning anti-cancerous agents such as the proapoptotic protein TRAIL (tumor necrosis factor–related apoptosis-induced ligand) offers a promising approach toward tumor cell killing via on-site delivery[28, 29] whereas the approach called enzyme-activating prodrug therapy (as known as, for example, gene-directed enzyme prodrug therapy (GDEPT) and suicide gene therapy) in the direction of improving the specificity of chemotherapy, in which the transgenes encode enzymes that convert specific less toxic prodrugs to toxic metabolites[4, 30]. In addition, oncolytic viruses that were originally suggested by the clinicians who witnessed tumor regression after spontaneous viral infections were delivered by MSCs as the carriers for a new wave of oncolytic virotherapies[31]. Progress has also been made in understanding the combination of surgery, radiation, and chemotherapy with cell-based delivery systems where therapeutic biomolecules are delivered from tumor-targeting stem cells[20]. Furthermore, those stem cell-based therapies has been reported in treating a wide spectrum of cancers including breast cancer, malignant brain tumors, prostate cancer and gastrointestinal malignancy[20].

1.4 MESENCHYMAL STEM CELLS (MSCS)

Mesenchymal stem cells (MSCs) are multipotent cells that can be derived from multiple adult tissues, including bone marrow and fat[32, 33]. MSCs are the basis for the first approved stem cell treatment in humans outside of bone marrow transplant (Prochymal®, Osiris Therapeutics) and for over 400 ongoing trials listed on clinicaltrials.gov[34-36], among which there are also a number of ongoing clinical trials which are utilizing MSC for cancer therapy (Table 1.1)[28].

1.4.1 MSCs in cancer therapy

Systemically infused MSCs preferentially home to and integrate with tumors in the body, including both primary breast tumors and lung metastases. This phenomenon is presumably due to recruitment of MSCs by inflammatory and other cytokines produced by the tumor cells and makes them appealing vectors for localized delivery of therapeutics[37-39].

As vehicles for delivering effective, targeted therapy to isolated tumors and metastatic disease, MSC have been readily engineered to express anti-proliferative, pro-apoptotic, anti-angiogenic agents that specifically target different cancer types. Many of these strategies have been validated in a wide range of studies evaluating treatment feasibility or efficacy, as well as establishing methods for real-time monitoring of stem cell migration *in vivo* for optimal therapy surveillance and accelerated development[20, 28].

The unmodified MSCs have been shown to have anti-tumor effects both *in vitro* and in different mouse models of cancer. This is attributed to the factors released by MSCs that have antitumor properties reducing the proliferation of, for example, breast cancer cells[28, 40]. Human MSCs injected intravenously (*i.v.*) in a mouse model of Kaposi's sarcoma were shown to home to sites of tumorigenesis and potently inhibit tumor growth[41]. However MSCs derived from the bone marrow may give rise to tumor myofibroblasts and promote the growth of gastric tumors[42] and MSCs are reported to promote tumor chemotherapy resistance via secretion of omega-3 and oxo family fatty acids[43]. Intriguingly, a recent paper from the Weinberg laboratory found that a delicate crosstalk between MSCs and cancer cells plays roles in both inducing cancer stem cells and regulating the phenotype of tumor-associated MSCs[44].

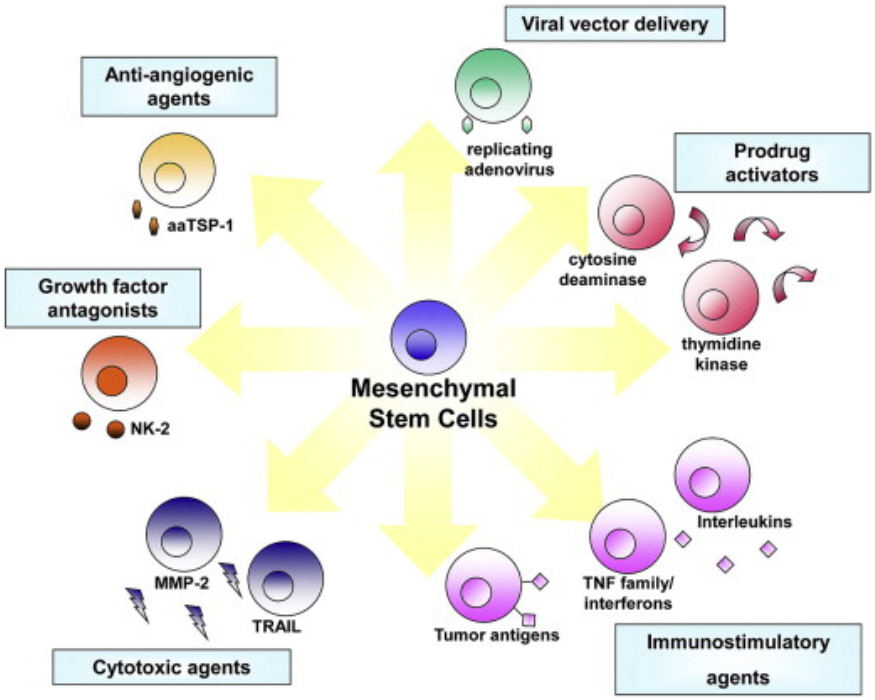

Figure 1.2. Transgene strategies potentiating MSC for tumor therapy. Reprinted by permission from Elsevier: Advanced Drug Delivery Reviews[28], copyright 2011.

In recent years, due to the controversy whether native/unmodified MSC promotes or inhibits tumor growth, there has been considerable interest using genetically modified MSCs, as trophic vehicles for delivery of drugs, proteins, and other therapeutic agents specifically to different cancer types. The advantage of using MSCs for drug delivery versus using other tumor-tropic cells such as macrophages include the immunoprivileged status of MSCs, homing abilities and intratumoral distribution, availability, genotypic and phenotypic stability, expandability, and proven safety record in clinical trials[32, 33]. Given the possibility of MSC regulation of tumor function it would be desirable to have viable drug-containing MSCs with stable functional properties until integration, distribution and drug release within tumors; however, once this has occurred, MSCs should die in order to avoid effects that facilitate tumor progression. The safe use of MSCs to treat cancer or non-cancer diseases in patients that have undiagnosed, early-stage cancer requires understanding the fate and functions of MSCs *in vivo* and their interactions with tumors (Figure 1.2).

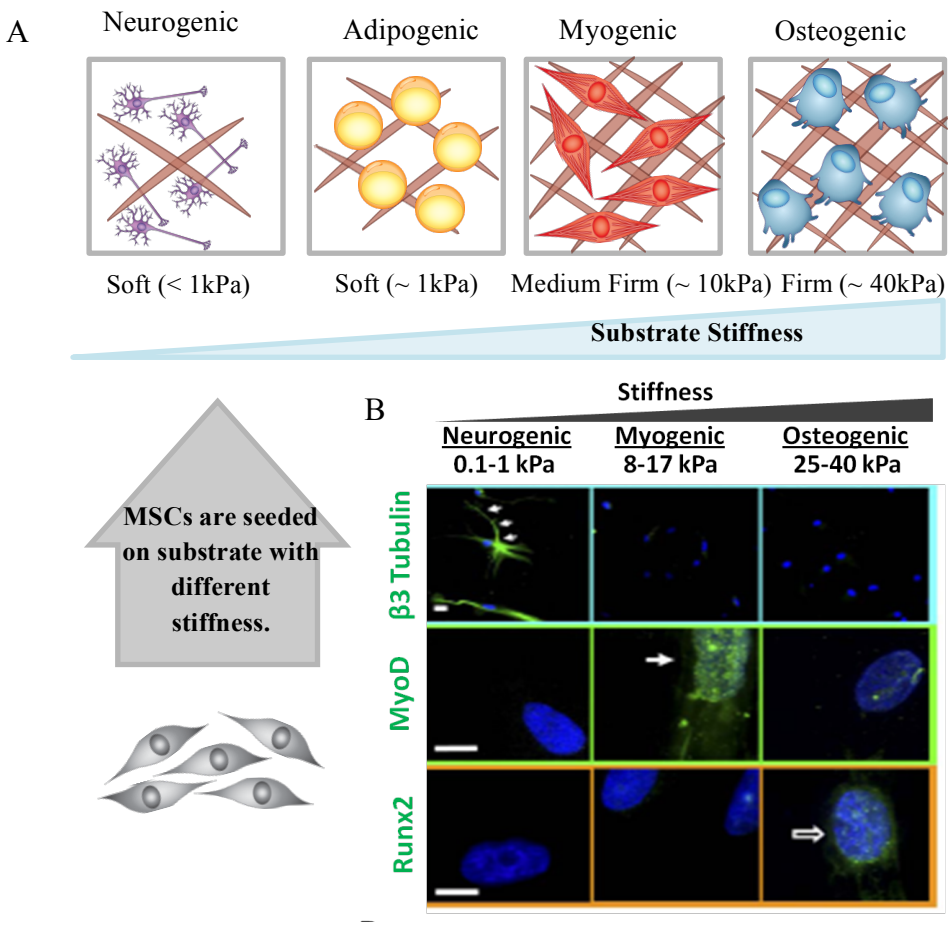

Figure 1.3. Influence of mechanical and physical properties of the ECM on cell behavior. (**A**) Mesenchymal stem cells (MSCs) within tissues experience very different degrees of ECM elasticity, ranging from very soft surroundings (such as those found in the brain and adipose tissue) to very stiff and rigid environments (such as those found within bones or at the bone surface). By recapitulating these different ECM elasticities *in vitro*, it was found that MSCs differentiate optimally into neurons, adipocytes, skeletal muscle cells or osteoblasts at elasticities that match the physiological ECM stiffness of their corresponding natural niche. (**B**) The neuronal cytoskeletal marker β3-tubulin is expressed in branches (arrows) of initially naive MSCs and only on the soft, neurogenic matrices. The muscle transcription factor MyoD1 is upregulated and nuclear localized (arrow) only in MSCs on myogenic matrices. The osteoblast transcription factor CBFα1 (*i.e.*, RunX2, arrow) is likewise expressed only on stiff, osteogenic gels. Scale bar: 5 μm. Reprinted by permission from Elsevier: Cell[45], copyright 2006.

1.4.2 Tools to image MSCs in cancer microenvironment *in vivo*

The clinical translation of MSC based therapies will depend on how successfully the robust surveillance systems are designed to simultaneously monitor the long-term fate of MSC,

the pharmacokinetics of MSC delivered therapeutics and ultimately the therapeutic efficacy of MSC *in vivo*. Several strategies can be pursued to visualize stem cell behavior *in vivo*.

Researchers have previously engineered different stem cell types including human MSC to stably express the bioluminescent enzyme firefly luciferase (Fluc)[46, 47]. After implanting stem cells into the cerebral hemispheres of nude mice contralateral to pregrafted tumors, NSC migration could be followed non-invasively in real-time along their migratory path towards tumors. A similar study was designed with MSC modified to secrete both S-TRAIL and Fluc[29]. Utilizing hybrid (fluorescence and bioluminescence) reporter constructs, dual bioluminescence and intravital imaging *in vivo*, the entire process of tumor formation, MSC migration, MSC dispersion throughout the tumor and MSC killing of glioma cells was monitored non-invasively in a longitudinal fashion. This allows not only the imaging gross MSC migration in real-time, but also to visualize tumor penetration by MSC at the single cell level.

Given the need for stem cell imaging techniques in larger animals or humans (where bioluminescent imaging is precluded by limited depth of tissue penetration), magnetic resonance imaging (MRI) and positron emission tomography (PET) have been evaluated for feasibility of stem cell tracking. Superparamagnetic particles have been conjugated to different stem cell types that have successfully demonstrated feasibility of imaging migration and peri- or intratumoral localization by MRI in mice[46, 48]. MSCs transduced with either adenoviruses and retroviruses expressing the HSV1-tk PET reporter gene suggest that engineered MSCs can be noninvasively imaged with 9-(4-18F-fluoro-3-[hydroxymethyl]butyl)guanine (18F-FHBG) after their transplantation in rats[49]. Recently, the reporter gene imaging of implanted human MSCs by using clinical positron emission tomography (PET)-computed tomography (CT) scanning suggests that human MSC can be translated in large animals[50]. In one study, embryonic stem cells transduced

with thymidine kinase and injected directly into murine hearts could be imaged with PET at high spatial resolution using the thymidine kinase-specific PET reporter probe [^{18}F]-FHBG[51]. Interestingly, teratomas formed in this study by embryonic stem cells could effectively be treated by systemic administration of ganciclovir. This indicates that the ganciclovir-thymidine kinase therapeutic regimen could be toxic to thymidine kinase expressing, non-immortalized stem cells themselves, and thus serve as a reporter-suicide for additional control in the prevention of tumor formation[51]. A few recent studies have explored the non-invasive tracking of MSC migration and sodium iodide symporter (NIS) transgene expression in real time prior to therapy in a mouse model of breast[52] and heapatocellular cancer[53] by Single-photon emission computed tomography (SPECT) and PET imaging respectively. SPECT imaging performed in mice injected with MSC-NIS and (99 m) TcO(4) revealed non-specificity of hNIS gene expression at earlier time points, however, at later time points, this expression depleted in non-target tissues and persisted at the tumor site. Based on these imaging/biodistribution data, mice received a therapeutic dose of (131) I 14D following MSC-NIS injection which resulted in a significant reduction in tumor growth as compared to controls[52]. This study reveals that the ability to non-invasively track MSC migration and transgene expression in real time prior to therapy is a major advantage for developing efficient stem cell based therapies. In conclusion, imaging surveillance of stem cell biodistribution and fate will be vital to successful implementation of stem cell delivery in cancer treatment. Several technologies are currently feasible for stem cell tracking, including bioluminescence, MRI and PET imaging, and are likely to contribute to future translational research.

Also, MSC spatiotemporally organize themselves in tumors, contributing to different microenvironments, and differentiating into various tumor stroma cells. The significance and the

mechanisms of this organization are unclear. Previous approaches of understanding cell fate and environment have been limited by low spatial and/or temporal resolution, required genetic modifications of cells, and/or could not detect multiple molecules. Today, high-resolution two-photon intravital microscopy (IVM)[54], coupled with spatiotemporal FRET-based aptamer microenvironment sensors (SMS)[55] can be used. Such studies would allow probing the spatiotemporal localization of MSCs and measuring the status of critical signaling molecules or events. By coupling these approaches with gain and loss of function studies, it will be possible to directly study the interactions between MSCs and tumors *in vivo*.

1.4.3 MSCs in mechanobiology

In the recent decade, it has become clear that mechanical and biophysical cues play an integral role in maintaining stem cell functions[56]. Mechanical signals received by the local extracellular matrix (ECM), including particularly stiffness, have been shown to regulate short and long-tern cellular activities, including morphology and cell differentiation[45]. Multiple recent publications have established that tissue and matrix stiffness is sufficient to drive expression of genes involved in MSC differentiation[45, 57-60]. Specifically, under compliant matrix stiffness (Young's modulus of less than 1 kPa), MSCs assume a neurogenic differentiation profile. At progressively higher matrix stiffness (5 to 75 kPa), MSCs differentiate to myogenic and osteogenic fates (Figure 1.3)[45, 57-60]. Importantly, the range of stiffness to which MSCs respond encompasses those found in normal breast and lung tissues (less than 1 kPa), as well as invasive cancers (10-15 fold higher stiffness)[61-63]. MSC differentiation is inherently a transcriptional program with each lineage defined by expression of characteristic transcription factors. This therefore allows us to use promoters regulating genes involved in MSC differentiation to drive expression of matrix stiffness-responsive reporters or therapeutics. Supporting our hypothesis

that MSCs can specifically respond to differences in tissue stiffness at the metastatic niche is the observation that MSCs injected intravenously in a mouse model of cancer specifically assumed an osteogenic differentiation profile in the metastatic lung but not in the normal lung[38, 64, 65].

Intriguingly it is shown that matrix stiffness directs 3-Dimension MSC differentiation in a similar manner to what was observed on 2-Dimension environments, but by altering integrin clustering rather than cell morphology[66]. In a covalently crosslinked hyaluronic acid hydrogel, however, it was shown that MSCs are differentiated into adipocytes independently of matrix stiffness, and once matrix is degraded, MSCs spread and undergo osteogenesis[67]. Whether this latter finding is related to the changes in hydrogel mechanical properties resulting from degradation is unclear, but combining these studies with a recent finding that the stress relaxation of gels regulates spreading, proliferation, and differentiation of MSCs[68, 69] suggests that matrix-stiffness-driven differentiation in 3-dimensions requires a labile environment where cells can generate traction forces and reorganize ligand binding.

It is said that force can be transmitted from the matrix to the nucleus through physical connections between cytoskeletal and nucleoskeletal proteins, but how matrix stiffness influences long-term gene expression and cell fate is just beginning to be understood at the molecular level. Yes-associated protein (YAP) and transcriptional coactivator with PDZ-binding motif (TAZ) were shown to play a functional role in MSC differentiation by promoting expression of mechanosensitive genes upon matrix stiffening[70]. Also, it was shown that matrix stiffening causes nuclear stiffening in MSCs by stabilizing the turnover of the nucleoskeletal protein lamin-A through phosphorylation, which then increases nuclear localization of YAP and other mechanosensitive transcription factors to drive osteogenesis[71]. To sum up, these studies are beginning to provide mechanistic understanding of how matrix stiffness directs stem cell fates.

1.5 SUMMARY

There is an unmet need to develop novel platform technology for future application to therapies targeting features of interest (*e.g.*, aberrant tissue stiffness) in certain disease states (*e.g.*, primary tumors and metastases in various organ systems). Cell engineering is an emerging way to detect, monitor or treat diseases or conditions by generating new features (*e.g.*, mechano-sensing) or enhancing existing functions (*e.g.*, tumor homing). This work aims to depict the methods using engineered MSCs to detect and treat diseases including metastatic breast cancer. We initially tested the concept of using transplanted MSCs as the basis for a simple cancer blood test. MSCs were engineered to express humanized *Gaussia* luciferase (hGluc). In a minimally invasive fashion, hGluc secreted by MSCs into circulation as a reporter for cancer presence, was assayed to probe whether MSCs co-localize with and persist in cancerous tissue (Chapter 2). Leveraging the central role of the mechanoenvironment in cancer metastasis, we present a mechanoresponsive cell system (MRCS) to selectively identify and treat cancer metastases by targeting the unique biophysical cues in the tumor niche both *in vitro* (Chapter 3) and *in vivo* (Chapter 4). Our MRCS employs mechanosensitive-promoter-driven, mesenchymal stem cell (MSC)-based vectors, which selectively homes to and targets cancer metastases in response to specific mechanical cues to deliver therapeutics to effectively kill cancer cells as demonstrated in a metastatic breast cancer mouse model (Chapter 5). We have further explored the potential mechanism of the activity of MRCS in the metastatic niche, *i.e.*, the correlation between collagen crosslinking and tissue-stiffness elevation at the metastatic sites where our MRCS is specifically activated by the unique, cancer associated mechano-cues (Chapter 6). In the summary, the overall impact from our platform technology on the fields of disease diagnosis, cell therapeutics

and mechanobiology as well as future directions of the study are discussed (Chapter 7). Chapter 2 is based on a publication[72] and Chapter 3-6 are based a manuscript currently under revision.

Table 1.1. The use of MSCs for localized drug delivery to tumors

Agent	Mechanism	Advantage of Using MSCs
Type I interferons	antiproliferative and proapoptotic	-high degree of toxicity when free IFNs are administered systemically -MSCs can deliver IFNs and locally release them in tumors
Interleukin-12	IL-12 acts on several immune cells including T, natural killer, and natural killer T cells and induces interferon-γ (IFN-γ)	-free IL-12 is toxic when delivered systemically, because it causes a widespread immune response -MSCs can deliver IL-12 specifically to tumors and release it locally
Chemokines (CX3CL1)	-at least in part by inducing migration and activation of immune cells	-MSCs locally deliver CX3CL1, avoid recruitment of immune cells to normal organs
Oncolytic viruses	- target replicating tumor cells and cause their death	-MSCs act as delivery vehicles to protect the viruses from neutralization by the body, and minimize the overall viral dose and systemic toxicity -tropism of MSCs for tumors lead to preferentially accumulation in tumors
Proapoptotic molecules (*e.g.*, TRAIL)	-tumor necrosis factor related apoptosis inducing ligand (TRAIL) is a pro-apoptotic molecule with relatively selective killing of cancer cells -MSCs were much more resistant to TRAIL-mediated cytotoxicity than tumor cells	-TRAIL short half life in blood and possible systemic toxicity warrants the use of MSCs as delivery vehicles to tumors
Prodrug converting enzymes	-One such enzyme is yeast cytosine deaminase-uracil ribosyltransferase fusion (abbreviated as CD). This enzyme can convert 5-fluorocytidine (FC) to the highly toxic 5-fluorouracil	-targeted delivery with MSCs

	(FU) -sodium iodide symporter (NIS) can be effective in both imaging MSC biodistribution by selective tumor concentration of $^{99m}TcO_4^-$ or iodide-123, and in concentrating iodide-131 for cancer therapy -herpes simplex thymidine kinase could act as a prodrug converting enzyme for gancyclovir.	
Nano and microparticles	-drugs are encapsulated within particles -particles are taken up by MSCs and delivered to tumors	-no genetic modifications of MSCs -targeted delivery of anticancer drugs to tumors -MSC-particles-drugs integrate to and distribute within tumors -MSCs may be more resistant to some drugs than cancer cells, but will eventually be killed by the drugs

Modified from Droujinine. *et al*[40] (Supplementary Table 4).

1.6 REFERENCES

1. Hanahan, D. & Weinberg, R.A. Hallmarks of cancer: the next generation. *Cell* **144**, 646-674 (2011).
2. Paget, S. The distribution of secondary growths in cancer of the breast. 1889. *Cancer metastasis reviews* **8**, 98-101 (1989).
3. Poste, G. & Fidler, I.J. The pathogenesis of cancer metastasis. *Nature* **283**, 139-146 (1980).
4. Altaner, C. Prodrug cancer gene therapy. *Cancer Lett* **270**, 191-201 (2008).
5. Hortobagyi, G.N. Can we cure limited metastatic breast cancer? *Journal of clinical oncology : official journal of the American Society of Clinical Oncology* **20**, 620-623 (2002).
6. Ali, S.M., Harvey, H.A. & Lipton, A. Metastatic breast cancer: overview of treatment. *Clinical orthopaedics and related research*, S132-137 (2003).
7. Hedley, B.D. & Chambers, A.F. Tumor dormancy and metastasis. *Advances in cancer research* **102**, 67-101 (2009).
8. Jones, S.E. Metastatic breast cancer: the treatment challenge. *Clinical breast cancer* **8**, 224-233 (2008).
9. Rivera, E. Management of metastatic breast cancer: monotherapy options for patients resistant to anthracyclines and taxanes. *American journal of clinical oncology* **33**, 176-185 (2010).
10. Cox, T.R. & Erler, J.T. Remodeling and homeostasis of the extracellular matrix: implications for fibrotic diseases and cancer. *Disease models & mechanisms* **4**, 165-178 (2011).
11. Erler, J.T. et al. Hypoxia-induced lysyl oxidase is a critical mediator of bone marrow cell recruitment to form the premetastatic niche. *Cancer cell* **15**, 35-44 (2009).
12. Levental, K.R. et al. Matrix crosslinking forces tumor progression by enhancing integrin signaling. *Cell* **139**, 891-906 (2009).
13. Leight, J.L., Wozniak, M.A., Chen, S., Lynch, M.L. & Chen, C.S. Matrix rigidity regulates a switch between TGF-beta1-induced apoptosis and epithelial-mesenchymal transition. *Molecular biology of the cell* **23**, 781-791 (2012).
14. Wong, C.C. et al. Hypoxia-inducible factor 1 is a master regulator of breast cancer metastatic niche formation. *Proceedings of the National Academy of Sciences of the United States of America* **108**, 16369-16374 (2011).
15. Erler, J.T. & Giaccia, A.J. Lysyl oxidase mediates hypoxic control of metastasis. *Cancer research* **66**, 10238-10241 (2006).
16. Erler, J.T. et al. Lysyl oxidase is essential for hypoxia-induced metastasis. *Nature* **440**, 1222-1226 (2006).
17. Bondareva, A. et al. The lysyl oxidase inhibitor, beta-aminopropionitrile, diminishes the metastatic colonization potential of circulating breast cancer cells. *PloS one* **4**, e5620 (2009).
18. Wong, C.C. et al. Inhibitors of hypoxia-inducible factor 1 block breast cancer metastatic niche formation and lung metastasis. *J Mol Med (Berl)* **90**, 803-815 (2012).
19. McPherson, J.M., Sawamura, S.J. & Conti, A. Preparation of [3H]collagen for studies of the biologic fate of xenogenic collagen implants in vivo. *The Journal of investigative dermatology* **86**, 673-677 (1986).
20. Shah, K. Stem cell therapeutics for cancer. (John Wiley & Sons, Hoboken, N.J.; 2013).
21. Weissman, I.L. Translating stem and progenitor cell biology to the clinic: barriers and opportunities. *Science* **287**, 1442-1446 (2000).
22. Smith, S., Neaves, W. & Teitelbaum, S. Adult stem cell treatments for diseases? *Science* **313**, 439 (2006).
23. Sagar, J., Chaib, B., Sales, K., Winslet, M. & Seifalian, A. Role of stem cells in cancer therapy and cancer stem cells: a review. *Cancer Cell Int* **7**, 9 (2007).
24. Thomson, J.A. et al. Embryonic stem cell lines derived from human blastocysts. *Science* **282**, 1145-1147 (1998).
25. Serakinci, N. et al. Adult human mesenchymal stem cell as a target for neoplastic transformation. *Oncogene* **23**, 5095-5098 (2004).
26. Sylvester, K.G. & Longaker, M.T. Stem cells: review and update. *Arch Surg* **139**, 93-99 (2004).
27. Pierige, F., Serafini, S., Rossi, L. & Magnani, M. Cell-based drug delivery. *Advanced drug delivery reviews* **60**, 286-295 (2008).
28. Shah, K. Mesenchymal stem cells engineered for cancer therapy. *Advanced drug delivery reviews* **64**, 739-748 (2012).
29. Sasportas, L.S. et al. Assessment of therapeutic efficacy and fate of engineered human mesenchymal stem cells for cancer therapy. *Proceedings of the National Academy of Sciences of the United States of America* **106**, 4822-4827 (2009).

30. Aboody, K.S. et al. Neural stem cell-mediated enzyme/prodrug therapy for glioma: preclinical studies. *Science translational medicine* **5**, 184ra159 (2013).
31. Alonso, M.M. et al. ICOVIR-5 shows E2F1 addiction and potent antiglioma effect in vivo. *Cancer research* **67**, 8255-8263 (2007).
32. Karp, J.M. & Leng Teo, G.S. Mesenchymal stem cell homing: the devil is in the details. *Cell stem cell* **4**, 206-216 (2009).
33. Ankrum, J. & Karp, J.M. Mesenchymal stem cell therapy: Two steps forward, one step back. *Trends in molecular medicine* **16**, 203-209 (2010).
34. Cyranoski, D. Chinese genomics giant BGI plots commercial path. *Nature biotechnology* **30**, 1159-1160 (2012).
35. Trounson, A., Thakar, R.G., Lomax, G. & Gibbons, D. Clinical trials for stem cell therapies. *BMC medicine* **9**, 52 (2011).
36. Giordano, A., Galderisi, U. & Marino, I.R. From the laboratory bench to the patient's bedside: an update on clinical trials with mesenchymal stem cells. *Journal of cellular physiology* **211**, 27-35 (2007).
37. Reagan, M.R. & Kaplan, D.L. Concise review: Mesenchymal stem cell tumor-homing: detection methods in disease model systems. *Stem Cells* **29**, 920-927 (2011).
38. Wang, H. et al. Trafficking mesenchymal stem cell engraftment and differentiation in tumor-bearing mice by bioluminescence imaging. *Stem Cells* **27**, 1548-1558 (2009).
39. Loebinger, M.R., Eddaoudi, A., Davies, D. & Janes, S.M. Mesenchymal stem cell delivery of TRAIL can eliminate metastatic cancer. *Cancer research* **69**, 4134-4142 (2009).
40. Droujinine, I.A., Eckert, M.A. & Zhao, W. To grab the stroma by the horns: from biology to cancer therapy with mesenchymal stem cells. *Oncotarget* **4**, 651-664 (2013).
41. Khakoo, A.Y. et al. Human mesenchymal stem cells exert potent antitumorigenic effects in a model of Kaposi's sarcoma. *J Exp Med* **203**, 1235-1247 (2006).
42. Quante, M. et al. Bone marrow-derived myofibroblasts contribute to the mesenchymal stem cell niche and promote tumor growth. *Cancer cell* **19**, 257-272 (2011).
43. Roodhart, J.M. et al. Mesenchymal stem cells induce resistance to chemotherapy through the release of platinum-induced fatty acids. *Cancer cell* **20**, 370-383 (2011).
44. Li, H.J., Reinhardt, F., Herschman, H.R. & Weinberg, R.A. Cancer-stimulated mesenchymal stem cells create a carcinoma stem cell niche via prostaglandin E2 signaling. *Cancer discovery* **2**, 840-855 (2012).
45. Engler, A.J., Sen, S., Sweeney, H.L. & Discher, D.E. Matrix elasticity directs stem cell lineage specification. *Cell* **126**, 677-689 (2006).
46. Ozdemir, V. et al. Shifting emphasis from pharmacogenomics to theragnostics. *Nature biotechnology* **24**, 942-946 (2006).
47. Shah, K. Imaging neural stem cell fate in mouse model of glioma. *Curr Protoc Stem Cell Biol* **Chapter 5**, Unit 5A 1 (2009).
48. Song, M. et al. MRI tracking of intravenously transplanted human neural stem cells in rat focal ischemia model. *Neurosci Res* **64**, 235-239 (2009).
49. Roelants, V. et al. Comparison between adenoviral and retroviral vectors for the transduction of the thymidine kinase PET reporter gene in rat mesenchymal stem cells. *J Nucl Med* **49**, 1836-1844 (2008).
50. Willmann, J.K. et al. Imaging gene expression in human mesenchymal stem cells: from small to large animals. *Radiology* **252**, 117-127 (2009).
51. Sweeney, T.J. et al. Visualizing the kinetics of tumor-cell clearance in living animals. *Proceedings of the National Academy of Sciences of the United States of America* **96**, 12044-12049 (1999).
52. Dwyer, R.M. et al. Mesenchymal Stem Cell-mediated delivery of the sodium iodide symporter supports radionuclide imaging and treatment of breast cancer. *Stem Cells* **29**, 1149-1157 (2011).
53. Knoop, K. et al. Image-guided, tumor stroma-targeted 131I therapy of hepatocellular cancer after systemic mesenchymal stem cell-mediated NIS gene delivery. *Molecular therapy : the journal of the American Society of Gene Therapy* **19**, 1704-1713 (2011).
54. Jain, R.K., Munn, L.L. & Fukumura, D. Dissecting tumour pathophysiology using intravital microscopy. *Nature reviews. Cancer* **2**, 266-276 (2002).
55. Zhao, W. et al. Cell-surface sensors for real-time probing of cellular environments. *Nature nanotechnology* **6**, 524-531 (2011).
56. Shin, J.W. & Mooney, D.J. Improving Stem Cell Therapeutics with Mechanobiology. *Cell stem cell* **18**, 16-19 (2016).

57. Rowlands, A.S., George, P.A. & Cooper-White, J.J. Directing osteogenic and myogenic differentiation of MSCs: interplay of stiffness and adhesive ligand presentation. *American journal of physiology. Cell physiology* **295**, C1037-1044 (2008).
58. Pek, Y.S., Wan, A.C. & Ying, J.Y. The effect of matrix stiffness on mesenchymal stem cell differentiation in a 3D thixotropic gel. *Biomaterials* **31**, 385-391 (2010).
59. Park, J.S. et al. The effect of matrix stiffness on the differentiation of mesenchymal stem cells in response to TGF-beta. *Biomaterials* **32**, 3921-3930 (2011).
60. Tse, J.R. & Engler, A.J. Stiffness gradients mimicking in vivo tissue variation regulate mesenchymal stem cell fate. *PloS one* **6**, e15978 (2011).
61. Krouskop, T.A., Wheeler, T.M., Kallel, F., Garra, B.S. & Hall, T. Elastic moduli of breast and prostate tissues under compression. *Ultrasonic imaging* **20**, 260-274 (1998).
62. Lopez, J.I., Kang, I., You, W.K., McDonald, D.M. & Weaver, V.M. In situ force mapping of mammary gland transformation. *Integrative biology : quantitative biosciences from nano to macro* **3**, 910-921 (2011).
63. Samani, A., Zubovits, J. & Plewes, D. Elastic moduli of normal and pathological human breast tissues: an inversion-technique-based investigation of 169 samples. *Physics in medicine and biology* **52**, 1565-1576 (2007).
64. Bonfield, T.L. & Caplan, A.I. Adult mesenchymal stem cells: an innovative therapeutic for lung diseases. *Discovery medicine* **9**, 337-345 (2010).
65. Ortiz, L.A. et al. Mesenchymal stem cell engraftment in lung is enhanced in response to bleomycin exposure and ameliorates its fibrotic effects. *Proceedings of the National Academy of Sciences of the United States of America* **100**, 8407-8411 (2003).
66. Huebsch, N. et al. Harnessing traction-mediated manipulation of the cell/matrix interface to control stem-cell fate. *Nat Mater* **9**, 518-526 (2010).
67. Khetan, S. et al. Degradation-mediated cellular traction directs stem cell fate in covalently crosslinked three-dimensional hydrogels. *Nat Mater* **12**, 458-465 (2013).
68. Chaudhuri, O. et al. Substrate stress relaxation regulates cell spreading. *Nat Commun* **6**, 6364 (2015).
69. Chaudhuri, O. et al. Hydrogels with tunable stress relaxation regulate stem cell fate and activity. *Nat Mater* **15**, 326-334 (2016).
70. Dupont, S. et al. Role of YAP/TAZ in mechanotransduction. *Nature* **474**, 179-183 (2011).
71. Swift, J. et al. Nuclear lamin-A scales with tissue stiffness and enhances matrix-directed differentiation. *Science* **341**, 1240104 (2013).
72. Liu, L. et al. Exogenous marker-engineered mesenchymal stem cells detect cancer and metastases in a simple blood assay. *Stem Cell Res Ther* **6**, 181 (2015).

CHAPTER 2

EXOGENOUS MARKER-ENGINEERED MESENCHYMAL STEM CELLS DETECT CANCER AND METASTASES IN A SIMPLE BLOOD ASSAY

Authors: **Linan Liu**[1,2], Shirley X. Zhang[1,2], Rangoli Aeran[1,3], Wenbin Liao[1,2], Mengrou Lu[1], George Polovin[1,2,4], Egest J. Pone[1,2], Weian Zhao[1,2,5]

Author Affiliations:

[1]Department of Pharmaceutical Sciences, Sue and Bill Gross Stem Cell Research Center, Chao Family Comprehensive Cancer Center and Edwards Life sciences Center for Advanced Cardiovascular Technology, 845 Health Sciences Road, University of California-Irvine, Irvine, California, 92697, USA.

[2]Department of Biomedical Engineering, University of California-Irvine, Irvine, California, 92697, USA.

[3]Department of Molecular Biology & Biochemistry, University of California-Irvine, Irvine, California, 92697, USA.

[4]Department of Biological Sciences, California State University, Long Beach, 1250 Bellflower Blvd, Long Beach, CA 90840, USA.

[5]Department of Biological Chemistry, University of California-Irvine, Irvine, California, 92697, USA.

2.1 ABSTRACT

Mesenchymal stem cells (MSCs) are adult multipotent stem cells that possess regenerative and immunomodulatory properties. They have been widely investigated as therapeutic agents for a variety of disease conditions, including tissue repair, inflammation, autoimmunity and organ transplantation. Importantly, systemically-infused MSCs selectively home to primary and metastatic tumors, though the molecular mechanisms of tumor tropism of MSC remain incompletely understood. We have exploited the active and selective MSC homing to cancer microenvironments to develop a rapid and selective blood test for the presence of cancer. We tested the concept of using transplanted MSC as the basis for a simple cancer blood test. MSCs were engineered to express humanized *Gaussia* luciferase (hGluc). In a minimally invasive fashion, hGluc secreted by MSC into circulation, as a reporter for cancer presence, was assayed to probe whether MSCs co-localize with and persist in cancerous tissue. *In vitro,* hGluc secreted by engineered MSC was detected stably over a period of days in the presence of serum. *In vivo* imaging showed that MSC homed to breast cancer lung metastases and persisted longer in tumor-bearing mice than in tumor-free mice ($P < 0.05$). hGluc activity in blood of tumor-bearing mice was significantly higher than in their tumor-free counterparts ($P < 0.05$). Both *in vitro* and *in vivo* data show that MSCs expressing hGluc can identify and report small tumors or metastases in a simple blood test format. Our novel and simple stem cell-based blood test can potentially be used to screen, detect and monitor cancer and metastasis at early-stages and during treatment.

Keywords: mesenchymal stem cells, cancer detection, point-of-care, blood test

2.2 INTRODUCTION

Cancer is a leading cause of human morbidity and mortality, and its origins, biomarkers and detection remain difficult to pinpoint [1]. While early detection has proven to be a useful and often necessary first step to effectively manage and treat cancer [2], it remains a challenge to identify cancer at early-stages, especially small tumors and metastases which account for over 90% of cancer mortality [3, 4]. Methods of cancer detection based on imaging are non-invasive, but common drawbacks include high cost, low specificity or resolution, and the use of potential irritating contrast agents [2]. For instance, positron emission tomography (PET), computed tomography (CT), and their combinations (PET-CT), are widely used for identifying and staging tumors, but require high doses of ionizing radiation and have limited specificity and resolution [5]. Other imaging modalities, such as magnetic resonance imaging (MRI) and ultrasound, do not use radiation but are still unable to achieve spatial resolution smaller than several millimeters [6, 7]. On the other hand, tissue biopsies are invasive and suffer from false negatives for heterogeneous tumors, and obtaining biopsies from multiple small disseminated tumors (*e.g.* metastases) is impractical**.** Cancer screening also utilizes tests for biomarkers, including circulating tumor cells, exosomes, proteins and nucleic acids. Recently, scientists have developed nanoparticle-based synthetic biomarkers composed of mass-encoded peptides that can be released upon tumor protease cleavage, and then detected in urine [8, 9]. Such approaches, however, still rely on passive delivery of nanoparticles to tumor via the enhanced permeability and retention (EPR) effect and on limited types of endogenous proteins, both of which are cancer type-specific. Nevertheless, cancer biomarker discovery has led to only a few biomarkers used in clinical diagnosis since cancer biomarkers frequently suffer from low sensitivity and specificity [10].

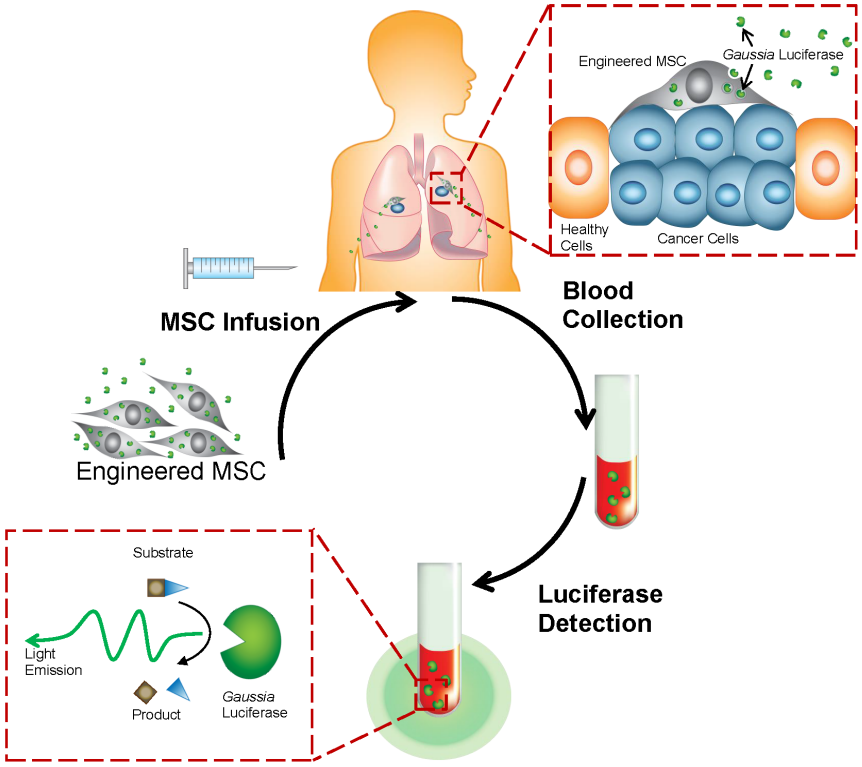

Figure 2.1. Using engineered mesenchymal stem cells (MSCs) to detect cancer. Engineered MSCs (gray) secreting humanized *Gaussia* luciferase (hGluc, green) are systemically administered into patients with cancer (breast cancer lung metastasis in this case). Engineered MSCs home to tumor (cyan) niche and persist, secreting hGluc into blood. Then patient blood can be collected and hGluc activity measured.

In particular, cancer heterogeneity and evolution makes it challenging to rely on molecular biomarkers for cancer detection [1]. For example, the commonly used cancer biomarkers prostate specific antigen (PSA) for prostate cancer and BRCA1/2 gene mutations for breast cancer can only identify about 25% and 10 to 25% of the patients in each cancer type, respectively [11]. Indeed, it has been widely accepted that a single biomarker typically lacks the sensitivity and specificity that is necessary for useful diagnosis. Intriguingly, recent research indicates that most cancers are caused by stochastic events rather than predictable mutations [12].

Thus, finding biomarkers that recognize multiple types of cancers with no common genetic basis is likely less promising than previously thought. In summary, there is clearly an unmet clinical need for sensitive early-stage cancer and metastasis tests that can "universally" identify many types of cancers independently of specific biomarkers from healthy controls and other conditions that share similar symptoms (*e.g.*, inflammation), as well as to discriminate different (sub)types of cancers at different stages.

Cells, including immune and stem cells, act as autonomous and adaptive agents and these properties have recently been used for cancer treatment and drug delivery [13-16]. In particular, mesenchymal stem (or stromal) cells (MSCs) have been tested as therapeutic agents due to their intrinsic regenerative and immunomodulatory features [17-22]. MSCs are under investigation for treating a wide array of diseases including diabetes, myocardial infarction, stroke and autoimmune diseases [23-25]. MSCs are also the world's first manufactured stem cell product to receive clinical approval (*i.e.*, Prochymal® manufactured by Osiris was approved in Canada to treat graft-versus-host disease (GvHD)) [25], suggesting they may be a safe source for diagnostic and therapeutic uses in humans. Importantly, systemically-infused MSCs preferentially home to and integrate with tumors, including both primary tumors and metastases in different anatomical locations [23]. As we have recently reviewed [21], mounting evidence now suggests that MSCs possess leukocyte-like, active homing mechanisms for tumor tropism involving a variety of adhesion molecules (*e.g.*, P-selectin and VCAM-1) and tumor-derived cytokines, chemokines, and growth factors (*e.g.*, CXCL12 and PDGF). This selective and active homing ability makes MSC an appealing vector for localized delivery of therapeutics to treat cancers including gliomas, melanomas, breast cancer and lung metastases in ongoing clinical trials [14, 23]. In addition, MSCs engineered with probes (such as luciferase) have been used to detect and image

tumors *in situ* [18, 26]. However, imaging methods such as PET/SPECT and MRI which are currently used for cell tracking after infusion are limited by the same aforementioned disadvantages of cancer detection [2].

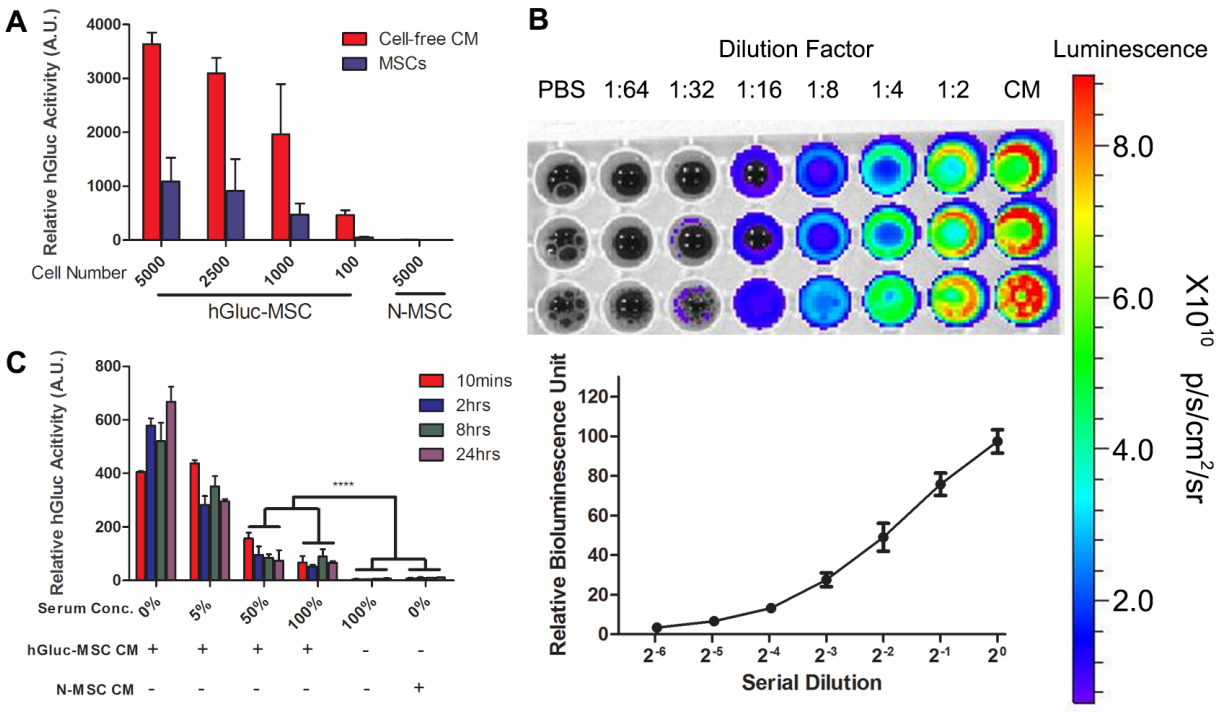

Figure 2.2. Humanized *Gaussia* luciferase (hGluc) is secreted *in vitro* and is stable in blood. **(A)** Mesenchymal stem cells expressing humanized *Gaussia* luciferase (hGluc-MSC) and native MSCs (N-MSC) were seeded onto 96 well plates. 24 hours later cell-free conditioned medium (CM) was harvested. The hGluc substrate coelenterazine (CTZ) was added with a final concentration of 20 µM. hGluc activity was measured immediately using a plate reader (Absorbance at wavelengths 300-700nm, exposure time = 2s). **(B)** Serial dilution of hGluc-MSC CM was performed in PBS and CTZ was added at a final concentration of 20 µM. hGluc activity was measured with an IVIS Lumina (exposure time = 0.5 second). Color scale: Min = $6.64e^{8}$; Max = $8.93e^{9}$. **(C)** CM of hGluc-MSC was harvested and incubated with human serum for 10 minutes, 2 hours, 8 hours or 24 hours at 37°C. A final concentration of 20 µM of CTZ was added and hGluc activity was measured immediately (exposure time = 2s). hGluc activity was detectable in 100% serum. **** $P < 0.0001$. Error bar: mean ± SD.

In this article, we present the concept of using exogenous MSC as the basis for a simple cancer blood test (Figure 2.1). Here we hypothesize that due to their tumor tropism property,

MSC engineered with a secreted reporter can actively and specifically home to tumor sites regardless of the type and location of the tumors, and persist there longer compared to MSC in healthy microenvironments. MSCs engineered to express humanized *Gaussia* luciferase (hGluc) [27-30] were systemically administered to mice harboring breast cancer cells, exhibited tumor tropism and persistence, and secreted hGluc into the bloodstream of tumor-bearing mice. Thus, MSC engineered with secreted reporters can potentially be developed into a blood test for broad cancer screening and monitoring.

2.3 RESULTS

2.3.1 Humanized *Gaussia* luciferase is secreted from engineered MSC *in vitro* and is stable and detectable in blood

Human bone marrow mesenchymal stem cells (MSCs) were stably transduced with lentivirus to express secreted humanized *Gaussia* luciferase (hGluc) as described above. In order to determine whether hGluc is secreted in an active form by MSC, cell-free conditioned medium (CM) was harvested from hGluc-MSC 24 hours after MSC seeding at different concentrations (100, 1000, 2500 or 5000 cells per cm^2). The substrate coelenterazine (CTZ) was added and hGluc activity was measured for both cells and CM (Figure 2.2A). Measured hGluc activity increased with increasing cell number (Figure 2.2A). In addition, hGluc activity in CM was 3-6 fold higher than inside cells (Figure 2.2A), indicating that hGluc expressed by engineered MSC is secreted in active form, as expected. hGluc-MSC CM was serially diluted with PBS and hGluc activity was measured *in vitro* and found to exhibit a linear function of concentration, in agreement with earlier reports [31-33] (Figure 2.2B). To demonstrate whether luciferase activity from hGluc-MSC is detectable and sufficiently stable in blood, human serum either directly

(100%) or serially diluted in PBS as mixed with hGluc-MSC CM. hGluc activity remained detectable ($P < 0.0001$) after 24 hours co-incubation and hGluc activity was not decreased significantly over time (Figure 2.2C), indicating that hGluc-MSC can be a stable marker in blood assays *in vitro*. Finally, since both firefly luciferase (Fluc-tdT, tdT: tdTomato red fluorescent protein) and hGluc would be used *in vivo* (below), any potential cross-reactivity between Fluc-tdT and hGluc-MSC was measured (Figure 2.S1). These two luciferases were substrate-specific and no cross-reaction was observed, as reported. Overall, these data show that hGluc expressed by engineered MSC is secreted *in vitro*, is stable in human serum for up to 24 hours and exhibits substrate-specific enzyme activity.

2.3.2 Engineered MSCs home to tumor sites and persist longer in the lungs of the tumor-bearing mice

As MSCs are reported to naturally home to tumor sites [17, 18] we then tested this phenomenon in our experiment as a preliminary step to using MSC that secrete hGluc as a diagnostic tool for cancer detection and localization. Human breast cancer-derived MDA-MB 231 cells were labeled with eGFP or Fluc-tdT and implanted intravenously (*i.v.*) into immunodeficient NOD-SCID gamma (NSG) mice (Figure 2.3) to establish a simple *in vivo* mouse model of breast cancer that has metastasized in the lungs [34, 35]. Tumor mass was observed in lung both *in vivo* (Figure 2.3A) and *ex vivo* (Figure 2.3B, 2.3D) while no tumor-related signal was seen in healthy lungs (Figure 2.3A, 2.3C). As hGluc is secreted by MSC, and due to its diluted and limited signal under whole animal imaging conditions with IVIS Lumina [36] (data not shown), we used MSC engineered with intracellular Fluc-tdT [37] for real-time imaging and localization of MSC in tumors *in situ.* Fluc-tdT-MSC were simultaneously labeled with red fluorescent protein (RFP) to assess Fluc transduction efficiency and to image any co-localized

MSCs and tumor cells in subsequent *ex vivo* immunohistochemistry. Both Fluc activity and RFP signal from Fluc-tdT-MSC were observed *in vitro* (Figure 2.S2), demonstrating that engineered MSCs express Fluc (Figure 2.S2A) with high transduction efficiency (> 90% RFP^+, Figure 2.S2B-2.S2D).

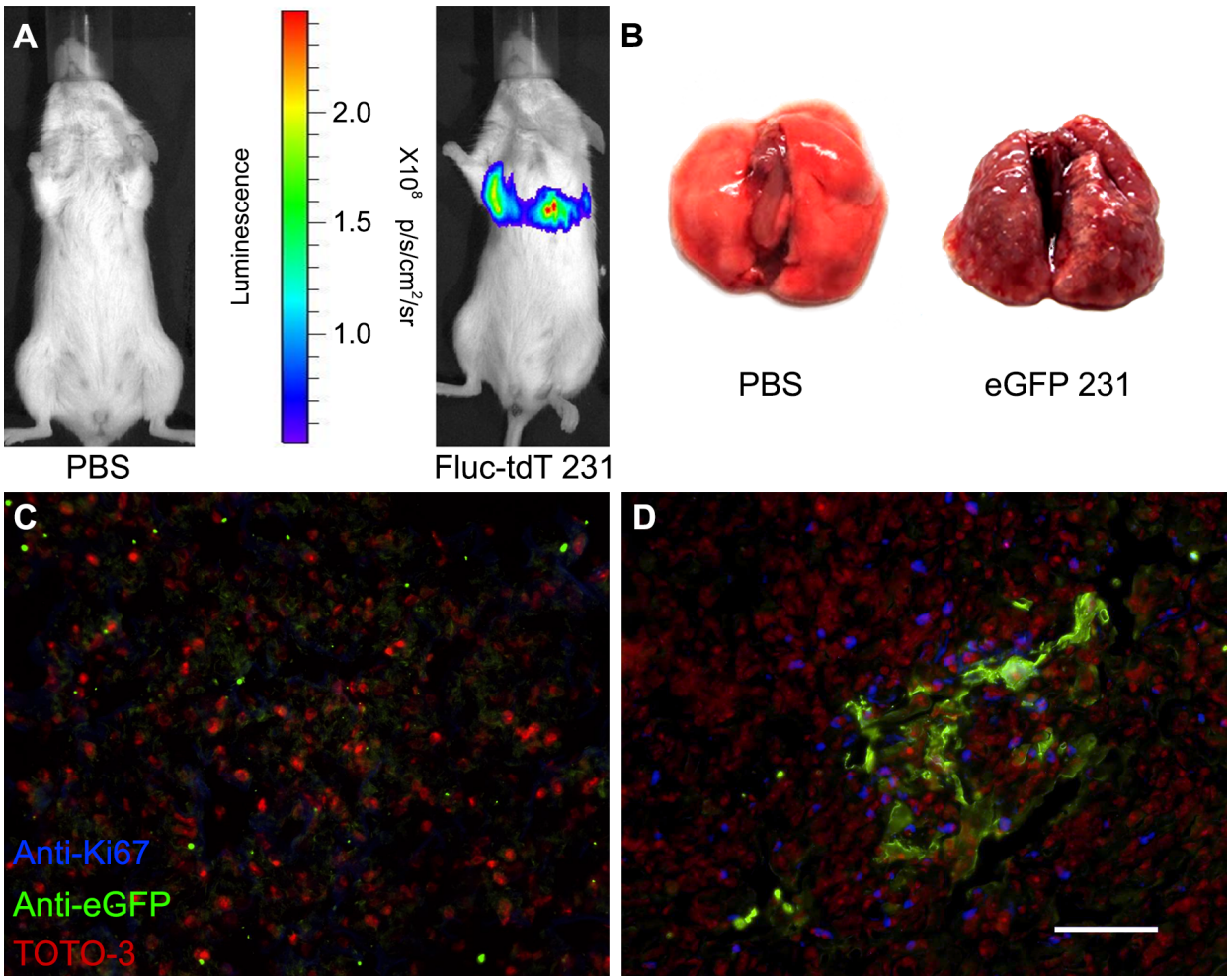

Figure 2.3. Human derived breast cancer is observed in xenotransplantation murine model. **(A)** 5 weeks after 0.5 x 10^6 Fluc-tdT-231 were seeded *i.v.*, NSG mice were injected *i.p.* with D-Luciferin (150mg/kg in DPBS) and *in vivo* Fluc activity was measured with IVIS Lumina 10 minutes after substrate administration. Exposure time = 5 seconds. Color scale: Min = $5.13e^7$; Max = $2.46e^8$. **(B)** Representative pictures of tumor-free (left) and tumor-bearing (right) lungs. 8 weeks after MDA-MB-231 breast cancer cells or PBS were seeded *i.v.*, NSG mice were euthanized and lungs were harvested. Frozen sections of lungs of **(C)** tumor-free mice and **(D)** eGFP-231 tumor-bearing mice sacrificed 5 weeks after cancer seeding was stained with anti-eGFP (green), anti-Ki67 (blue) and TOTO-3 (red). Scale bar: 50 µm.

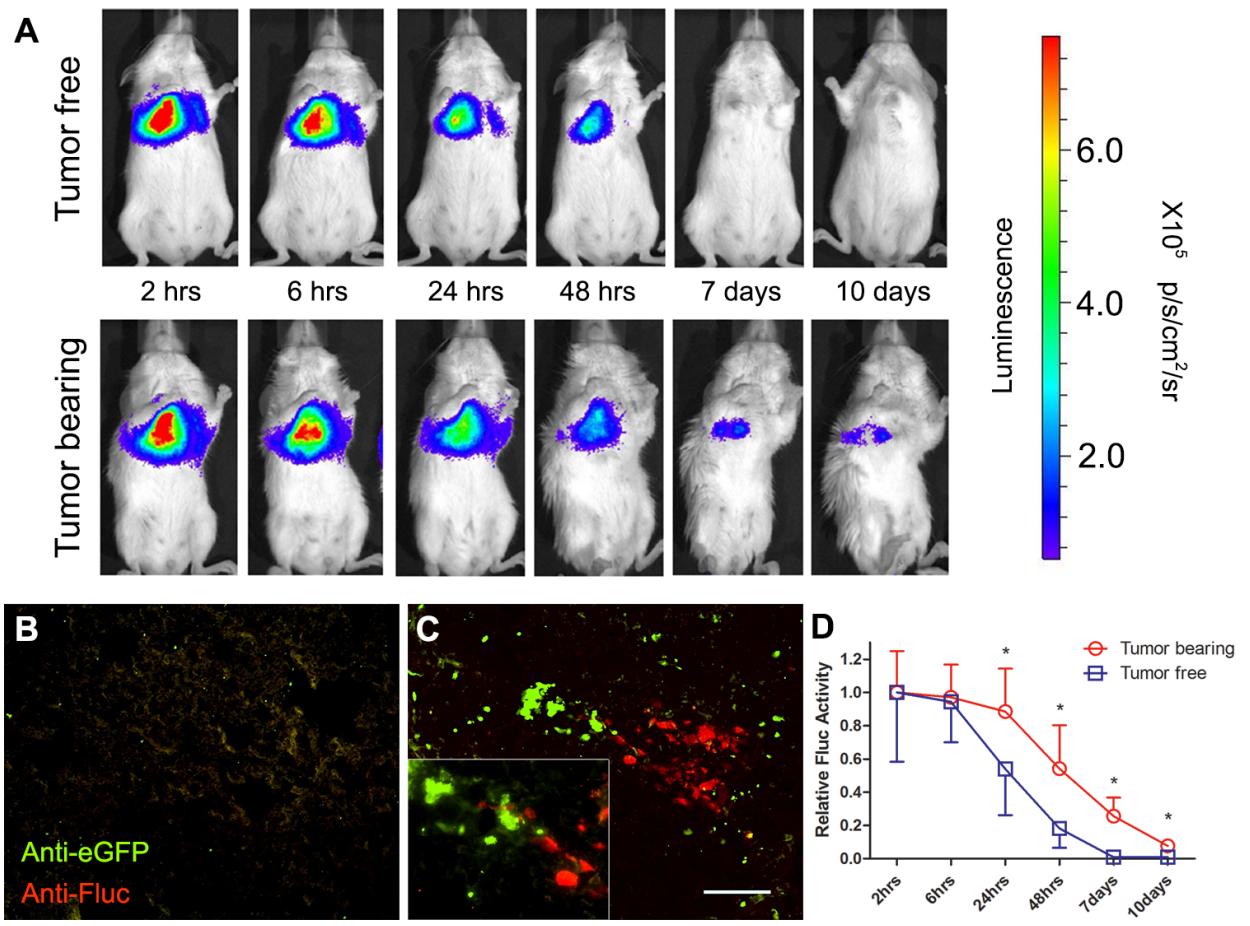

Figure 2.4. Mesenchymal stem cells home to tumor site and persist longer than in healthy mice. (A) 5 weeks after eGFP-231 were seeded *i.v.* into NSG mice, 10^6 Fluc-tdT-MSC were administered systemically into both tumor-free (top) and tumor-bearing (bottom) mice. Then mice were injected *i.p.* with D-Luciferin (150mg/kg in DPBS) and *in vivo* Fluc activity was measured at different time points (2 hours, 6 hours, 24 hours, 7 days and 10 days after MSC infusion) using an IVIS Lumina to begin data acquisition 10 minutes after substrate administration (exposure time = 60 seconds; $n = 4$ in each group). MSCs were cleared out faster in tumor-free mice. Color scale: Min = $6.50e^4$; Max = $7.50e^5$. Frozen sections of lungs of **(B)** tumor-free mice and **(C)** eGFP-231 tumor-bearing mice sacrificed 10 days after Fluc-tdT-MSC infusion were stained with anti-eGFP (green) and anti-Fluc (red) antibodies. MSC was observed to home to tumor niche. Scale bar: 50 μm. **(D)** Fluc activity measured at different time points was quantified and normalized to the time point of 2 hours. Error bar: mean ± SEM. * $P < 0.05$. $n = 4$ in each group.

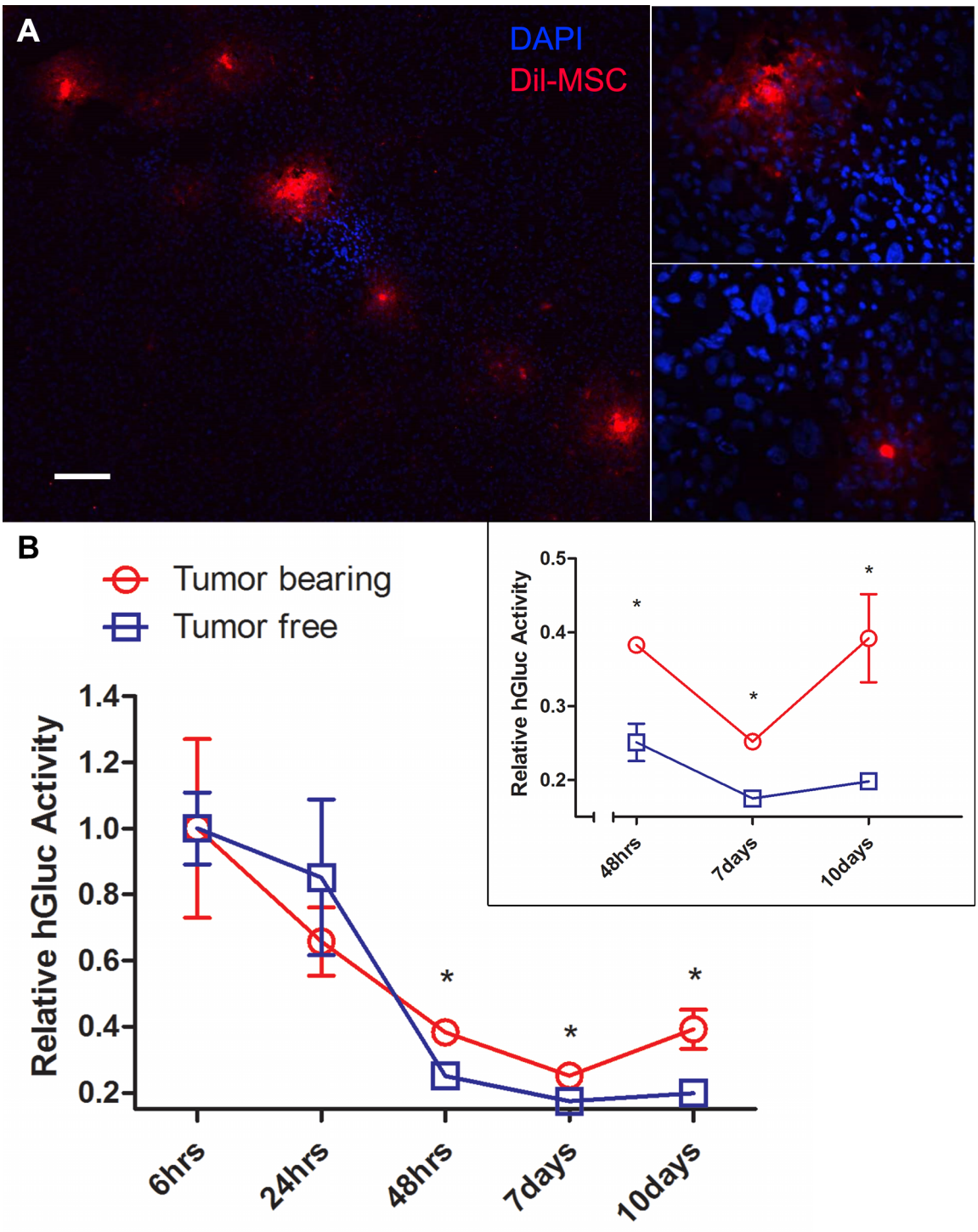

Figure 2.5. ***Gaussia*** **luciferase (hGluc) is active in murine blood and the signal is elevated in tumor-bearing mice. (A)** Frozen sections of lungs of tumor-bearing mice sacrificed 10 days after Dil-labeled hGluc-MSC administration were stained with DAPI and then imaged by fluorescence microscopy. MSCs (red) were observed to home to tumor niche (dense blue). Scale bar: 100 μm. **(B)** 5 weeks after Fluc-tdT-231 were seeded *i.v.* into NSG mice, 10^6 (*continued*)

(*continued*) hGluc-MSC were administered systemically into both tumor-free and tumor-bearing mice. Then murine blood was harvested and hGluc activity was measured at different time points (6 hours, 24 hours, 7 days and 10 days after MSC infusion) with IVIS Lumina immediately after substrate was added. hGluc activity measured at different time points was quantified and normalized to the time point of 6 hours. The inset graph shows that the hGluc activity in blood between tumor-bearing and tumor-free mice are significant from 48 hours after MSC infusion. Error bar: mean ± SEM. * P <0.05. Exposure time = 30 seconds. n = 4 in each group.

In order to investigate any differences in MSC homing between cancer-bearing and healthy mice, 10^6 Fluc-tdT-MSC were systemically infused into mice with or without breast cancer. Mice were anesthetized and *in vivo* Fluc activity was measured after *i.p.* administration of D-luciferin substrate into mice at the indicated time points. *In vivo* imaging demonstrated that MSCs were detectable in tumor-bearing mice for as long as 10 days after systemic administration (Figure 2.4A). *Ex vivo* immunohistochemistry data confirmed that engineered MSC homed to the tumor niche *in vivo* (Figure 2.4C, 2.5A). As we hypothesized, engineered MSC persisted significantly longer in tumor-bearing lungs, especially at later time points (Figure 2.4A), consistent with several previous studies performed on different cancer models [17, 21, 38]. We then quantified the Fluc signal and found that significant differences between tumor-bearing and tumor-free mice emerged 24 hours after MSC infusion and lasted until 10 days after infusion (Figure 2.4D, n = 4, P < 0.05). In order to test if MSC tumor tropism is cancer-type independent, we infused Fluc-tdT-MSC into mice with lung metastasis of colon cancer. Similar results were observed, showing tumor homing ability of MSC is independent from the type of cancer (Figure 2.S3). These results revealed that engineered MSC could home to and stay in tumor-bearing lungs for a significantly longer time compared to tumor-free lungs. Therefore, the *in vivo* persistence of engineered MSC in tumor-bearing compared to healthy animals may provide a viable "marker" for broad cancer detection.

2.3.3 hGluc secreted by engineered MSC can be assayed in the blood of tumor-bearing mice

We next investigated whether MSCs that were engineered to express hGluc can be used to detect metastasis of breast cancer to the lungs. hGluc was chosen as the reporter in this study because of its high sensitivity, lack of nonspecific cross-reactivity to other substrates (*e.g.*, Figure 2.S1), and linear signal over a wide concentration range (Figure 2.2B). In addition, hGluc has a short half-life *in vivo* (20 minutes), allowing for repeated real-time testing without undesirable excessive signal accumulation, but a long half-life *in vitro* (6 days), allowing for convenient sample storage [32]. As hGluc is secreted, it cannot be used as a marker to co-localize MSC and tumor as seen in Figure 2.C for intracellular Fluc. Therefore, in this set of experiments, we stained hGluc-MSC with the Dil lipophilic dye before they were infused *i.v.* into mice. Like Fluc-tdT-MSC, Dil-MSC were detectable in the tumor niche up to 10 days post-infusion (Figure 2.5A). Mouse blood was collected at the indicated time points and hGluc activity was measured. Although the detected signal decayed rapidly over time as expected, the difference of hGluc activity in blood between tumor-bearing and tumor-free mice was significant starting from 48 hours after MSC administration and lasting until 10 days post-infusion (Figure 2.5B), suggesting that systemically-infused hGluc-MSC can be used for the potential development of a simple blood assay for cancer detection in this murine model. In summary, this set of data supports the feasibility of using engineered MSC with secreted hGluc as a blood test for the presence of cancer.

2.4 DISCUSSION

Early detection of cancer, and especially metastasis, is a necessary and often critical first

step to effectively treat and eradiate cancer. Traditional imaging tools and molecular biomarker-based assays are typically complex, expensive and/or invasive for routine screening for most cancers; most importantly, they frequently do not possess the sensitivity and specificity to identity heterogeneous cancers at early-stages. In our study, we developed a stem cell-based detection system that can detect cancer, including metastases, by collecting small amounts of blood with a minimally invasive procedure. Our engineered MSC could home to tumor sites and persist there for significantly longer durations compared to healthy mice. The signal derived from engineered stem cells lasted longer compared to current imaging tracers [5] and no repeat administration was needed. With one single administration, the presence of tumor could be monitored continuously through a prolonged period of time, making MSC a convenient tool for real-time cancer detection. Compared to acellular systems (*e.g.*, antibodies and nanoparticles), the natural interactions between MSC and tumor involve complex adaptive sensing and responding systems that enable more efficient and specific reporting of cancer and metastases. This intrinsic biological property of tumor homing therefore potentially allows our stem cell approach to "universally" identify many cancers regardless of their origins, types and anatomical sites. In addition, stem cell-based probe delivery also circumvents many hurdles associated with passive delivery (*i.e.*, by direct administration or polymeric nanoparticles via the EPR effect), including penetrating the endothelium and the increased pressure associated with tumors. Therefore, our simple, noninvasive stem cell-based blood test might be useful for routine cancer screening, detecting small tumors and metastases, and monitoring cancer progression and recurrence during the course of treatment.

Since MSCs possess not only tumor tropism but also tropism for bone marrow and sites of inflammation and injury [19, 22], it remains important to distinguish those conditions from cancer

when using MSC-based methods to detect cancer. In addition, given high cancer heterogeneity, our next generation systems aim to engineer MSC with activatable, cancer type-specific probes to further increase the assay specificity. The long-term goal is to establish a panel of tests that can effectively discriminate between cancer (sub)types and stages and distinguish between cancer and other disorders that share similar symptoms, including inflammation and injury.

MSCs were chosen in our current (first generation) system because they can be easily obtained from multiple adult tissues [39], including bone marrow and fat, therefore avoiding ethical concerns. MSCs are also relatively easy to expand in culture, and can be readily engineered to express functional therapeutics or reporters [13, 22]. Importantly, the clinically-approved Prochymal® and hundreds of other ongoing clinical trials have demonstrated that allogeneic MSC are generally safe for use in the human without harsh immunosuppressive regimens. Nonetheless, as MSCs may themselves participate in cancer progression or regression, [21] further considerations are required. The interactions between MSC and cancer remain incompletely understood [13, 21], with different reports indicating conflicting findings from endogenous and exogenous MSC on cancer progression [21, 40, 41]. Thus, safety tests and optimizations will likely be required to better control the fate of our engineered MSCs after cancer detection though no obvious MSC-derived cancer enhancement was observed within our detection window (Figure 2.S4). To mitigate this potential issue, for example, a suicide gene [42] can be engineered into our MSC-based system so that after completion of the cancer detection test, the remaining engineered MSCs can be eliminated using exogenously administered drugs. Also, our system may be used as companion diagnostics combined with other treatments, for example, identifying certain patients and monitoring side effects. Finally, our cell-based blood assay may represent a new platform for monitoring the fate and functions of transplanted cells as well as for assessing

the *in vivo* microenvironment where they reside.

We demonstrate for the first time, to the best of our knowledge, a simple blood test for cancer detection. This test is based on the premise of exploiting the natural tumor-homing ability of MSC to further engineer them to express a secreted luciferase with optimal biocompatibility and kinetic parameters. Similar to our current murine studies, these "reporter MSCs" could be developed to identify the presence of small tumors or metastases in humans that would otherwise be undetectable by existing imaging modalities. We hope this simple, "off the shelf" allogeneic stem cell-based diagnostic test can be used to screen, detect and monitor cancer on a routine basis.

2.5 MATERIALS AND METHODS

Cell Lines and Cell Culture

Human bone marrow MSCs were obtained from the Texas A&M Health Science Center and were expanded to within passages 3-6. The cells were routinely maintained in Minimum Essential Medium α (MEM α, Life Technologies) supplemented with 15% fetal bovine serum (FBS, Atlanta Biologicals, GA) and 1% Penicillin-Streptomycin (PenStrep, 100 U/ml, Life Technologies) at 37°C in a humidified incubator containing 5% CO_2. The human breast cancer cell line MDA-MB-231 was obtained from American Type Culture Collection (ATCC, VA). These cells were grown in Leibovitz's L-15 medium containing L-glutamine (Corning, NY), and supplemented with 10% FBS and 1 U/ml PenStrep at 37°C in a humidified incubator without CO_2. The human colon cancer cell line LoVo was obtained from ATCC. These cells were grown in Kaighn's Modification of Ham's F-12 Medium (F-12K, ATCC), and supplemented with 10% FBS and 1 U/ml PenStrep at 37°C in a humidified incubator with 5% CO_2. The 293T-LV cell line (Gen Target, CA) was cultured in Dulbecco's Modified Eagle Medium (DMEM, Life

Technologies) supplemented with 15% FBS, Non-Essential Amino Acid (NEAA, 1X, 100 U/ml, Life Technologies) and 1 U/ml PenStrep at 37°C in a humidified incubator containing 5% CO_2.

Generation of Lentiviral Vectors

The following lentiviral vectors were used in this study: LV-eGFP, LV-Fluc-tdT and LV-hGluc. The sequences of interest from pUCBB-eGFP (Addgene #32548), pcDNA3.1(+)/Luc2=tdT (Addgene #32904) and pSV40-Gluc (New England BioLabs) were cloned into the promoterless lentiviral transfer vector LV-PL4 (GenTarget, CA).

Lentiviral Transduction

All lentiviral constructs were packaged (pMD2.G, Addgene #12259; pRSV-Rev, Addgene #12253; pMDLg/pRRE, Addgene #12251) as lentiviral (LV) vectors in 293T-LV cells [43] using Lipofectamine® LTX and PLUS™ Reagents (Life Technologies). MSCs and breast cancer cells were transduced with LVs by incubating virions in a culture medium containing 100 μg/ml protamine sulfate (Sigma). After selection with medium containing 10 μg/ml Puromycin (MP Biomedicals, CA), cells were visualized for fluorescent protein expression using fluorescence microscopy.

In Vitro Bioluminescence Assays

LV-Fluc-tdT MSCs (Fluc-tdT-MSC) expressing firefly luciferase (Fluc), or LV-hGluc MSCs (hGluc-MSC) expressing humanized *Gaussia* luciferase (hGluc) were seeded in serially diluted concentrations. After the cells were washed with PBS (Lonza), luciferase substrates (150 μg/ml D-luciferin for Fluc, Perkin Elmer, MA or 20 μM coelenterazine (CTZ) for hGluc, NanoLight Technologies, AZ) were added and the activities of Fluc and hGluc were then imaged as previously described [32]. Conditioned medium (CM) of hGluc-MSC was harvested and filtered.

5 µl CM was then mixed with human serum (Atlanta Biologicals, GA) with or without PBS dilution to final serum concentrations of 0%, 5%, 50% or 100%, incubated at 37°C at various times as indicated and hGluc activity was measured with 20 µM CTZ (final concentration in a final volume of 200 µl). Mouse blood was collected as described [44] and added into ¼ volume of EDTA (Sigma) solution (50 mM, pH = 8.0). 5 µl blood was mixed with 100 µl of 100 µM CTZ and hGluc activity was measured immediately. All bioluminescent assays were performed with an IVIS Lumina (Caliper LifeSciences, MA) or a plate reader (BioTek, VT). All samples above were measured in triplicate.

Cell Implantation and Imaging in Vivo

$0.5x10^6$ ($2.5x10^6$/ml in DPBS) LV-Fluc-tdT MDA-MB-231 (Fluc-tdT-231) or LV-eGFP MDA-MB-231 (eGFP-231) breast cancer cells or LoVo colon cancer cells were implanted intravenously (*i.v.*) into NOD-SCID gamma (NSG) mice (5 weeks, #005557, The Jackson Laboratory). 5 weeks later, *in vivo* Fluc activity from Fluc-tdT-231 cells was measured as described [45]. Briefly, *in vivo* Fluc signal was imaged with IVIS Lumina 10 minutes after intraperitoneal (*i.p.*) injection of D-luciferin (150mg/kg in DPBS, Lonza) into mice. 10^6 hGluc-MSC or Fluc-tdT-MSC ($5x10^6$/ml in DPBS) were systemically infused into the mice harboring of breast cancer cells and into healthy control mice. hGluc-MSC were labeled with the Dil lipophilic dye (5 µl/10^6 cells, Life Technologies) by incubation at 37°C for 20 minutes before infusion. Mice were anesthetized with 2~3% of isoflurane (Western Medical Supply, CA) and *in vivo* Fluc activity was measured at the indicated time points. Imaging was performed with the IVIS Lumina (n = 4 in each case). All animal experiments and procedures were performed after the approval from the University of California-Irvine (UCI) Institution of Animal Care and Use

Committee (IACUC protocol number 2012-3062) and conducted according to the Animal Welfare Assurance (#A3416.01).

Tissue Processing and Immunohistochemistry

Tissues were collected and flash frozen in Tissue-Tek® O.C.T™ Compound (Sakura Finetek, CA), with or without overnight fixation in 4% paraformaldehyde (Amresco, OH), and with overnight incubation in 30% sucrose solution (Amresco, OH). Sections 8µm thick were taken by cryostat and stained following an immunohistochemistry protocol for eGFP (sheep polyclonal IgG, Pierce Biotechnology) and Fluc (rabbit polyclonal IgG, Abcam). Briefly, slides were fixed in acetone (Thermo Fisher Scientific) at -20°C for 10 minutes, permeabilized in 0.1% Triton X-100 (Sigma) for 10 minutes, and blocked in 0.1% Triton X-100 with 5% normal donkey serum (Sigma) for 30 minutes. Primary antibodies were diluted 1:100 from the stock solution in 0.05% Tween-20 in PBS and applied overnight at 4°C. Slides were washed in 1X PBS, then secondary antibodies (donkey anti-sheep IgG conjugated to Alexa Fluor® 488, donkey anti-rabbit IgG conjugated to Alexa Fluor® 594, Jackson Immunoresearch, PA) were diluted 1:500 from the stock solution in 0.05% Tween-20 in PBS and applied for 30 minutes at room temperature. TOTO-3 Iodide (2.4 µM, Life Technologies) was added to the secondary antibody incubation. DAPI (50 µg/ml, Life Technologies) in PBS was applied to slides for 10 minutes before mounting. Slides were washed in PBS and mounted with DPX (Sigma) or Fluoromount-G (Southern Biotech, AL).

Statistical Analysis

Data were analyzed by Student's *t* test when comparing 2 groups and by ANOVA when comparing more than 2 groups. Data were expressed as mean ± SD or mean ± SEM, and differences were considered significant at $P < 0.05$.

2.6 ACKNOWLEDGMENTS

This work was supported by the National Institutes of Health (1DP2CA195763-01) and in part by the American Heart Association (13BGIA17140099). S.X.Z. was supported by Cardiovascular Applied Research and Entrepreneurship (CARE) fellowship (NIH/NHLBI T32). W.L. was supported by the California Institute for Regenerative Medicine (CIRM) fellowship (TG2-01152) and G.P. was supported by CIRM training grant (TB1-01182).

2.7 AUTHOR CONTRIBUTIONS

L.L. designed the study, carried out the *in vitro* and *in vivo* experiments, processed tissues, analyzed data, interpreted the results, and drafted the manuscript. S.X.Z. processed tissues, analyzed data, prepared figures and drafted the manuscript. R.A. carried out the *in vitro* bioluminescence assay and analyzed data. W.L. carried out the *in vivo* experiments and analyzed the data. M.L. prepared the figures and participated in drafting the manuscript. G.P. participated in the *in vivo* imaging, processed tissues and analyzed the data. E.J.P. participated in designing the study and edited the manuscript. W.Z. was responsible for conception and design of the research, interpreted the results, and revised the manuscript.

2.8 SUPPLEMENTAL MATERIAL

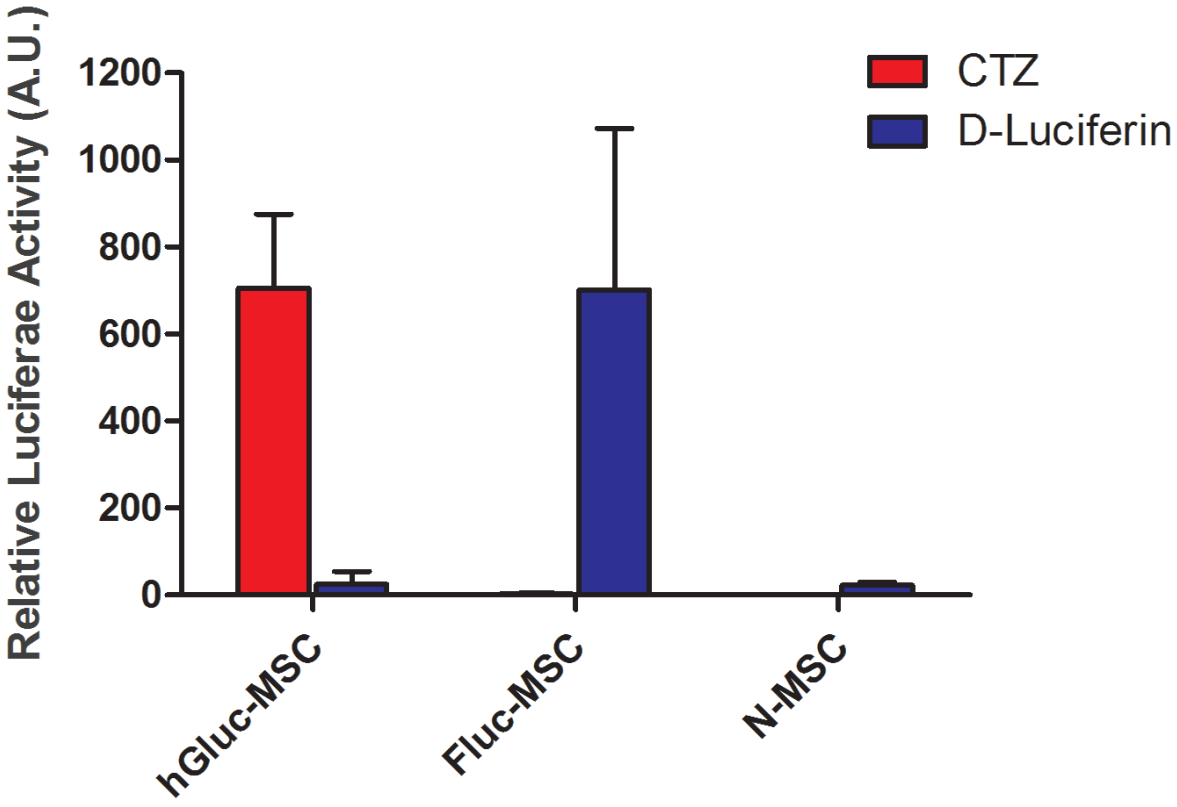

Figure 2.S1. Firefly and humanized *Gaussia* luciferases are substrate-specific and not cross-reactive. hGluc-MSC, Fluc-tdT-MSC (Fluc-MSC) and N-MSC were seeded in 96-well plate. The firefly luciferase substrate D-luciferin (final concentration = 150 µg/ml) or the humanized *Gaussia* luciferase substrate CTZ (final concentration = 20 µM) was added and luciferase activity was measured with a plate reader. Error bar: mean ± SD. Exposure time = 2s.

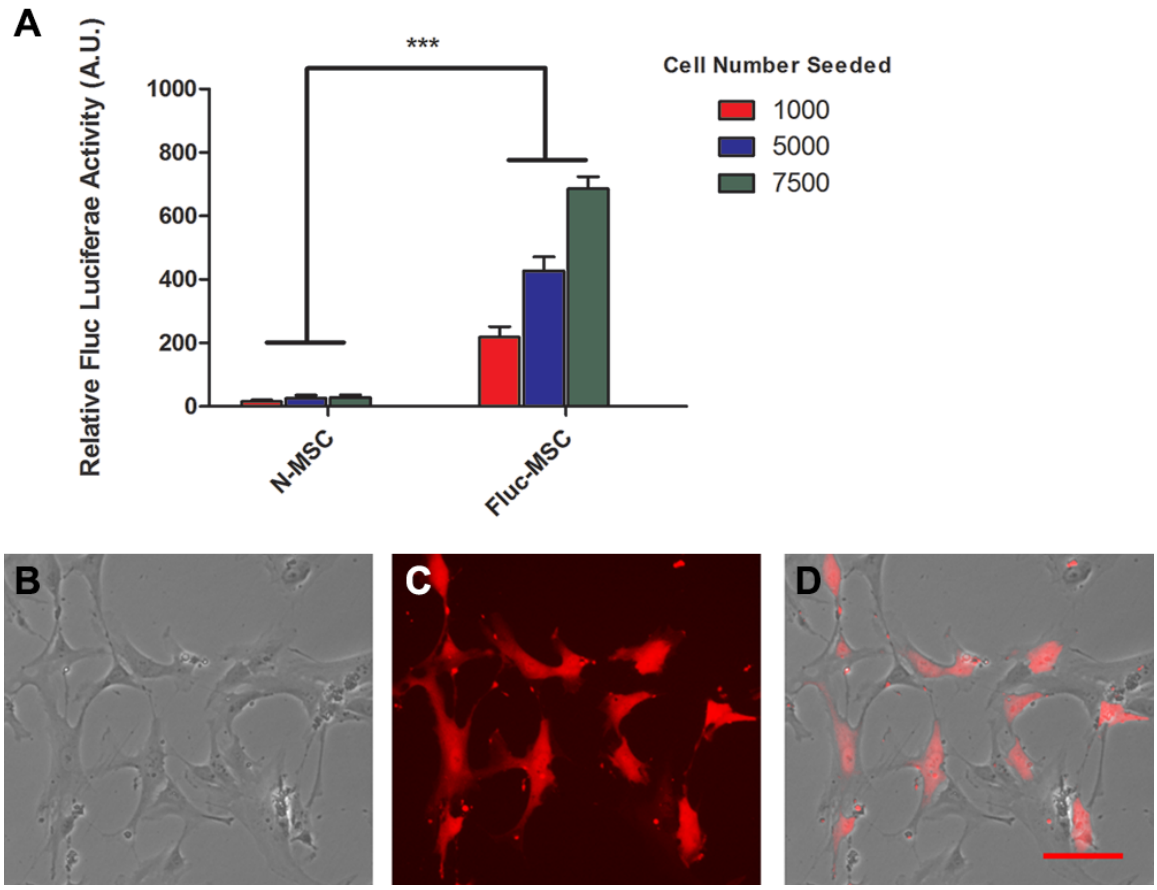

Figure 2.S2. Engineered mesenchymal stem cells (Fluc-tdT-MSC) express firefly luciferase (Fluc) and red fluorescent protein (tdT). (A) Fluc-tdT-MSC (Fluc-MSC) were seeded onto 96-well plate and 24 hours later D-luciferin was added at a final concentration of 150 µg/ml. Fluc activity was measured with a plate reader. Error bar: mean ± SD. Exposure time = 2s. *** P <0.001. **(B-D)** Fluc-tdT-MSC were imaged by fluorescence microcopy 24 hours after seeding. Scale bar: 50 µm.

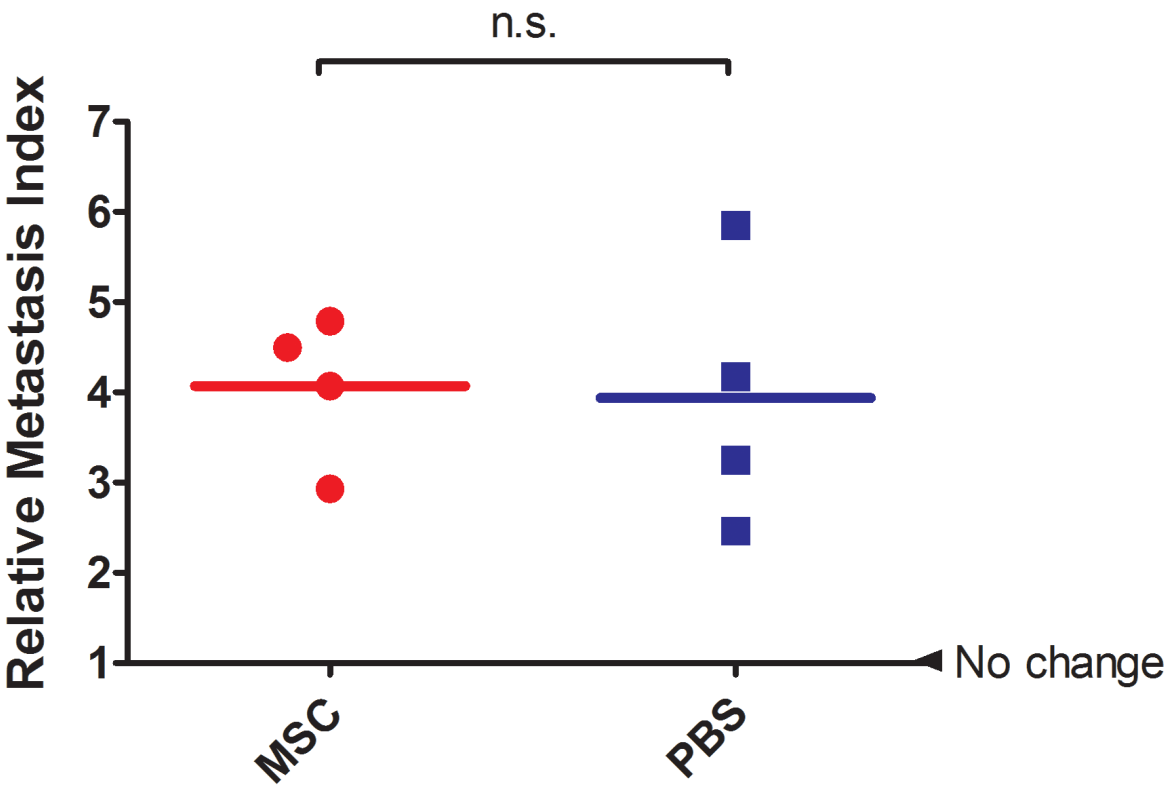

Figure 2.S3. Engineered mesenchymal stem cells (hGluc-MSC) infusion does not promote cancer metastasis *in vivo*. 5 weeks after Fluc-tdT-231 were seeded *i.v.* into NSG mice, 10^6 hGluc-MSC or PBS were administered systemically into tumor-bearing mice (Day 0). *In vivo* Fluc activity was measured with IVIS Lumina 10 minutes after substrate administration before (Day 0) and 10 days after MSC infusion (Day 10). Exposure time = 5 seconds. Relative Metastasis Index (RMI) = Luciferase activity on Day 10 (after) / Luciferase activity on Day 0 (before). $n = 4$ for each group. n.s. = not significant.

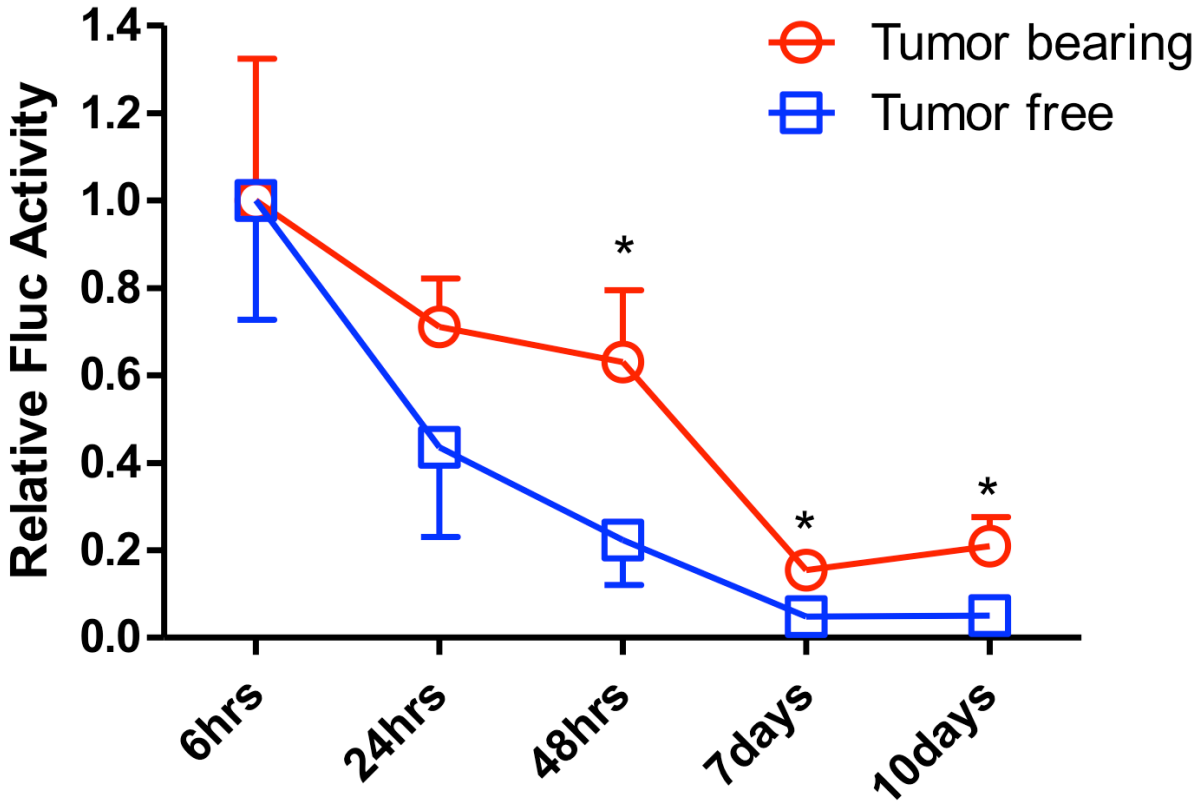

Figure 2.S4. Engineered mesenchymal stem cell (hGluc-MSC) infusion has no influence on the growth of cancer metastasis size *in vivo*. Five weeks after Fluc-tdT-231 were seeded intravenously into NSG mice, 10^6 hGluc-MSCs or PBS was administered systemically into tumor-bearing mice (day 0). *In vivo* Fluc activity was measured with IVIS Lumina 10 minutes after substrate administration before (day 0) and 10 days after MSC infusion (day 10). Exposure time = 5 s. Relative metastasis index (RMI) = Luciferase activity on day 10 (after) / Luciferase activity on day 0 (before). $n = 4$ for each group.

2.9 REFERENCES

1. Hanahan, D. & Weinberg, R.A. Hallmarks of cancer: the next generation. *Cell* **144**, 646-674 (2011).
2. Hussain, T. & Nguyen, Q.T. Molecular imaging for cancer diagnosis and surgery. *Advanced drug delivery reviews* **66**, 90-100 (2014).
3. Hedley, B.D. & Chambers, A.F. Tumor dormancy and metastasis. *Advances in cancer research* **102**, 67-101 (2009).
4. Mehlen, P. & Puisieux, A. Metastasis: a question of life or death. *Nature reviews. Cancer* **6**, 449-458 (2006).
5. Kapoor, V., McCook, B.M. & Torok, F.S. An introduction to PET-CT imaging. *Radiographics : a review publication of the Radiological Society of North America, Inc* **24**, 523-543 (2004).
6. Schick, F. Whole-body MRI at high field: technical limits and clinical potential. *European radiology* **15**, 946-959 (2005).
7. Buchberger, W., Niehoff, A., Obrist, P., DeKoekkoek-Doll, P. & Dunser, M. Clinically and mammographically occult breast lesions: detection and classification with high-resolution sonography. *Seminars in ultrasound, CT, and MR* **21**, 325-336 (2000).
8. Warren, A.D. et al. Disease detection by ultrasensitive quantification of microdosed synthetic urinary biomarkers. *Journal of the American Chemical Society* **136**, 13709-13714 (2014).
9. Kwong, G.A. et al. Mass-encoded synthetic biomarkers for multiplexed urinary monitoring of disease. *Nature biotechnology* **31**, 63-70 (2013).
10. Hanash, S.M., Baik, C.S. & Kallioniemi, O. Emerging molecular biomarkers--blood-based strategies to detect and monitor cancer. *Nature reviews. Clinical oncology* **8**, 142-150 (2011).
11. Schroder, F.H. et al. Prostate-cancer mortality at 11 years of follow-up. *The New England journal of medicine* **366**, 981-990 (2012).
12. Tomasetti, C. & Vogelstein, B. Cancer etiology. Variation in cancer risk among tissues can be explained by the number of stem cell divisions. *Science* **347**, 78-81 (2015).
13. Ankrum, J. & Karp, J.M. Mesenchymal stem cell therapy: Two steps forward, one step back. *Trends in molecular medicine* **16**, 203-209 (2010).
14. Shah, K. Mesenchymal stem cells engineered for cancer therapy. *Adv Drug Deliv Rev* **64**, 739-748 (2012).
15. Loebinger, M.R. & Janes, S.M. Stem cells as vectors for antitumour therapy. *Thorax* **65**, 362-369 (2010).
16. Studeny, M. et al. Mesenchymal stem cells: potential precursors for tumor stroma and targeted-delivery vehicles for anticancer agents. *Journal of the National Cancer Institute* **96**, 1593-1603 (2004).
17. Kidd, S. et al. Direct evidence of mesenchymal stem cell tropism for tumor and wounding microenvironments using in vivo bioluminescent imaging. *Stem Cells* **27**, 2614-2623 (2009).
18. Reagan, M.R. & Kaplan, D.L. Concise review: Mesenchymal stem cell tumor-homing: detection methods in disease model systems. *Stem Cells* **29**, 920-927 (2011).
19. Zhao, W., Phinney, D.G., Bonnet, D., Dominici, M. & Krampera, M. Mesenchymal stem cell biodistribution, migration, and homing in vivo. *Stem cells international* **2014**, 292109 (2014).
20. Ankrum, J.A., Ong, J.F. & Karp, J.M. Mesenchymal stem cells: immune evasive, not immune privileged. *Nature biotechnology* **32**, 252-260 (2014).
21. Droujinine, I.A., Eckert, M.A. & Zhao, W. To grab the stroma by the horns: from biology to cancer therapy with mesenchymal stem cells. *Oncotarget* **4**, 651-664 (2013).
22. Karp, J.M. & Leng Teo, G.S. Mesenchymal stem cell homing: the devil is in the details. *Cell stem cell* **4**, 206-216 (2009).
23. Bexell, D., Scheding, S. & Bengzon, J. Toward brain tumor gene therapy using multipotent mesenchymal stromal cell vectors. *Molecular therapy : the journal of the American Society of Gene Therapy* **18**, 1067-1075 (2010).
24. Phinney, D.G. & Prockop, D.J. Concise review: Mesenchymal stem/multipotent stromal cells: The state of transdifferentiation and modes of tissue repair - Current views. *Stem Cells* **25**, 2896-2902 (2007).
25. Liu, L. et al. From blood to the brain: can systemically transplanted mesenchymal stem cells cross the blood-brain barrier? *Stem cells international* **2013**, 435093 (2013).
26. Hingtgen, S.D., Kasmieh, R., van de Water, J., Weissleder, R. & Shah, K. A novel molecule integrating therapeutic and diagnostic activities reveals multiple aspects of stem cell-based therapy. *Stem Cells* **28**, 832-841 (2010).

27. Chung, E. et al. Secreted Gaussia luciferase as a biomarker for monitoring tumor progression and treatment response of systemic metastases. *PloS one* **4**, e8316 (2009).
28. Tannous, B.A. & Teng, J. Secreted blood reporters: insights and applications. *Biotechnology advances* **29**, 997-1003 (2011).
29. Bovenberg, M.S., Degeling, M.H. & Tannous, B.A. Enhanced Gaussia luciferase blood assay for monitoring of in vivo biological processes. *Analytical chemistry* **84**, 1189-1192 (2012).
30. El-Amouri, S.S., Cao, P., Miao, C. & Pan, D. Secreted luciferase for in vivo evaluation of systemic protein delivery in mice. *Molecular biotechnology* **53**, 63-73 (2013).
31. Tannous, B.A., Kim, D.E., Fernandez, J.L., Weissleder, R. & Breakefield, X.O. Codon-optimized Gaussia luciferase cDNA for mammalian gene expression in culture and in vivo. *Molecular therapy : the journal of the American Society of Gene Therapy* **11**, 435-443 (2005).
32. Tannous, B.A. Gaussia luciferase reporter assay for monitoring biological processes in culture and in vivo. *Nature protocols* **4**, 582-591 (2009).
33. Welsh, J.P., Patel, K.G., Manthiram, K. & Swartz, J.R. Multiply mutated Gaussia luciferases provide prolonged and intense bioluminescence. *Biochemical and biophysical research communications* **389**, 563-568 (2009).
34. Fantozzi, A. & Christofori, G. Mouse models of breast cancer metastasis. *Breast cancer research : BCR* **8**, 212 (2006).
35. Wang, C.Y. & Brown, P.H. Animal Models for Breast Cancer Prevention Research. *Genetically Engineered Mice for Cancer Research: Design, Analysis, Pathways, Validation and Pre-Clinical Testing*, 497-526 (2012).
36. Close, D.M., Xu, T., Sayler, G.S. & Ripp, S. In vivo bioluminescent imaging (BLI): noninvasive visualization and interrogation of biological processes in living animals. *Sensors (Basel)* **11**, 180-206 (2011).
37. Prescher, J.A. & Contag, C.H. Imaging Mouse Models of Human Cancer. *Genetically Engineered Mice for Cancer Research: Design, Analysis, Pathways, Validation and Pre-Clinical Testing*, 235-260 (2012).
38. Elman, J.S. et al. Pharmacokinetics of natural and engineered secreted factors delivered by mesenchymal stromal cells. *PloS one* **9**, e89882 (2014).
39. Caplan, A.I. & Correa, D. The MSC: an injury drugstore. *Cell stem cell* **9**, 11-15 (2011).
40. El-Haibi, C.P. et al. Critical role for lysyl oxidase in mesenchymal stem cell-driven breast cancer malignancy. *Proceedings of the National Academy of Sciences of the United States of America* **109**, 17460-17465 (2012).
41. Li, H.J., Reinhardt, F., Herschman, H.R. & Weinberg, R.A. Cancer-stimulated mesenchymal stem cells create a carcinoma stem cell niche via prostaglandin E2 signaling. *Cancer Discov* **2**, 840-855 (2012).
42. Aboody, K.S. et al. Neural stem cell-mediated enzyme/prodrug therapy for glioma: preclinical studies. *Science translational medicine* **5**, 184ra159 (2013).
43. Dull, T. et al. A third-generation lentivirus vector with a conditional packaging system. *Journal of virology* **72**, 8463-8471 (1998).
44. Donovan, J. & Brown, P. Blood collection. *Current protocols in neuroscience / editorial board, Jacqueline N. Crawley ... [et al.]* **Appendix 4**, Appendix 4G (2005).
45. Kong, Y. et al. Whole-body imaging of infection using bioluminescence. *Current protocols in microbiology* **Chapter 2**, Unit 2C 4 (2011).

CHAPTER 3

CONSTRUCTION OF MECHANO-RESPONSIVE CELL SYSTEM (MRCS)

Authors: **Linan Liu**[1,2,3†], Shirley X. Zhang[1,2,3†], Wenbin Liao[1,2,3], Chi W. Wong[1,2,3], Claire C. Chen[1,2], Henry P. Farhoodi[1,2], Aude I. Ségaliny[1,2,3], Jenu V. Chacko[3], Lily P. Nguyen[1,2], Mengrou Lu[1,2], George Polovin[1,2,3], Egest J. Pone[1,2,3], Timothy L. Downing[3], Devon A. Lawson[2,4], Michelle A. Digman[3,5,6], Weian Zhao[1,2,3,7]

Author Affiliations:

[1]Department of Pharmaceutical Sciences and Edwards Life sciences Center for Advanced Cardiovascular Technology, 845 Health Sciences Road, University of California-Irvine, Irvine, California, 92697, USA.

[2]Sue and Bill Gross Stem Cell Research Center and Chao Family Comprehensive Cancer Center, 845 Health Sciences Road, University of California-Irvine, Irvine, California, 92697, USA.

[3]Department of Biomedical Engineering, University of California-Irvine, Irvine, California, 92697, USA.

[4]Department of Physiology & Biophysics, University of California-Irvine, Irvine, California, 92697, USA.

[5]Laboratory for Fluorescence Dynamics, University of California-Irvine, California, 92697, USA.

[6]Centre for Bioactive Discovery in Health and Ageing, School of Science and Technology, University of New England, Armidale, New South Wales, 2351, Australia.

[7]Department of Biological Chemistry, University of California-Irvine, Irvine, California, 92697, USA.

† These authors contributed equally to this work.

3.1 ABSTRACT

It has been established that tissue mechanical properties regulate MSC fate: tissue and matrix stiffness is sufficient to drive expression of genes involved in MSC differentiation. We hypothesize that that increased matrix stiffness is a fundamental property of the metastatic niche that can be targeted with MSC-based, mechano-responsive therapies. In order to develop a new paradigm for the treatment of breast cancer metastases by targeting the mechano-environment of the metastatic niche, we have constructed mechanosensitive-promoter-driven, MSC-based vectors, as known as mechano-responsive cell system (MRCS). We have successfully established the MRCS expressing reporters (e.g., eGFP and firefly luciferase) that selectively respond to stiff substrates (E > 10 kPa) *in vitro*. Our approach to treating metastases has the potential to not only reduce the deleterious effects of systemic chemotherapy, but also more effectively treat metastatic breast cancer with the overall goal of elimination of metastases.

Keywords: mechano-sensing, stiffness, mesenchymal stem cell, YAP/TAZ

3.2 INTRODUCTION

Multiple recent publications have established that tissue and matrix stiffness is sufficient to drive expression of genes involved in mesenchymal stem cell (MSC) differentiation[1-5]. Specifically, under compliant matrix stiffness (Young's modulus of less than 1 kPa), MSCs assume a neurogenic differentiation profile. At progressively higher matrix stiffness (5 to 75 kPa), MSCs differentiate to myogenic and osteogenic fates (Figure 1.2)[1-5]. Importantly, the range of stiffness to which MSCs respond encompasses those found in normal breast and lung tissues (less than 1 kPa), as well as invasive cancers (10-15 fold higher stiffness)[6-8]. MSC differentiation is inherently a transcriptional program with each lineage defined by expression of characteristic transcription factors. This therefore allows us to use promoters regulating genes involved in MSC differentiation to drive expression of matrix stiffness-responsive reporters or therapeutics. Supporting our hypothesis that MSCs can specifically respond to differences in tissue stiffness at the metastatic niche is the observation that MSCs injected intravenously in a mouse model of cancer specifically assumed an osteogenic differentiation profile in the metastatic lung but not in the normal lung[9-11].

We hypothesize that the promoters of genes upregulated in response to specific ranges of matrix stiffness capture and synthesize the regulatory inputs responsive to discrete ranges of stiffness. Using these promoters to drive expression of a reporter or therapeutic therefore allows us to create a mechano-responsive cell system (MRCS) (Figure 3.1) that responds to ranges of matrix stiffness found in the metastatic niche.

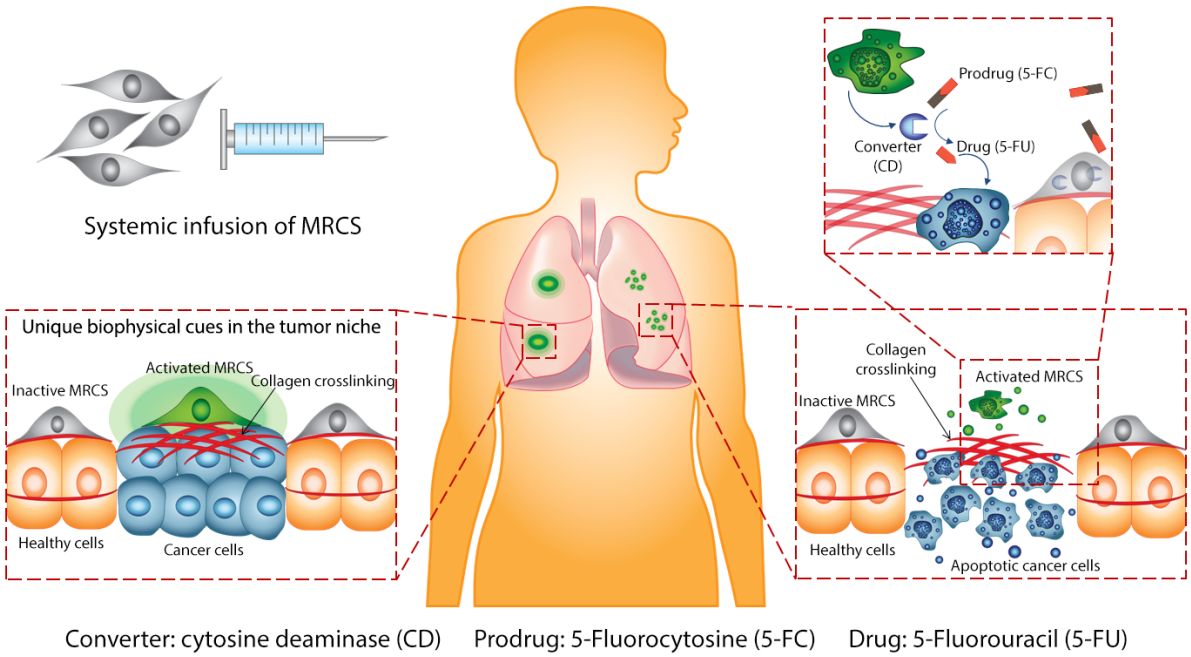

Figure 3.1. The concept of mechano-responsive cell system (MRCS) for targeting breast cancer metastases in the lung. The tumor-homing MRCS are locally activated by specific ranges of stiffness linked to collagen crosslinking found at the metastatic niche (red crosshatching) thereby expressing or secreting reporters and therapeutics (Left side), and selectively treating cancer metastases using converter enzyme cytosine deaminase (CD) and prodrug 5-Fluoroucytosine (5-FC) (right side).

3.3 RESULTS

Existing literature has established that matrix stiffness is sufficient to direct MSC differentiation, with genes being regulated in response to a range of matrix stiffness[1-5]. We took advantage of the endogenous ability of MSCs to respond to matrix stiffness to drive expression of reporters with stiffness-responsive promoters.

3.3.1 Cloning of the matrix stiffness-responsive promoters

Engler *et al*. have previously performed microarray analysis of MSCs exposed to different ranges of matrix stiffness to define genes specifically expressed under each set of conditions[1]. We used this data as a starting point to design the MRCS to respond to matrix

stiffness inputs. This includes cloning the approximately 3.0 kBp promoters of the *TUBB3* (β3-tubulin, neurogenic lineage), *MYOD1* (MyoD, myogenic lineage), and *RUNX2* (RunX2 or CBFα1, osteogenic lineage) gene promoters from human genomic DNA with PCR. These promoters then were sub-cloned into a promoterless vector to drive expression of a destabilized version of green fluorescent protein (GFPd) (Figure 3.S1). GFPd has a half-life of 60-90 minutes, allowing near-real time imaging of promoter activity. We have successfully cloned these promoters from human genomic DNA (data not shown). *TUBB3* is induced at stiffness of less than one 1 kPa, *MYOD1* is strongly expressed within the range of 9-25 kPa, and *RUNX2* at stiffness greater than 25 kPa[1, 7, 12].

Moreover, to create a MRCS that responds to a physiological range of stiffness found in the metastatic niche of the lungs, we engineered MRCS with a Yes-associated protein (YAP) / transcriptional coactivator with PDZ-binding motif (TAZ, also known as WWTR1) synthetic promoter (see Methods). When activated, YAP/TAZ drives the expression of downstream reporters including enhanced green fluorescent protein (eGFP) (MRCS-eGFP) for *in vitro* imaging or firefly luciferase (MRCS-Luc) for later *in vivo* imaging. YAP/TAZ can also drive expression of anti-tumor agents (*i.e.*, MRCS-CD) (Figure 3.2A and 3.S1). YAP/TAZ have previously been reported as sensors and mediators of mechanical cues via, for instance, cytoskeleton and Rho GTPase[13, 14]. On soft substrates *in vitro* (< 1 kPa), YAP remain inactivated in the cytoplasm, but on stiff substrates *in vitr*o (> 10 kPa), YAP localize to the nucleus and become activated as transcriptional factors[13, 14]. Importantly, YAP/TAZ have also been reported to be key upstream factors that regulate lineage-specific transcription factors (including Runt-related transcription factor 2 (*RUNX2*), an osteogenic marker) and drive MSC differentiation including osteogenesis[15]. YAP/TAZ is regulated by biophysical cues via nuclear localization thus

affecting their function as transcriptional factors[13, 14]. In effect, YAP/TAZ serve as an on/off switch for the MRCS gene expression triggered by the substrate stiffness in our study (Figure 3.2).

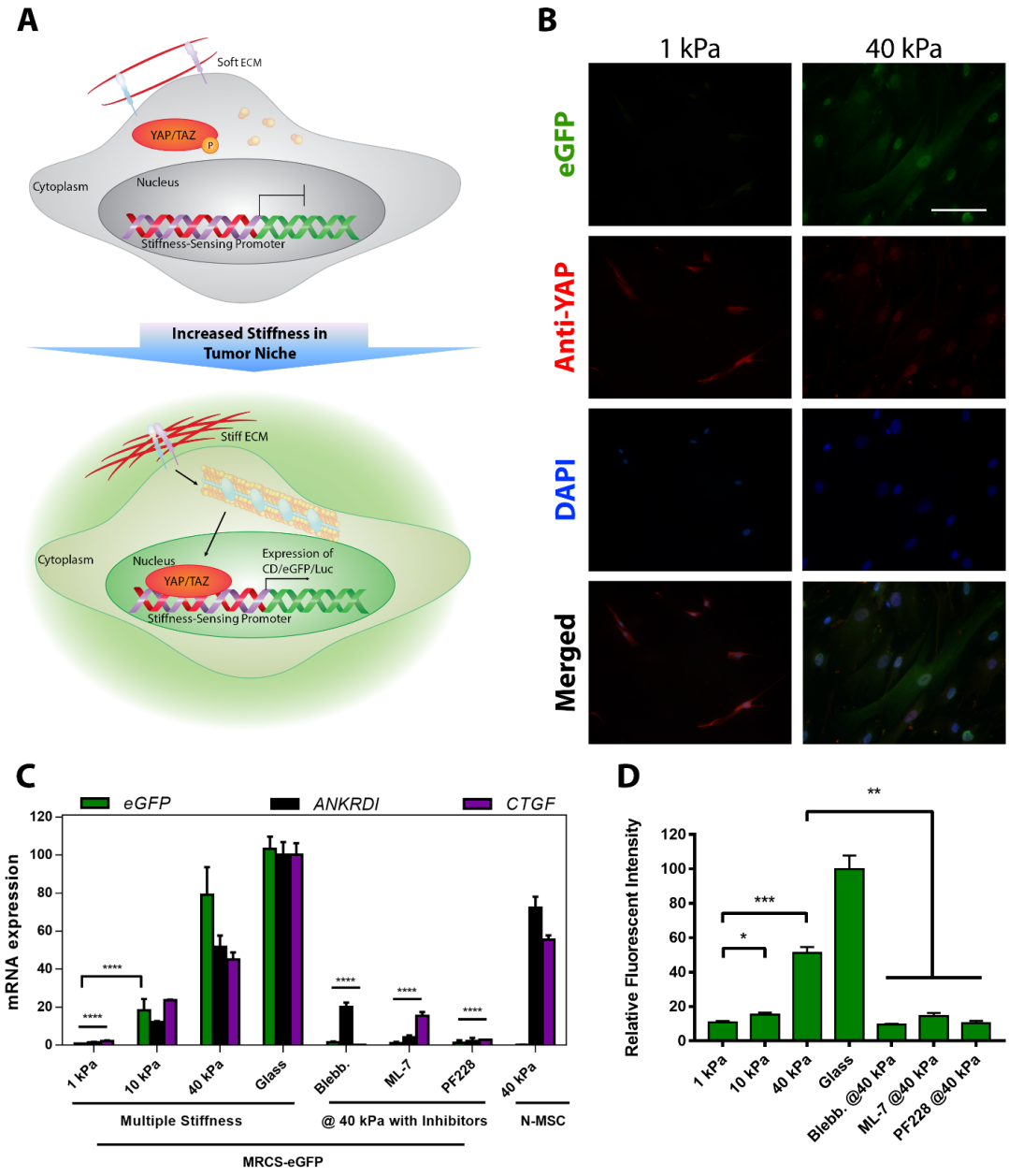

Figure 3.2. Mechano-responsive cell system (MRCS) *in vitro* validation. (**A**) The schematic of a proposed mechanism of how MRCS works. When the stiffness of extracellular matrix (ECM) increases, YAP/TAZ will be activated and relocalized into nucleus. Then YAP/TAZ can be bound to the synthetic stiffness-sensing promoter in MRCS and drive (*continued*)

(*continued*) the expression of the downstream reporters (e.g., eGFP and luciferase (Luc)) and/or therapeutics (e.g., cytosine deaminiase (CD)). *Note*: This schematic is simplified to clarify the major components in MRCS mechanism. (**B**) Representative images of MRCS-eGFP plated on soft (~ 1 kPa) and firm (~ 40 kPa) polyacrylamide gels. eGFP (green) was turned on responding to higher stiffness. YAP (red) relocalization is also regulated by stiffness, *i.e.*, concentrated in nuclei on stiffer substrates. Scale bar = 100 μm. (**C**) Quantitative reverse-transcriptase-PCR (RT qPCR) analysis of MRCS-eGFP on hydrogels. Expression of eGFP (green) and YAP/TAZ downstream factors (*CTGF*, purple and *ANKRDI*, black) was increased on stiff substrate and was downregulated on soft substrate or with mechanosenisng inhibitors, showing that MRCS is stiffness specific. Error bar: mean ± S.D.. (**D**) Quantification of fluorescent intensity of eGFP (stained with antibody) from MRCS-eGFP seeded on different stiffness or on firm (~ 40 kPa) substrates treated with 10 μM ML-7 (myosin light-chain kinase inhibitors) or 20 μM PF228 (focal adhesion kinase inhibitor), respectively, suggests that MRCS sensing is reversibly stiffness-dependent. **P* < 0.05, ***P* < 0.01 and ****P* < 0.001. Error bar: mean ± S.E.M..

For all experiments, we utilize human bone marrow MSCs from the Texas A&M Health Science Center (passage 3-6). For transduction of constructs, we use lenti-viral transduction, which results in permanent and robust transfection of MSCs with minimal toxicity (Figure 3.S1). We have found culture of the constructed MRCS on tissue culture plastic does not lead to aberrant activation of promoters.

3.3.2 Validation and optimization of the MRCS *in vitro*

We have chosen *TUBB3*, *MYOD1* and *RUNX2* promoters for the initial screening process due to previous validated reports that variable levels of matrix stiffness are sufficient to induce their transcription[1, 7, 12]. We also screened multiple other gene promoters identified as regulated in response to matrix stiffness to ensure coverage of the entire range of physiological stiffness (including neurogenic: *TUBB4*, *GDNF*, and *STAT3*; myogenic: *MYOG*, *PAX7*, and *MEOX2*; osteogenic: *BGLAP*, *SMAD1* and *BMP6*) as well as promoters bound to key upstream transcriptional factors of *TUBB3*, *MYOD1* and *RUNX2* (YAP/TAZ, for example).

To validate the mechano-sensing property of our MRCS in response to a physiological range of stiffness that were observed in lung metastases, cells were seeded on tunable

polyacrylamide hydrogels with various stiffness (~ 1 kPa, ~ 10 kPa and ~ 40 kPa) found in normal and transformed tissues.[1, 13] Lineage has been verified by morphological characterization (Figure 3.S2) and staining for markers (data not shown) of neurogenic, myogenic and osteogenic differentiation (including NeuN, myogenin, and osteocalcin, respectively)[16, 17]. We have found that on soft substrate (~1kPa), MSCs are rounded like neurogenic or adipogenic cells while on stiff substrates MSCs are more stretched out, render a spindle (~10kPa) or polygon (> 40kPa)-like morphological change like myogenic or osteogenic cells (Figure 3.S2A-3.S2D). In previous experiments, inhibition of stiffness response in MSCs on myogenic matrices with blebbistatin for hours led to a dramatic reduction in *MYOD1* transcription that was rapidly restored upon removal of blebbistatin inhibition[1]. This strongly suggests that the transcriptional changes that occur in response to matrix stiffness are reversible and dynamic. With retroviral transduction, which results in stable and robust engineered MSCs, we have observed that the morphology of MSCs on the stiff tunable hydrogels (~40kPa) was changed to those reported on softer (<10kPa) gels with treatment with inhibitors of focal adhesion kinase (FAK) (PF228, Pfizer)[18] and myosin light chain kinase (blebbistatin and ML7, Sigma)[19], which abrogate important signaling downstream of matrix stiffness and integrin activation (Figure 3.S2E-3.S2G). It suggests that the engineered MSCs sense specifically dependent on matrix stiffness.

To confirm the selective activation of our MRCS-eGFP responding to various stiffness, MRCS-eGFP were seeded on tunable hydrogels as abovementioned. As expected, on soft hydrogel (~ 1 kPa), YAP remained in the cytoplasm, and no eGFP signal could be detected (Figure 3.2B, 3.S2A), whereas on stiffer hydrogels (> 10 kPa), YAP localized to the nuclei and eGFP was expressed, typically within 24-48 hours after cell seeding (Figure 3.2B, 3.S2B and 3.S2C). The intensity of reporter expression correlates positively with the substrate stiffness, *i.e.*,

stiffer hydrogel resulted in stronger eGFP signal. As controls, MRCS-eGFP plated on glass (the highest stiffness used) showed strong activation of YAP/TAZ and eGFP expression (Figure 3.S2D). MRCS-eGFP treated with blebbistatin, an inhibitor of mechanotransduction which impedes important signaling downstream of matrix stiffness and integrin activation,[1, 13] showed no eGFP expression and YAP remained in the cytoplasm, even on stiff substrates (Figure 3.S2E). Two other mechanotransduction inhibitors, ML-7 and PF228, a myosin light-chain kinase (MLCK) inhibitor and focal adhesion kinase (FAK) inhibitor, respectively, similarly deactivated YAP and downstream eGFP expression (Figure 3.S2F, 3.S2G). In order to acquire more robust signal and confirm the expression of eGFP, immunostaining was performed and representative images of MRCS-eGFP on hydrogels were taken. Similar results were displayed (Figure 3.2B). More importantly, the quantification of eGFP signal intensity demonstrates an over 5-fold increase when MRCS were seeded on stiff (~40kPa) gels and presents a similar expression level as on the soft (~1kPa) gel in the presence of mechano-inhibitors (Figure 3.2D). This set of data demonstrates that YAP activation in response to altered stiffness is MLCK/FAK dependent. We further characterized the expression of eGFP mRNA and two additional genes (*CTGF* and *ANKRDI*) that are transcriptionally regulated by YAP/TAZ using quantitative reverse-transcriptase PCR (RT qPCR). Consistent to the imaging data, expression of *eGFP*, *CTGF* and *ANKRDI* was specifically activated on stiffer hydrogels (Figure 3.2C). Notably, Furthermore, show a noticeable difference between the expression levels of eGFP and the other YAP-induced markers. A possible reason is that a gene's mRNA level does not predict its protein expression level[20, 21]. MRCS engineered to produce firefly luciferase (MRCS-Luc) were similarly prepared and characterized (Figure 3.3). Collectively, these data indicate that our MRCS is stiffness-

specific and can respond to a range of matrix stiffness reversibly and dynamically to drive downstream gene expression.

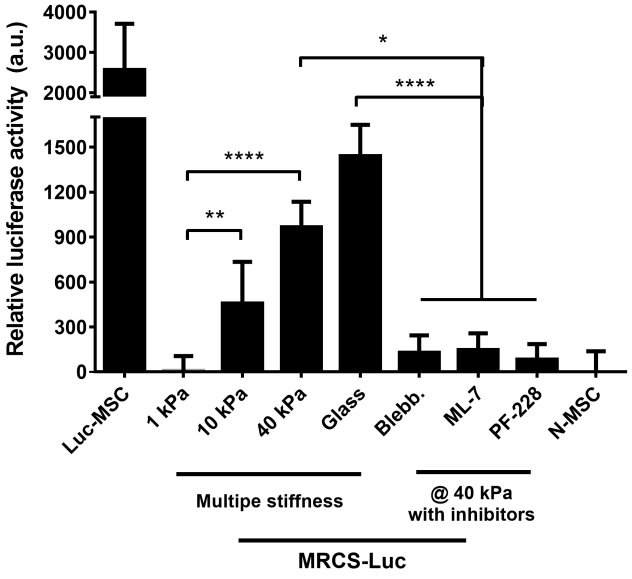

Figure 3.3. **MRCS-Luc are stiffness specific *in vitro*.** MRCS-Luc were seeded on substrates with different stiffness. It shows that luciferase activity was upregulated on stiff substrate and downregulated on soft substrate or with mechano-sensing inhibitors. *$P < 0.05$, **$P < 0.01$ and ****$P < 0.0001$. Error bar: mean ± S.D.. Luc-MSC: Constitutive positive control; N-MSC: Native MSCs.

3.4 DISCUSSION AND FUTURE DIRECTION

Therefore, we have constructed YAP/TAZ promoter into our MRCS that can be activated in response to a range of matrix stiffness and validated the ability of our promoter-based system to respond to a physiologically-relevant range of matrix stiffness. We have been optimizing these promoters to respond more specifically and more efficiently to matrix stiffness inputs.

In order to find out more minimal promoter or essential elements that can sense certain stiffness, we will further isolate fragments of, for example, *TUBB3*, *MYOD1* and *RUNX2* promoters, sub-clone them into the promoterless vector, nucleofect the constructs into MSCs and

screen them on hydrogel as abovementioned. We will also include multiple other gene promoters identified as regulated in response to matrix stiffness to ensure coverage of the entire range of physiological stiffness (including neurogenic: *TUBB4*, *GDNF*, and *STAT3*; myogenic: *MYOG*, *PAX7*, and *MEOX2*; osteogenic: *BGLAP*, *SMAD1* and *BMP6*)[1] as abovementioned.

Although previous reports suggest the proximal 3 kBp of each gene is sufficient to regulate their transcription, it is possible that response to other stimuli (such as hypoxia or inflammation) may interfere with mechano-specific activation. If it occurs, we will remove response elements to hypoxia and inflammation, such as HIF-1α and NF-KB consensus sequences, via well-established whole-plasmid site-directed mutagenesis[22, 23]. Numerous previous reports suggest that viral transduction and engineering of MSCs do not affect recruitment to primary tumors or metastases[24-26].

As one of our long-term goals is to establish an MRCS that is uniquely and specifically responsive to matrix stiffness but not to nonspecific factors (e.g., hypoxia and inflammation), we will also collaborate with Dr. Qing Nie's laboratory[27] at University of California-Irvine and perform a bioinformatics analysis to identify transcriptional stiffness response elements: sequences in the promoters of genes that respond to specific ranges of stiffness by activating or repressing transcription. The analysis will be based on existing microarray analyses of MSCs exposed to matrices of varying stiffness: by comparing the promoters of co-regulated genes with a tool such as cis-Regulatory Elements in the Mammalian Genome (cREMaG), we can identify conserved sequences in common between these genes. We anticipate that we can use these response elements to design synthetic promoters to construct stiffness "rulers" to quantitatively assess matrix stiffness by measuring transcriptional response (*i.e.*, transcription of a fluorescent

protein). We anticipate that this technique will allow us to interrogate a wider range of stiffness by measuring the relative expression level of each reporter.

3.5 MATERIALS AND METHODS

Cell lines and cell culture

Human bone marrow MSCs were obtained from the Texas A&M Health Science Center and were expanded to passages 3-6 for further use (*i.e.*, transduction, assays, injection, *etc.*). The cells were routinely maintained in Minimum Essential Medium α (MEM α, Life Technologies) supplemented with 15% fetal bovine serum (FBS, Atlanta Biologicals, GA) and 1% Penicillin-Streptomycin (PenStrep, 100 U/ml, Life Technologies) at 37°C in a humidified incubator containing 5% CO_2. The human breast cancer cell line MDA-MB-231 was obtained from American Type Culture Collection (ATCC, VA). These cells were grown in Leibovitz's L-15 medium containing L-glutamine (Corning, NY), and supplemented with 10% FBS and 1 U/ml PenStrep at 37°C in a humidified incubator without CO_2. The 293T-LV cell line (Gen Target, CA) was cultured in Dulbecco's Modified Eagle Medium (DMEM, Life Technologies) supplemented with 15% FBS, Non-Essential Amino Acid (NEAA, 1X, 100 U/ml, Life Technologies) and 1 U/ml PenStrep at 37°C in a humidified incubator containing 5% CO_2.

Generation of lentiviral vectors and lentiviral transduction

The following lentiviral vectors were used in this study: LV-*CMV*::eGFP, LV-*CMV*::Luc-RFP, LV-*CMV*::CD, LV-MRCS-eGFP, LV-MRCS-Luc and LV-MRCS-CD. The sequences of interest from pUCBB-eGFP[28] (a gift from Claudia Schmidt-dannert, Addgene #32548), pcDNA3.1(+)/Luc2=tdT (a gift from Christopher Contag[29], Addgene #32904), pSelect-zeo-*Fcy*::*Fur* (InvivoGen, CA) and 8xGTIIC-luciferase[13] (a gift from Stefano Piccolo, Addgene

#34615) were cloned into the promoterless lentiviral transfer vector LV-PL4 (GenTarget, CA). All MSCs and breast cancer cells were transduced as previously described[30]. Briefly all lentiviral constructs were packaged (gifts from Didier Trono, pMD2.G, Addgene #12259; pRSV-Rev, Addgene #12253; pMDLg/pRRE, Addgene #12251) as lentiviral (LV) vectors in 293T-LV cells_using Lipofectamine® LTX and PLUS™ Reagents (Life Technologies)[30]. Cells were transduced with LVs by incubating virions in a culture medium containing 100 μg/ml protamine sulfate (Sigma). Cells transduced with LVs containing empty vectors (EV) were used as a control. After selection with medium containing 10 μg/ml Puromycin (MP Biomedicals, CA), fluorescent protein-expressing cells were visualized for fluorescent protein expression using fluorescence microscopy (Eclipse Ti, Nikon, Japan).

Hydrogel synthesis and immunocytochemistry (in vitro)

Polyacrylamide tunable-hydrogels coated with collagen were synthesized as previously described[31]. The stiffness of hydrogels was attuned by adjusting the ratio of acrylamide and bis-acrylamide[31]. Cells were seeded in drop to evenly spread onto the hydrogels and harvested for further assays 24-48 hours later according to previous literature[13]. In order to test if the MRCS is stiffness-dependent, in some experiments, 50 μM (−)-Blebbistatin (Sigma), 10 μM ML-7 (Sigma) or 20 μM PF 573228 (PF228, Sigma) were added to the MRCS after attachment. Cells were briefly fixed in 4% paraformaldehyde (PFA, Amresco, OH) and permeablized in 0.1% IGEPAL® CA-630 (Sigma). Primary antibodies (mouse anti-YAP 1: 100; sheep anti-CD 1: 200; chicken anti-eGFP 1: 500) were incubated overnight in Phosphate Buffered Saline (PBS, Lonza) with 0.1% Triton X-100 (Sigma) and 2% goat (Thermo Fisher Scientific) or donkey serum (Sigma) (for double-staining). Secondary antibodies were diluted 1: 500 and were applied for 30 minutes at room temperature. Slides were washed in PBS and mounted with Fluoromount-G

(Southern Biotech, AL). DAPI (50 μg/ml, Life Technologies) in PBS was added onto samples before mounting. All the antibodies used in this experiment are provided in Table 3.1 (Primary antibodies) and Table 3.2 (Secondary antibodies; Jackson ImmunoResearch Laboratories). Quantification of protein expression was conducted by normalizing the average of fluorescent intensity within the cells to the glass control using the NIS-Elements AR software (Nikon, Japan) after background subtraction. Triplicated samples were used for the analysis.

Quantitative Reverse transcriptase PCR (RT qPCR)

Hydrogels were synthesized and cells were seeded as above mentioned. In order to test the expression of certain mRNA regulated by mechano-cues *in vitro*, cells were then harvested from hydrogels, glass coverslip or tissue culture plates in TRIzol (Invitrogen) for total RNA extraction with DNase I (Thermo Fisher Scientific) treatment to remove DNA contamination according to the manufacturer's protocol. cDNA synthesis was performed with Oligo(dT) (Invitrogen) primed SuperScript® III RNase H Reverse Transcriptase (Invitrogen) and Power SYBR® Master Mix (Life Technologies). RT qPCR was performed ion quadruplicates on an Applied Biosystems® ViiA™ 7 Real-Time PCR System and data were analyzed with ViiA™ 7 Software v1.2. Relative gene expression levels were normalized to the endogenous gene *GAPDH*. Sequences of primers[13, 32, 33] used in this experiment (Integrated DNA Technologies (IDT)) are provided in Table 3.3.

In vitro bioluminescence assays

LV-*CMV*::Luc MSCs (Luc-MSC) expressing firefly luciferase (Luc) and LV-MRCS-Luc MSCs (MRCS-Luc) were seeded onto collagen-coated hydrogels with different stiffness as described[13]. After the cells were washed with PBS, D-luciferin (150 μg/ml in PBS, Perkin Elmer,

MA) was added and the activity of Luc was then measured. All samples above were measured at least in triplicate.

Statistical analysis

Data were analyzed by Student's *t* test when comparing 2 groups and by ANOVA when comparing more than 2 groups. Data were expressed as mean ± S. D. or mean ± S. E. M., and differences were considered significant at $P < 0.05$.

3.6 ACKNOWLEDGMENTS

We thank Dr. D.-K. Kang, Dr. M. M. Ali and Dr. J. Zimak for discussion and comments. We are grateful to K. Zhang and Dr. X. E. Guo for kind help on *in vitro* experiments and discussion. We thank Dr. F. Grun, the director of the UCI Mass Spectrometry Facility (Department of Chemistry, University of California-Irvine) for his precious advice and help with the mass spectrometry training and analysis. We thank Dr. K. Aboody, Dr. T. Synold and Dr. M. Metz from City of Hope for sharing their LC-MS/MS method for prodrug conversion. We thank California NanoSystems Institute (CNSI) at University of California-Los Angeles for AFM. This work was supported by the National Institutes of Health (1DP2CA195763-01) and Department of Defense (W81XWH-13-1-0326). S.X.Z. was supported by a Cardiovascular Applied Research and Entrepreneurship fellowship (NIH/NHLBI T32). W.L. was supported by a California Institute for Regenerative Medicine (CIRM) fellowship (TG2-01152), C.C.C. was supported by National Science Foundation Graduate Research Fellowship (NSF GRFP), A.I.S. received a fellowship from the Fondation ARC Pour La Recherche Sur Le Cancer (SAE20150602901) and G.P. was supported by a CIRM training grant (TB1-01182).

3.7 AUTHOR CONTRIBUTIONS

L.L. designed and performed experiments, analyzed and interpreted data, drafted the manuscript and coordinated the project. S.X.Z. performed the *in vivo* experiments, tissue processing, histology, mass spectrometry exams and AFM micro-indentation test, analyzed data and drafted the manuscript. W.L. designed and performed the *in vivo* experiments and edited the manuscript. C.W.W. engineered the cells, conducted the immunocytochemistry, qPCR, XTT and Transwell assays, *in vitro* luciferase assays, mass spectrometry exams, bone marrow flush, flow cytometry and analyzed the data. C.C.C. carried out the qPCR, XTT assays and *in vitro* luciferase assays and analyzed the data and participated in the mass spectrometry exams. H.P.F. performed tissue processing, immunohistochemistry and SHG imaging and edited the manuscript. A.I.S. designed and performed the mass spectrometry exams, designed the histology assays, conducted the flow cytometry assay and analyzed the data. J.V.C. and M.A.D. performed SHG imaging, analyzed the data and edited the manuscript. L.P.N. participated in the *in vivo* experiments and the mass spectrometry exams, performed the histology assays and acquired the data. M.L. engineered the cells, helped to prepare the figures and performed cloning and manuscript editing. G.P. contributed to *in vivo* experiments, participated in immunohistochemistry and manuscript editing. T.L.D edited the manuscript. D.A.L. edited the manuscript. E.J.P. conducted the flow cytometry assay, edited the manuscript and interpreted the data. W.Z. was responsible for conception and design of the research, interpreted the results, revised the manuscript and supervised the overall project.

3.8 SUPPLEMENTAL MATERIAL

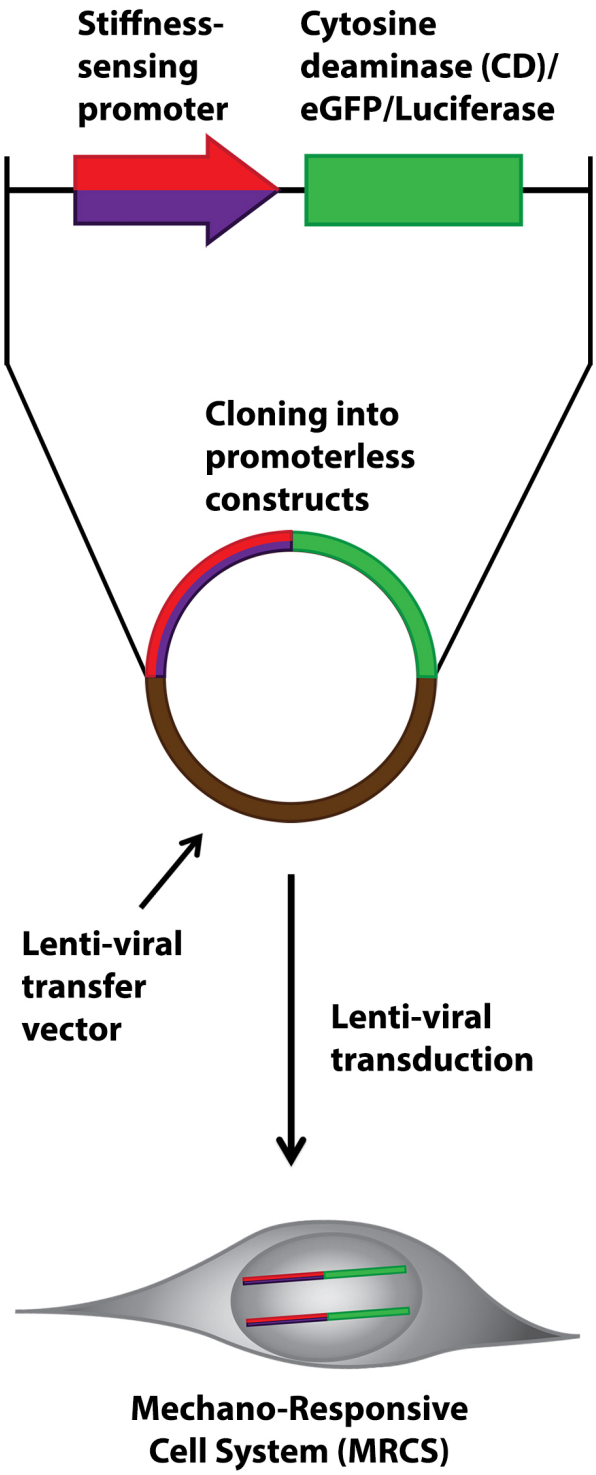

Figure 3.S1. Construction of mechano-responsive cell system (MRCS). The scheme of cell engineering. Promoters of genes responsive to specific ranges of stiffness are cloned into promoterless vectors to drive expression of eGFP, luciferase, and/or cytosine deaminiase (CD). Then the constructs are transduced into mesenchymal stem cells (MSCs) to produce stable engineered MSCs (*i.e.*, MRCS).

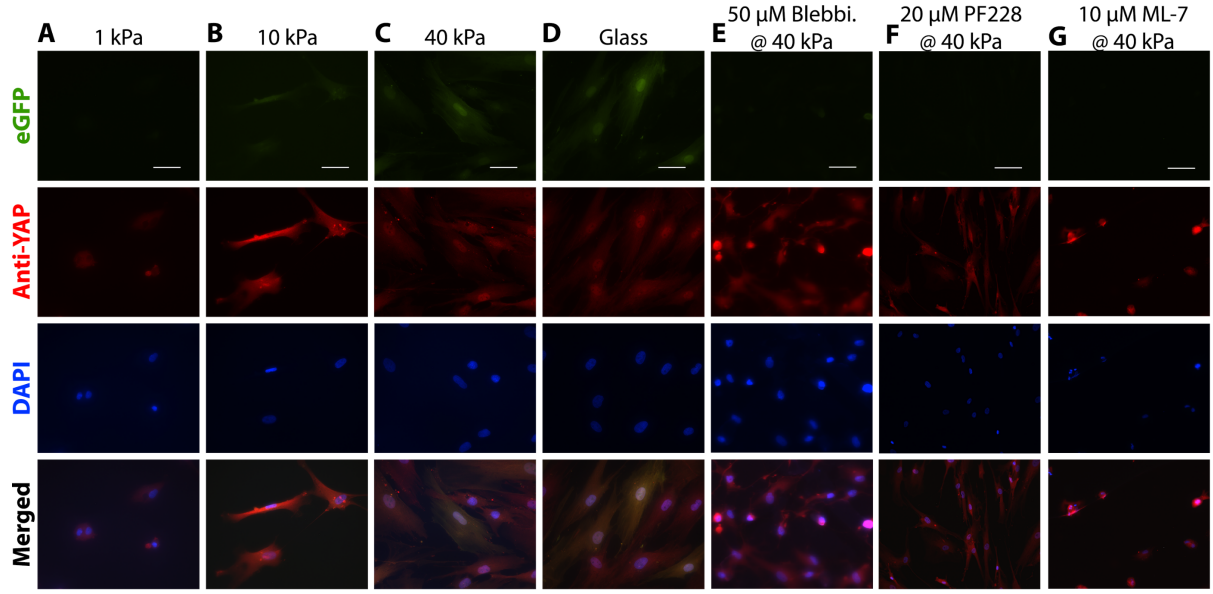

Figure 3.S2. Further mechano-responsive cell system (MRCS-eGFP) *in vitro* validation. (**A** to **D**) MRCS-eGFP were plated on soft (~ 1 kPa), medium (~ 10 kPa), firm (~ 40 kPa) polyacrylamide gel or glass. eGFP (green) was turned on responding to higher stiffness (> 10 kPa). YAP (red) relocalization is also regulated by stiffness, *i.e.*, concentrated in nuclei on stiffer substrates (> 10 kPa). (**E** to **G**) When MRCS-eGFP on firm (~ 40 kPa) substrates were treated with 50 µM blebbistatin, 10 µM ML-7 (myosin light-chain kinase inhibitors) or 20 µM PF228 (focal adhesion kinase inhibitor), respectively, eGFP (green) was turned off and YAP (red) was localized in cytoplasm, suggesting that MRCS sensing is reversibly stiffness-dependent. DAPI (blue, nuclear counterstain) is also displayed. Scale bar = 100 µm.

Table 3.1. Primary antibodies

Antigen	Company	Catalog #	Dilution	Notes
Annexin V	Bioss Antibodies	bs-0398R	1: 100	Fig.5.2
Cytosine Deaminase	Bioss Antibodies	bs-2950R	1: 100	Fig.5.S4&6.2
Cytosine Deaminase	Pierce (Thermo Fisher)	PA185365	1: 200	Fig.4.1&4.2
eGFP	Abcam	ab111258	1: 100	Fig.5.S5
eGFP	Abcam	ab13970	1: 500	Fig.3.2
eGFP	Pierce (Thermo Fisher)	OSE00001G	1: 100	Fig.6.2
Firefly Luciferase	Abcam	ab21176	1: 100	Fig.5.S4&5.S5
Firefly Luciferase	Abcam	ab181640	1: 100	Fig.6.2
Lysyl Oxidase (LOX)	Abcam	ab31238	1: 100	Fig.6.1&6.S1
PARP p85 Fragment	Promega	G7341	1: 100	Fig.6.3,6.4&6.S3
YAP	Santa Cruz Biotechnology	sc-101199	1: 100	[13]Fig3.2,3.S2&4.2
CD45R/B220	BioLegend	103212	N/A	Fig.5.3
CD11b	BioLegend	101206	N/A	Fig.5.3
CD3e	TONBO Biosciences	50-0031-U100	N/A	Fig.5.3
Ly-6G (Gr-1)	TONBO Biosciences	60-5931-U025	N/A	Fig.5.3

Table 3.2. Secondary antibodies

Tag	Species	Catalog #	Dilution
Alexa Fluor® 488	Donkey α Chicken	ab63507(Abcam)	1: 1000
Alexa Fluor® 488	Donkey α Goat	705-545-147	1: 500
Alexa Fluor® 488	Donkey α Rabbit	711-545-152	1: 500
Alexa Fluor® 488	Donkey α Sheep	713-545-003	1: 500
Rhodamine (TRITC)	Donkey α Goat	705-025-147	1: 500
Rhodamine (TRITC)	Donkey α Rabbit	711-025-152	1: 500
Alexa Fluor® 594	Goat α Mouse	115-585-062	1: 500
Alexa Fluor® 647	Donkey α Rabbit	711-605-152	1: 500

All secondary antibodies were purchased from Jackson ImmunoResearch Laboratories except for ab63507.

Table 3.3. Primers used in qPCR

Name	Sequence	Notes
GAPDH-C-F1	5’ – CTC CTG CAC CAC CAA CTG CT – 3’	[13]
GAPDH-C-R2	5’ – GGG CCA TCC ACA GTC TTC TG – 3’	
ANKRDI-C-F	5’ – AGT AGA GGA ACT GGT CAC TGG – 3’	
ANKRDI-C-R	5’ – TGG GCT AGA AT GTC TTC AGA T – 3’	
CTGF-C-F	5’ – AGG AGT GGG TGT GTG ACG A – 3’	
CTGF-C-R	5’ – CCA GGC AGT TGG CTC TAA TC – 3’	
GFP-F	5’ – CTG CTG CCC GAC AAC CAC – 3’	[32]
GFP-R	5’ – ACC ATG TGA TCG CGC TTC TC – 3’	
CDy-F	5’ – ACC ATG GTC ACA GGA GGC AT – 3’	[33]
CDy-R	5’ – TTC TCC AGG GTG CTG ATC TC – 3’	

All primers were purchased from Integrated DNA Technologies (IDT).

3.8 REFERENCES

1. Engler, A.J., Sen, S., Sweeney, H.L. & Discher, D.E. Matrix elasticity directs stem cell lineage specification. *Cell* **126**, 677-689 (2006).
2. Rowlands, A.S., George, P.A. & Cooper-White, J.J. Directing osteogenic and myogenic differentiation of MSCs: interplay of stiffness and adhesive ligand presentation. *American journal of physiology. Cell physiology* **295**, C1037-1044 (2008).
3. Pek, Y.S., Wan, A.C. & Ying, J.Y. The effect of matrix stiffness on mesenchymal stem cell differentiation in a 3D thixotropic gel. *Biomaterials* **31**, 385-391 (2010).
4. Park, J.S. et al. The effect of matrix stiffness on the differentiation of mesenchymal stem cells in response to TGF-beta. *Biomaterials* **32**, 3921-3930 (2011).
5. Tse, J.R. & Engler, A.J. Stiffness gradients mimicking in vivo tissue variation regulate mesenchymal stem cell fate. *PloS one* **6**, e15978 (2011).
6. Krouskop, T.A., Wheeler, T.M., Kallel, F., Garra, B.S. & Hall, T. Elastic moduli of breast and prostate tissues under compression. *Ultrasonic imaging* **20**, 260-274 (1998).
7. Lopez, J.I., Kang, I., You, W.K., McDonald, D.M. & Weaver, V.M. In situ force mapping of mammary gland transformation. *Integrative biology : quantitative biosciences from nano to macro* **3**, 910-921 (2011).
8. Samani, A., Zubovits, J. & Plewes, D. Elastic moduli of normal and pathological human breast tissues: an inversion-technique-based investigation of 169 samples. *Physics in medicine and biology* **52**, 1565-1576 (2007).
9. Wang, H. et al. Trafficking mesenchymal stem cell engraftment and differentiation in tumor-bearing mice by bioluminescence imaging. *Stem Cells* **27**, 1548-1558 (2009).
10. Bonfield, T.L. & Caplan, A.I. Adult mesenchymal stem cells: an innovative therapeutic for lung diseases. *Discovery medicine* **9**, 337-345 (2010).
11. Ortiz, L.A. et al. Mesenchymal stem cell engraftment in lung is enhanced in response to bleomycin exposure and ameliorates its fibrotic effects. *Proceedings of the National Academy of Sciences of the United States of America* **100**, 8407-8411 (2003).
12. Kotlarchyk, M.A., Botvinick, E.L. & Putnam, A.J. Characterization of hydrogel microstructure using laser tweezers particle tracking and confocal reflection imaging. *Journal of physics. Condensed matter : an Institute of Physics journal* **22**, 194121 (2010).
13. Dupont, S. et al. Role of YAP/TAZ in mechanotransduction. *Nature* **474**, 179-183 (2011).
14. Halder, G., Dupont, S. & Piccolo, S. Transduction of mechanical and cytoskeletal cues by YAP and TAZ. *Nature reviews. Molecular cell biology* **13**, 591-600 (2012).
15. Hong, J.H. et al. TAZ, a transcriptional modulator of mesenchymal stem cell differentiation. *Science* **309**, 1074-1078 (2005).
16. Gang, E.J. et al. Skeletal myogenic differentiation of mesenchymal stem cells isolated from human umbilical cord blood. *Stem Cells* **22**, 617-624 (2004).
17. Zuk, P.A. et al. Human adipose tissue is a source of multipotent stem cells. *Molecular biology of the cell* **13**, 4279-4295 (2002).
18. Slack-Davis, J.K. et al. Cellular characterization of a novel focal adhesion kinase inhibitor. *The Journal of biological chemistry* **282**, 14845-14852 (2007).
19. Dhawan, J. & Helfman, D.M. Modulation of acto-myosin contractility in skeletal muscle myoblasts uncouples growth arrest from differentiation. *Journal of cell science* **117**, 3735-3748 (2004).
20. Gygi, S.P., Rochon, Y., Franza, B.R. & Aebersold, R. Correlation between protein and mRNA abundance in yeast. *Mol Cell Biol* **19**, 1720-1730 (1999).
21. de Sousa Abreu, R., Penalva, L.O., Marcotte, E.M. & Vogel, C. Global signatures of protein and mRNA expression levels. *Mol Biosyst* **5**, 1512-1526 (2009).
22. Mole, D.R. et al. Genome-wide association of hypoxia-inducible factor (HIF)-1alpha and HIF-2alpha DNA binding with expression profiling of hypoxia-inducible transcripts. *The Journal of biological chemistry* **284**, 16767-16775 (2009).
23. Chen, F.E., Huang, D.B., Chen, Y.Q. & Ghosh, G. Crystal structure of p50/p65 heterodimer of transcription factor NF-kappaB bound to DNA. *Nature* **391**, 410-413 (1998).
24. Loebinger, M.R., Eddaoudi, A., Davies, D. & Janes, S.M. Mesenchymal stem cell delivery of TRAIL can eliminate metastatic cancer. *Cancer research* **69**, 4134-4142 (2009).
25. Song, C. et al. Thymidine kinase gene modified bone marrow mesenchymal stem cells as vehicles for antitumor therapy. *Human gene therapy* **22**, 439-449 (2011).

26. Studeny, M. et al. Bone marrow-derived mesenchymal stem cells as vehicles for interferon-beta delivery into tumors. *Cancer research* **62**, 3603-3608 (2002).
27. Lei, J., Levin, S.A. & Nie, Q. Mathematical model of adult stem cell regeneration with cross-talk between genetic and epigenetic regulation. *Proceedings of the National Academy of Sciences of the United States of America* **111**, E880-887 (2014).
28. Vick, J.E. et al. Optimized compatible set of BioBrick vectors for metabolic pathway engineering. *Appl Microbiol Biotechnol* **92**, 1275-1286 (2011).
29. Patel, M.R. et al. Longitudinal, noninvasive imaging of T-cell effector function and proliferation in living subjects. *Cancer research* **70**, 10141-10149 (2010).
30. Liu, L. et al. Exogenous marker-engineered mesenchymal stem cells detect cancer and metastases in a simple blood assay. *Stem Cell Res Ther* **6**, 181 (2015).
31. Tse, J.R. & Engler, A.J. Preparation of hydrogel substrates with tunable mechanical properties. *Curr Protoc Cell Biol* **Chapter 10**, Unit 10 16 (2010).
32. Mangeat, B. et al. Broad antiretroviral defence by human APOBEC3G through lethal editing of nascent reverse transcripts. *Nature* **424**, 99-103 (2003).
33. Kucerova, L. et al. Cytosine deaminase expressing human mesenchymal stem cells mediated tumour regression in melanoma bearing mice. *J Gene Med* **10**, 1071-1082 (2008).

CHAPTER 4

THE MRCS CANCER KILLING IN VITRO IN RESPONSE TO STIFFNESS

4.1 ABSTRACT

Cancer metastases are responsible for most of the cancer deaths. We hypothesize that that increased matrix stiffness is a fundamental property of the metastatic niche that can be targeted with MSC-based, mechano-responsive therapies. After we had constructed the mechano-responsive cell system (MRCS), we have also successfully validated the MRCS as therapeutics (*e.g.*, expressing cytosine deaminase (CD)) that selectively respond to stiff substrates (E > 10 kPa) with a turn-on ratio over 50%, covert prodrug and kill cancer cells *in vitro*.

Keywords: mesenchymal stem cell; cancer killing; mechano-sensing; bystander effect; cytosine deaminase; 5-fluorocytosine; 5-fluorouracil; co-culture; LC/MS/MS

4.2 INTRODUCTION

Besides other anti-cancer agents, a large number of enzyme-prodrug systems (as known as suicide genes) have been developed and used in cell and/or gene therapies[1]. The most frequently used enzymes for cell and/or gene therapies are non-mammalian in origin and different from any endogenous enzymes in circulation, satisfying the general condition to be expressed in concentrations for sufficient conversion of prodrug to achieve high therapeutic efficiency. The disadvantage compared to the enzymes of mammalian origin is that they are likely to be immunogenic, which can be improved by gene humanization. The enzyme-prodrug systems most well characterized and experimentally tested in clinical trials are cytosine deaminase (CD)/5-fluorocytosine (5-FC), Herpes simplex virus thymidine kinase/gancyclovir, and cytochrome P450/cytochrome P450 reductase. The choice of enzyme delivery system is dictated by the characteristics of the tumor[1, 2].

To design a MRCS for local drug activation, we utilized the reporters that were established as specific to the *in vitro* model mimicking the metastatic niche in Chapter 3. To the identified reporter constructs we replaced the eGFP with the gene for cytosine deaminase (CD). CD acts as a pro-drug convertase, converting the pro-drug 5-fluorocytosine (5-FC) into the potent anti-metabolite 5-fluorouracil (5-FU). This leads to localized activation of 5-FC via the bystander effect in which the apoptotic MRCS locally releases CD [3]. This technique has shown great promise and is currently the basis of a clinical trial using neural stem cells (NSC) for the treatment of glioblastoma[3, 4]. In addition, we made use of a vector in which CD is constitutively expressed as an important control to understand and quantify pulmonary and systemic toxicity of global MSC activation of 5-FC. MSCs will be transduced as described previously.

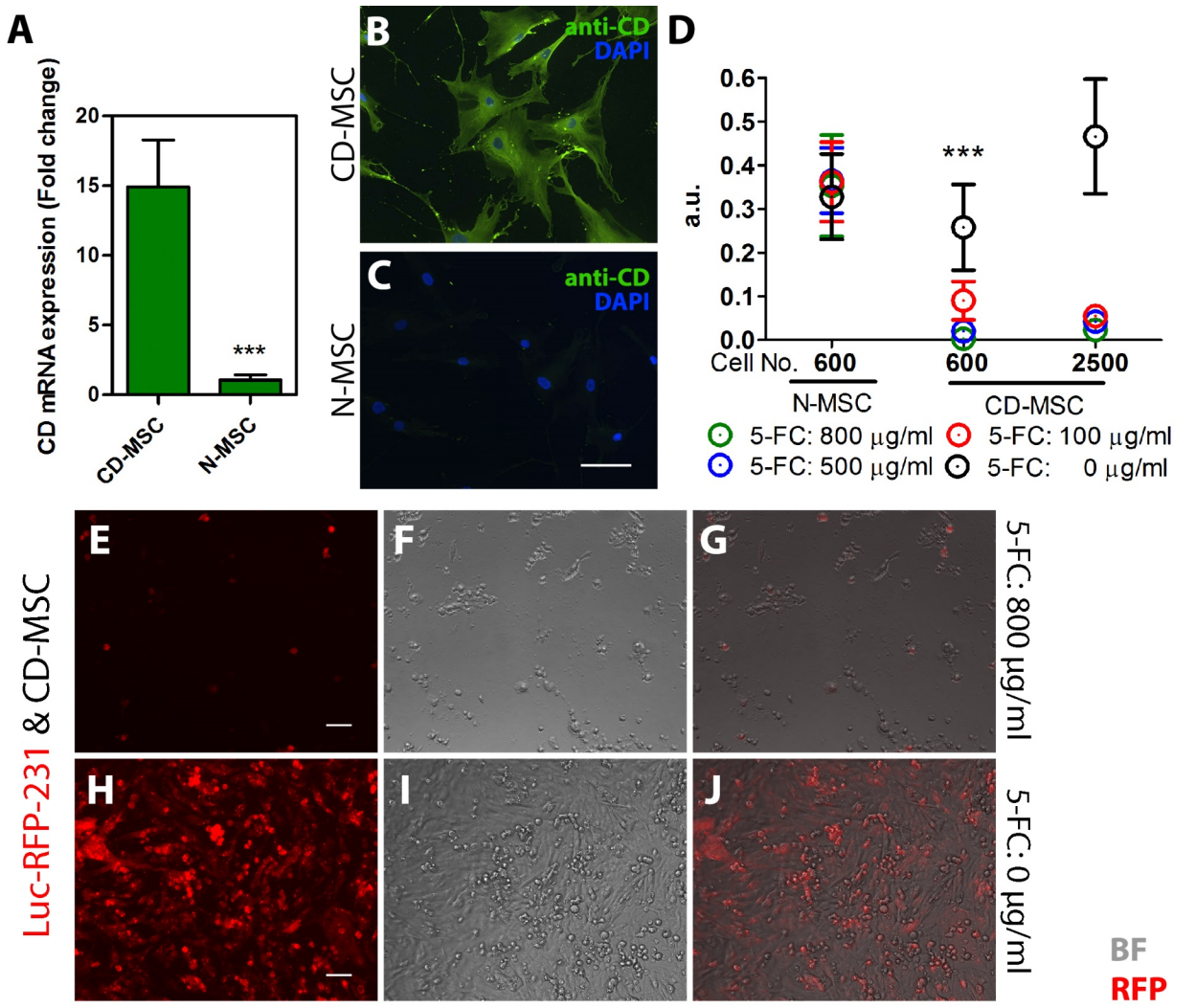

Figure 4.1. MSCs with constitutive cytosine deaminase (CD) expression (CD-MSC) able to kill cancer cells in the presence of 5-FC *in vitro.* The expression of *cytosine deaminase* (*CD*) was validated by (**A**) RT qPCR and (**B**) immunofluorescent staining. CD (green); DAPI (blue, nuclear counterstain). Native MSC (N-MSC) is included as a control in panel (**A** and **C**). In panel **a**, the CD mRNA expression of N-MSC was normalized to "1". N-MSC does not express CD. (**D**) XTT assay was performed to show that CD expressing MSCs are suicide agents in the presence of 5-FC at various concentrations. MSC proliferation is highly decreased only when both CD expressing MSCs and prodrug 5-FC exist. (**E** to **J**) Co-culture experiment was conducted with CD-MSC and RFP expressing MDA-MB-231 breast cancer cells (231: MSC = 2:1) with or without 800 μg/ml 5-FC. It shows that approximately 95% of breast cancer cells are killed and rest is apoptotic while no 5-FC control has a high confluency, showing CD-MSC-5-FC system is sufficient to kill adjacent breast cancer cells. RFP (red) and bright field (BF) are displayed. Scale bar = 100 μm. Error bar: mean ± S.D.. ***$P < 0.001$.

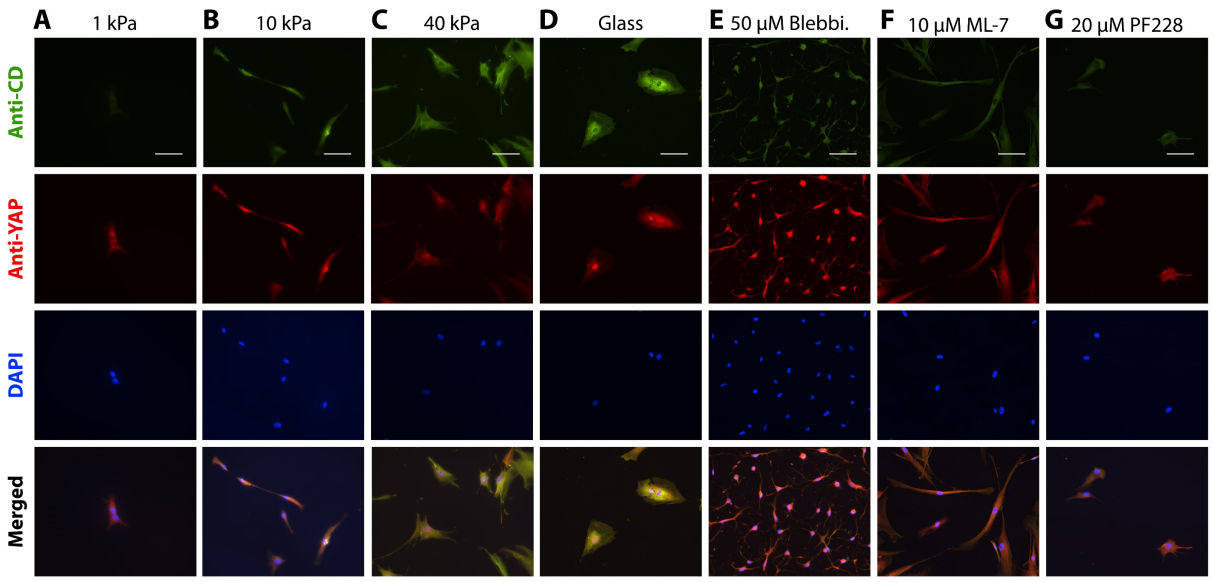

Figure 4.2. MRCS-CD responding to matrix stiffness *in vitro.* (**A** to **D**) MRCS-CD were plated on soft (~ 1 kPa), medium (~ 10 kPa), firm (~ 40 kPa) poly-acrylamide gel or glass, respectively. Note that cytosine deaminase (CD, green) was turned on responding to high stiffness (> 10kPa). YAP (red) relocalization is also regulated by stiffness. (**E** to **G**) When MRCS-CD plated on firm (~ 40kPa) poly-acrylamide gel were treated with 50 µM blebbistatin, 10 µM ML-7 (myosin light-chain kinase inhibitors) as well as 20 µM PF228 (focal adhesion kinase inhibitor), cytosine deaminase (CD) (green) was turned off and YAP (red) was localized in cytoplasm. These data show that MRCS-CD are stiffness specific *in vitro*. DAPI (blue, nuclear counterstain) are displayed. Scale bar = 100 µm.

4.3 RESULTS

4.3.1 Cytosine deaminase expressing MSCs killing cancer in the presence of 5-Fluocytosine

CD is a prodrug convertase that converts the inactive prodrug 5-FC to the active drug 5-fluorouracil (5-FU)[4]. This leads to localized tumor killing via the bystander effect in which the apoptotic MRCS locally releases CD[3] (Figure 3.1). This promising technique is currently being used in clinical trials, *e.g.*, 5-FU delivery by neural stem cells (NSCs) for treatment of glioblastoma[3]. To validate the effectiveness of this prodrug system, we first confirmed that MSCs engineered to constitutively express CD (abbreviated as CD-MSC) are able to sufficiently convert 5-FC to kill MDA-MB-231 breast cancer cells *in vitro* (Figure 4.1). Briefly, mRNA

expression level of CD from MSCs was first characterized (more than 15-fold change, Figure 4.1A). Robust CD expression was also confirmed with immunocytochemistry (Figure 4.1B, 4.1C). More importantly, CD-MSC can kill themselves in the presence of 5-FC, showing the feature as a "suicide gene" (Figure 4.1D-4.1J).

Co-culture experiments with CD-MSC and luciferase expressing MDA-MB-231 breast cancer cells was performed. It is shown that CD-MSC only kill breast cancer cells in the presence of 5-FC in culture (Figure 4.1E-4.1J and 4.S1). Titration assay of CD-MSC and 5-FC shows that 1) if MSCs : MDA-MB-231 cells < 10 : 1, a 5-FC concentration of 500 μg/ml is necessary and 2) if MSCs : MDA-MB-231 cells is no less than 2 : 1, then a high efficacy can still be achieved with a low 5-FC concentration (Figure 4.S2). Interestingly, it is also observed that MSCs show an inhibitory effect on the growth of MDA-MB-231 cells in co-culture, which is a beneficial addition over the treatment from our engineered cell. (Figure 4.S1C)

4.3.2 Validation of the MRCS-CD in response to different stiffness *in vitro*

In order to utilize MRCS to locally treat breast cancer metastasis in the lung, we engineered the cells to express CD instead of a reporter gene (Figure 3.S1). Briefly we constructed MRCS-CD with the aforementioned YAP/TAZ promoter that will drive the expression of CD in response to matrix stiffness. We first correlated CD transcription/translation with local stiffness by staining for CD (data not shown). To validate the stiffness-specific regulation of CD expression and conversion of 5-FC, MRCS-CD were seeded on polyacrylamide hydrogels with different stiffness. On soft hydrogel (~ 1 kPa), minimal level of CD was expressed (Figure 4.2A), but on stiffer hydrogels and glass (> 10 kPa), CD expression was turned on (Figure 4.2B-4.2D). Notably, we observed a "turned-on" ratio of 56% of MRCS-CD

on stiff substrate (~ 40 kPa) and of 100% on glass (Table 4.1). This expression pattern also correlated well with the localization of YAP. In the presence of mechanotransduction inhibitors, CD expression was turned off even on stiff hydrogel (~ 40 kPa) (Figure 4.2E-4.2G). Those data show that MRCS-CD can respond to certain stiffness *in vitro* and this sensing is reversibly stiffness-dependent. Quantification of the fluorescent signal of CD immunostaining indicates the similar results (Figure 4.3A). Briefly, MRCS-CD on stiff (40 kPa) gel show a more than 3-fold higher expression of CD than those on soft (1 kPa) gel. Meanwhile MRCS-CD on stiff gel with mechano-inhibitors shows a similar CD expression level as those on soft gel.

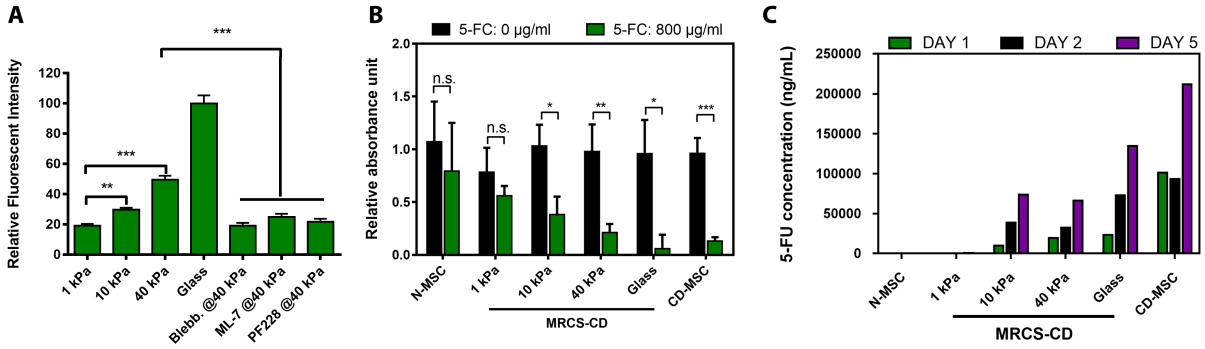

Figure 4.3. MRCS-CD can be activated depending on substrate stiffness *in vitro*. (**A**) Quantification of fluorescent signals of cytosine deaminase (CD) shows MRCS-CD responding to matrix stiffness *in vitro.* MRCS-CD were stained with antibody after plated on tunable polyacrylamide gels or glass as indicated, or treated with 50 μM blebbistatin, 10 μM ML-7 (myosin light-chain kinase inhibitors) as well as 20 μM PF228 (focal adhesion kinase inhibitor), respectively. The fluorescent signals of CD were analyzed and the relative fluorescent intensity is shown. These data indicate that MRCS-CD are stiffness specific *in vitro*. Error bar: mean ± S.E.M.. (**B**) MRCS-CD able to kill cancer cells in response to matrix stiffness and 5-FC *in vitro.* MRCS-CD were co-cultured with MDA-MB-231 breast cancer cells (231: MRCS = 2:1) with (800 μg/ml, green) or without (black) 5-FC on different stiffness. Total cell proliferation (XTT assay) is displayed. The data were normalized with breast cancer only (231: MRCS = 1:0) with or without 5-FC on each stiffness. It shows that MRCS-CD kill cancer cells in response to stiffness with 5-Fluorocytosine (5-FC) *in vitro.* Error bar: mean ± S.D.. n.s., not significant, $*P < 0.05$, $**P < 0.01$, $***P < 0.001$ and $****P < 0.0001$. (**C**) Conversion of 5-FC to 5-FU by MRCS-CD in response to matrix stiffness *in vitro.* MRCS-CD were seeded on different stiffness with 800 μg/ml 5-FC in growth medium for 1, 2 or 5 days. The concentration of 5-FU in the conditioned medium was detected by LC-MS/MS. The data demonstrate that the production of 5-FU by CD expressed by MRCS-CD respond to stiffness. CD-MSC: Constitutive positive control; N-MSC: Native MSCs.

4.3.3 MRCS-CD killing cancer in response to certain stiffness in the presence of 5-FC

To verify local production of functional CD and the efficacy of the bystander effect and test whether MRCS-CD could kill cancer specifically on high-stiffness substrates, MRCS-CD were co-cultured with MDA-MB-231 breast cancer cells on polyacrylamide hydrogels with or without 5-FC, and XTT assay was performed to quantify total cell proliferation (Figure 4.3B). On soft hydrogel (~ 1 kPa), there was no significant difference in cancer cell proliferation with or without the addition of 5-FC, consistent with the low expression of CD under these soft matrix conditions. When seeded on hydrogels with increased stiffness (10 and 40 kPa) or on glass, cell proliferation was significantly decreased in the presence of 5-FC in proportion to stiffness, suggesting that CD was expressed and converted the prodrug to its active form to kill the cancer cells. CD-MSC without a stiffness-sensing promoter showed significant difference in cell proliferation with or without 5-FC due to constitutive expression of CD, while native MSCs (N-MSC) showed no difference in total cell proliferation, as expected since they do not produce CD. This data demonstrates that MRCS-CD can selectively activate CD expression in response to matrix stiffness (*i.e.*, on stiff substrates) and convert 5-FC to kill adjacent cancer cells *in vitro*.

On the top of co-culture-cancer-killing assays performed above, it would be highly beneficial if the quantification of 5-FU conversion for both MRCS-CD and MSC-CD could be conducted as this appears to be a critical parameter in demonstrating the novelty of the platform and to provide a direct assessment of potency. We have utilized LC-MS/MS^4 in order to quantify the conversion of 5-FC to 5-FU by MRCS-CD and CD-MSC in conditioned medium, as shown in Figure 4.3C. Our data show after 5 days, the conversion of 5-FC to 5-FU is roughly half as

much for MRCS-CD as compared to CD-MSC on stiff substrates, and much lower for MRCS-CD on softer substrates, down to no conversion for MRCS-CD on very soft (~1 kPa) substrates. This suggests that MRCS-CD only converted prodrug in respond to stiff substrate and would not convert 5-FC to 5-FU on healthy tissues of off-target.

Table 4.1. "Turned-on" ratio of MRCS-CD on substrates with different stiffness

Substrate	Total Cell #	"Turned-on" Cell #	"Turned-on" Percentage
1 kPa	46	1	2.17%
10 kPa	30	4	13.33%
40 kPa	50	28	56.00%
Glass	29	29	100.00%

4.4 DISCUSSION AND FUTURE DIRECTION

Our system takes advantage of the ability of MSC to specifically home to metastases. The natural 'active' homing (and the subsequent integration) ability of MSC to tumors and metastases enables the efficient delivery of 'cargo' to the target site. This circumvents many hurdles associated with the passive delivery (*i.e.*, by direct administration or polymeric nanoparticles) including penetrating the endothelium, and the increased pressure associated with tumors. In particular, due to their small size, high dispersion to organs, and low vascularization, metastatic tumors may be less accessible to systemically infused chemotherapeutics or targeted nanoparticles. Such active and specific targeting combined with local and specific delivery of the pro-drug convertase/5-fluorocytosine system allows us to approach local therapeutic concentrations impossible with systemic infusion of chemotherapeutics with minimal side effects.

High systemic toxicity of 5-fluorouracil (5-FU), a potent cytotoxic chemotherapeutic, could be circumvented by initiating gene directed enzyme prodrug therapy[1]. The CD/5-FC

prodrug system relies on the ability of bacterial and/or yeast CD enzyme to convert the far less-toxic substrate 5-fluorocytosine (5-FC) to the highly toxic anti-cancer drug 5-FU. 5-FU is a small molecule capable of diffusion into and out of cells, resulting in significant bystander effect. When 5-FU is processed to, for example, 5-fluorouracil triphosphate, these molecular mechanisms cause inhibition of cell proliferation and cell death.

In the strong 5-FU-mediated bystander effect, direct cell-cell contact is not necessary for this process[5]. Several experimental studies have demonstrated that, besides the 5-FU-mediated bystander effect, a distant bystander effect contributes to the accomplishment of this therapy[6]. There have been several attempts to increase the efficiency of 5-FC prodrug conversion to 5-FU[1]. Yeast cytosine deaminase (iced) was shown to produce a 15-fold higher amount of 5-FU compared to bacterial CD[7]. Further improvement in the efficiency of prodrug conversion was accomplished by construction of bifunctional yeast fusion gene cytosine deaminase:uracil phosphoribosyltransferase (CD/ UPRT), which is also used in our MRCS. The gene product of a bifunctional chimeric protein efficiently catalyzes the direct conversion of 5-FC into the toxic metabolites 5-FU and its monophosphate. The CD activity is increased at least 100-fold over native yeast CD[8]. CD/UPRT gene as a prodrug converting enzyme was reported to exhibit improved 5-FC conversion efficiency and higher bystander effect *in vitro* and *in vivo*[9, 10]. Recently the high efficiency of this CD/UPRT fusion gene for suppression the growth of the tumor cells both *in vitro* and *in vivo* was shown in suicide gene therapy[11]. Similar high efficiency of this fusion gene was confirmed in stem cell based cancer gene therapy[12, 13].

In order to measure the 5-FU converted *in vivo*, thus to better understand the timeline of 5-FU production during the treatment, we collected the lungs and the sera of the animals at different time-points (details in Chapter 5). Based on the literature, we tried several extraction

methods and mobiles phases to extract the compound from the lungs. Most of the methods reported to extract 5-FU were mostly done from plasma/sera and used extraction buffers based on ethyl-acetate, methanol or a mix of ethyl-acetate, alcohol and acid[14-16]. As a control to determine our extraction yields, we used lungs containing 30 µg of 5-FU. So far, our results demonstrated that a mixture of ethyl-acetate and isopropanol was the best extraction buffer among what we tested together with a mobile phase containing acetonitrile with 0.2% acetic acid and a negative ion mode for the Electrospray Ionization (ESI). However, our yields remain very low (around 5%), and we are still optimizing the extraction by using larger volumes, re-extracting multiples times, playing with the solvent ratio, *etc.* In the plasma samples, we were only able to detect the 5-Bromouracil that we used as an internal standard, but we couldn't detect any 5-FU. The 5-FU has rapid total clearance, with a very short half-life of 10-20 minutes[17], and we might be below the limit of detection in our extraction conditions, which is 100 ng/ml in the described settings. That means that we need to have at least 400 ng/ml of the 5-FU in the circulation to start with, based on the current 5% extraction yield, and if we consider roughly 500 µl of plasma collected for 1 ml of blood and that the samples are re-solubilized in 100 µl for the mass spectrometry analysis. If the circulating or the local 5-FU concentrations in the lungs are below that, which is highly probable, we need to improve our extraction yield to at least 20-30%.

Additionally, as described in our *in vitro* assays, a negative ion mode for the mass analysis has been identified as the best since we could not discriminate the daughter ions of the 5-FC and 5-FU using the positive ion mode (strong C13 peak for the 5-FC daughter ion that overlaps with the 5-FU main daughter ion).

4.5 MATERIALS AND METHODS

Cell lines and cell culture

Human bone marrow MSCs were obtained from the Texas A&M Health Science Center and were expanded to passages 3-6 for further use (*i.e.*, transduction, assays, injection, etc.). The cells were routinely maintained in Minimum Essential Medium α (MEM α, Life Technologies) supplemented with 15% fetal bovine serum (FBS, Atlanta Biologicals, GA) and 1% Penicillin-Streptomycin (PenStrep, 100 U/ml, Life Technologies) at 37°C in a humidified incubator containing 5% CO_2. The human breast cancer cell line MDA-MB-231 was obtained from American Type Culture Collection (ATCC, VA). These cells were grown in Leibovitz's L-15 medium containing L-glutamine (Corning, NY), and supplemented with 10% FBS and 1 U/ml PenStrep at 37°C in a humidified incubator without CO_2. The 293T-LV cell line (Gen Target, CA) was cultured in Dulbecco's Modified Eagle Medium (DMEM, Life Technologies) supplemented with 15% FBS, Non-Essential Amino Acid (NEAA, 1X, 100 U/ml, Life Technologies) and 1 U/ml PenStrep at 37°C in a humidified incubator containing 5% CO_2.

Generation of lentiviral vectors and lentiviral transduction

The following lentiviral vectors were used in this study: LV-CMV::eGFP, LV-CMV::Luc-RFP, LV-CMV::CD, LV-MRCS-eGFP, LV-MRCS-Luc and LV-MRCS-CD. The sequences of interest from pUCBB-eGFP[18] (a gift from Claudia Schmidt-dannert, Addgene #32548), pcDNA3.1(+)/Luc2=tdT (a gift from Christopher Contag[19], Addgene #32904), pSelect-zeo-Fcy::Fur (InvivoGen, CA) and 8xGTIIC-luciferase[20] (a gift from Stefano Piccolo, Addgene #34615) were cloned into the promoterless lentiviral transfer vector LV-PL4 (GenTarget, CA). All MSCs and breast cancer cells were transduced as previously described[21]. Briefly all lentiviral constructs were packaged (gifts from Didier Trono, pMD2.G, Addgene #12259; pRSV-Rev,

Addgene #12253; pMDLg/pRRE, Addgene #12251) as lentiviral (LV) vectors in 293T-LV cells_using Lipofectamine® LTX and PLUS™ Reagents (Life Technologies)[21]. Cells were transduced with LVs by incubating virions in a culture medium containing 100 μg/ml protamine sulfate (Sigma). Cells transduced with LVs containing empty vectors (EV) were used as a control. After selection with medium containing 10 μg/ml Puromycin (MP Biomedicals, CA), fluorescent protein-expressing cells were visualized for fluorescent protein expression using fluorescence microscopy (Eclipse Ti, Nikon, Japan).

Hydrogel synthesis and immunocytochemistry (in vitro)

Polyacrylamide tunable-hydrogels coated with collagen were synthesized as previously described[22]. The stiffness of hydrogels was attuned by adjusting the ratio of acrylamide and bis-acrylamide[22]. Cells were seeded in drop to evenly spread onto the hydrogels and harvested for further assays 24-48 hours later according to previous literature[20]. In order to test if the MRCS is stiffness-dependent, in some experiments, 50 μM (−)-Blebbistatin (Sigma), 10 μM ML-7 (Sigma) or 20 μM PF 573228 (PF228, Sigma) were added to the MRCS after attachment. Cells were briefly fixed in 4% paraformaldehyde (PFA, Amresco, OH) and permeablized in 0.1% IGEPAL® CA-630 (Sigma). Primary antibodies (mouse anti-YAP 1: 100; sheep anti-CD 1: 200; chicken anti-eGFP 1: 500) were incubated overnight in Phosphate Buffered Saline (PBS, Lonza) with 0.1% Triton X-100 (Sigma) and 2% goat (Thermo Fisher Scientific) or donkey serum (Sigma) (for double-staining). Secondary antibodies were diluted 1: 500 and were applied for 30 minutes at room temperature. Slides were washed in PBS and mounted with Fluoromount-G (Southern Biotech, AL). DAPI (50 μg/ml, Life Technologies) in PBS was added onto samples before mounting. All the antibodies used in this experiment are provided in Table 3.1 (Primary antibodies) and Table 3.2 (Secondary antibodies; Jackson ImmunoResearch Laboratories).

Quantification of protein expression was conducted by normalizing the average of fluorescent intensity within the cells to the glass control using the NIS-Elements AR software (Nikon, Japan) after background subtraction. Triplicated samples were used for the analysis.

For the calculation of "turned-on ratio" of MRCS, a threshold was set to mean + 2 x S.D. of fluorescent signals of the cells seeded on 1 kPa hydrogel. Subsequently, the estimation of "turn on ratio" was done by applying the same threshold to different conditions, presented as percentage of "turned-on cells".

Quantitative Reverse transcriptase PCR (RT qPCR)

Hydrogels were synthesized and cells were seeded as above mentioned. In order to test the expression of certain mRNA regulated by mechano-cues *in vitro*, cells were then harvested from hydrogels, glass coverslip or tissue culture plates in TRIzol (Invitrogen) for total RNA extraction with DNase I (Thermo Fisher Scientific) treatment to remove DNA contamination according to the manufacturer's protocol. cDNA synthesis was performed with Oligo(dT) (Invitrogen) primed SuperScript® III RNase H Reverse Transcriptase (Invitrogen) and Power SYBR® Master Mix (Life Technologies). RT qPCR was performed ion quadruplicates on an Applied Biosystems® ViiA™ 7 Real-Time PCR System and data were analyzed with ViiA™ 7 Software v1.2. Relative gene expression levels were normalized to the endogenous gene GAPDH. Sequences of primers[12, 20, 23] used in this experiment (Integrated DNA Technologies (IDT)) are provided in Table 3.3.

In vitro XTT cell viability assays

MSCs (LV-MRCS-CD MSCs (MRCS-CD), LV-*CMV*::CD MSCs (CD-MSC) or native MSCs (N-MSC)) were seeded onto hydrogels with MDA-MB-231 breast cancer cells with a

ratio of 2: 1 (231: MSCs). Prodrug 5-Fluorocytosine (5-FC, 800 μg/ml in MSC growth medium, Sigma) was added after attachment. Reagents from XTT kit (2,3-Bis-(2-Methoxy-4-Nitro-5-Sulfophenyl)-2*H*-Tetrazolium-5 Carboxanilide, ATCC, VA) were mixed and added to cells after 5 days' co-culture. The color absorbance was measured after 2 hours' incubation at 37°C in a humidified incubator. Bioluminescent signals and color absorbance were measured with a plate reader (BioTek, VT). All samples above were measured at least in triplicate.

Sample preparation and Ultra high performance liquid chromatography-electrospray ionization tandem quadrupole mass spectrometry (UPLC-MS/MS)

MSCs (MRCS-CD, CD-MSC or N-MSC) were seeded at a density of $10^4/cm^2$ on the hydrogels with variant stiffness or cover slides. Cells were allowed to grow for 24 hours in MSC growth medium and were then treated with 800 μg/ml 5-FC (Day 0). On Day 1, 2 and 5 respectively, conditioned medium was collected for extraction. 200 μl of the conditioned medium from each condition was extracted using 1000 μl of ethyl acetate : isopropanol 1:1 (v:v) (Sigma). Organic phase was collected after centrifugation at 3,000 xg for 10 minutes. Additional protein precipitation was done by adding 80 μl of saturated ammonium sulfate solution. After centrifuging at 3,000 xg for 10 minutes, the organic layer was transferred into a new microcentrifuge tube and dried using a centrifugal vacuum concentrator (Speedvac, Thermo Fisher Scientific). The extracted compounds were reconstituted in 250 μl water containing 20% acetonitrile , and 100 μl was used for the UPLC-MS/MS.

Culture medium spiked with 400 μg/ml 5-FC and 5-FU were used to determine the extraction yield. A 6 points 5-FU standard curve (⅓ dilution starting from 10 μg/ml) with a $R^2 >$ 0.98 was used to quantify the 5-FU inside the samples. 5-FU standard solutions were prepared in

water 20% acetonitrile. 10 µl was injected into the UPLC system for analysis, and then eluted on an Acquity UPLC BEH C18 1.7um column (Waters). UPLC was performed using the Acquity UPLC system (Waters) with a mobile phase gradient starting with 98% of a mobile phase composed of 98% water, 2% acetonitrile and 0.2% acetic acid which progressively goes up to 95% of the second mobile phase (100% acetonitrile and 0.2% acetic acid) for the elution of the samples. Then, the samples are injected into the triple quad mass spectrometer (Waters Micromass Quattro Premier XE^{TM} Tandem Quadrupole Mass Spectrometer, Waters) for the mass analysis. The electrospray ionization was done using the negative ion mode, which generates a precursor to product ion transition of m/z 129 > 42 for the 5-FU. After teaching, the cone voltage and the collision cell energy have respectively been optimized at 20V (CV) and 30V(CE). Dwelling time was 0.285 seconds and total run time per sample was 3 minutes. MassLynx software was used for data acquisition, and QuantLynx software for the data analysis and quantification.

Statistical Analysis

Data were analyzed by Student's *t* test when comparing 2 groups and by ANOVA when comparing more than 2 groups. Data were expressed as mean ± S. D. or mean ± S. E. M., and differences were considered significant at $P < 0.05$.

4.6 SUPPLEMENTAL MATERIAL

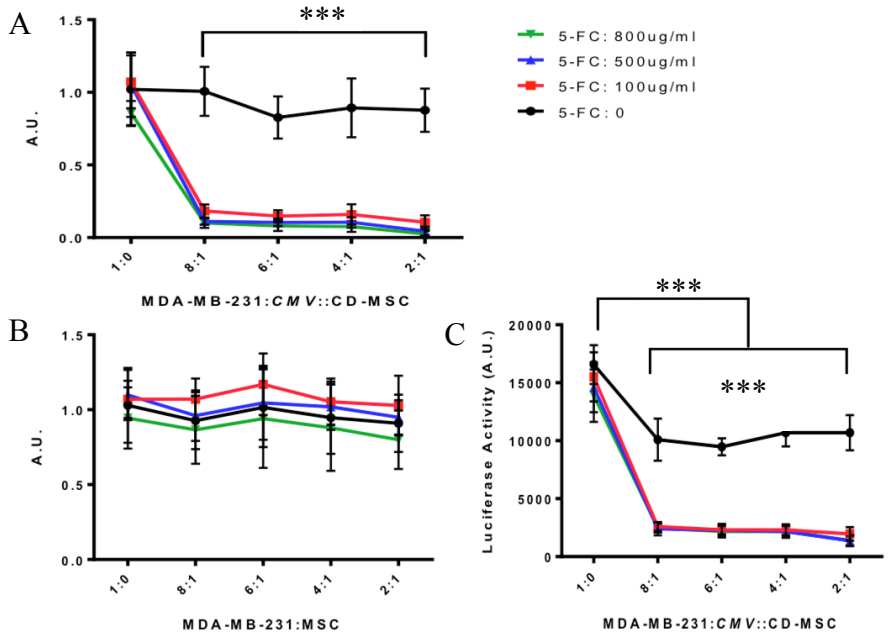

Figure 4.S1. CD expressing MSCs are able to kill cancer cells in the presence of 5-FC. Constitutively CD expressing MSCs were co-cultured with luciferase expressing MDA-MB-231 breast cancer cells for 6 days following with **(A, B)** XTT proliferation assay and **(C)** luciferase assay. **(A, B)** The total (MSCs and cancer cells) cell proliferation is highly decreased only when both CD expressing MSCs and pro-drug 5-FC exist. **(C)** Luciferase expressing cancer cells are killed by CD-MSC-5-FC system. Error bar: mean ± S.D.. ***$P < 0.001$.

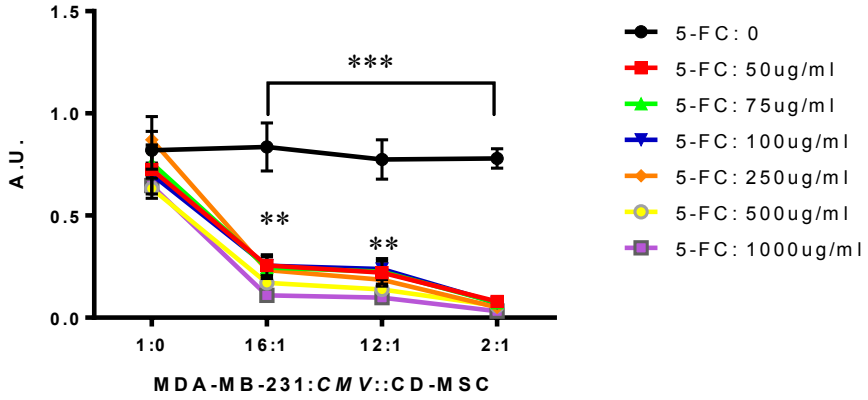

Figure 4.S2. Titration assay of CD-MSC and 5-FC. Constitutively CD expressing MSCs were co-cultured with luciferase expressing MDA-MB-231 breast cancer cells for 6 days following with XTT proliferation assay, with different MSC/MDA-MB-231 ratio and 5-FC concentration. The results indicate that 1) if MSCs : MDA-MB-231 cells < 10 : 1, a 5-FC concentration of 500 μg/ml is necessary and 2) if MSCs : MDA-MB-231 cells is no less than 2 : 1, then a high efficacy can still be achieved with a low 5-FC concentration. Error bar: mean ± S.D.. $^{**}P < 0.01$; $^{***}P < 0.001$.

4.7 REFERENCES

1. Altaner, C. Prodrug cancer gene therapy. *Cancer Lett* **270**, 191-201 (2008).
2. Shah, K. Stem cell therapeutics for cancer. (John Wiley & Sons, Hoboken, N.J.; 2013).
3. Aboody, K.S. et al. Targeting of melanoma brain metastases using engineered neural stem/progenitor cells. *Neuro-oncology* **8**, 119-126 (2006).
4. Aboody, K.S. et al. Neural stem cell-mediated enzyme/prodrug therapy for glioma: preclinical studies. *Science translational medicine* **5**, 184ra159 (2013).
5. Huber, B.E., Austin, E.A., Richards, C.A., Davis, S.T. & Good, S.S. Metabolism of 5-fluorocytosine to 5-fluorouracil in human colorectal tumor cells transduced with the cytosine deaminase gene: significant antitumor effects when only a small percentage of tumor cells express cytosine deaminase. *Proceedings of the National Academy of Sciences of the United States of America* **91**, 8302-8306 (1994).
6. Mullen, C.A., Coale, M.M., Lowe, R. & Blaese, R.M. Tumors expressing the cytosine deaminase suicide gene can be eliminated in vivo with 5-fluorocytosine and induce protective immunity to wild type tumor. *Cancer research* **54**, 1503-1506 (1994).
7. Kievit, E. et al. Yeast cytosine deaminase improves radiosensitization and bystander effect by 5-fluorocytosine of human colorectal cancer xenografts. *Cancer research* **60**, 6649-6655 (2000).
8. Erbs, P. et al. In vivo cancer gene therapy by adenovirus-mediated transfer of a bifunctional yeast cytosine deaminase/uracil phosphoribosyltransferase fusion gene. *Cancer research* **60**, 3813-3822 (2000).
9. Ramnaraine, M. et al. Direct and bystander killing of sarcomas by novel cytosine deaminase fusion gene. *Cancer research* **63**, 6847-6854 (2003).
10. Chung-Faye, G.A. et al. In vivo gene therapy for colon cancer using adenovirus-mediated, transfer of the fusion gene cytosine deaminase and uracil phosphoribosyltransferase. *Gene Ther* **8**, 1547-1554 (2001).
11. Erbs, P. et al. Modified vaccinia virus Ankara as a vector for suicide gene therapy. *Cancer Gene Ther* **15**, 18-28 (2008).
12. Kucerova, L. et al. Cytosine deaminase expressing human mesenchymal stem cells mediated tumour regression in melanoma bearing mice. *J Gene Med* **10**, 1071-1082 (2008).
13. Kucerova, L., Altanerova, V., Matuskova, M., Tyciakova, S. & Altaner, C. Adipose tissue-derived human mesenchymal stem cells mediated prodrug cancer gene therapy. *Cancer research* **67**, 6304-6313 (2007).
14. Breda, M. & Barattè, S. A review of analytical methods for the determination of 5-fluorouracil in biological matrices. *Analytical and bioanalytical chemistry* **397**, 1191-1201 (2010).
15. Büchel, B. et al. LC-MS/MS method for simultaneous analysis of uracil, 5, 6-dihydrouracil, 5-fluorouracil and 5-fluoro-5, 6-dihydrouracil in human plasma for therapeutic drug monitoring and toxicity prediction in cancer patients. *Biomedical chromatography* **27**, 7-16 (2013).
16. Chang, D.Y. et al. The growth of brain tumors can be suppressed by multiple transplantation of mesenchymal stem cells expressing cytosine deaminase. *Int J Cancer* **127**, 1975-1983 (2010).
17. Ensminger, W.D. et al. A clinical-pharmacological evaluation of hepatic arterial infusions of 5-fluoro-2′-deoxyuridine and 5-fluorouracil. *Cancer research* **38**, 3784-3792 (1978).
18. Vick, J.E. et al. Optimized compatible set of BioBrick vectors for metabolic pathway engineering. *Appl Microbiol Biotechnol* **92**, 1275-1286 (2011).
19. Patel, M.R. et al. Longitudinal, noninvasive imaging of T-cell effector function and proliferation in living subjects. *Cancer research* **70**, 10141-10149 (2010).
20. Dupont, S. et al. Role of YAP/TAZ in mechanotransduction. *Nature* **474**, 179-183 (2011).
21. Liu, L. et al. Exogenous marker-engineered mesenchymal stem cells detect cancer and metastases in a simple blood assay. *Stem Cell Res Ther* **6**, 181 (2015).
22. Tse, J.R. & Engler, A.J. Preparation of hydrogel substrates with tunable mechanical properties. *Curr Protoc Cell Biol* **Chapter 10**, Unit 10 16 (2010).
23. Mangeat, B. et al. Broad antiretroviral defence by human APOBEC3G through lethal editing of nascent reverse transcripts. *Nature* **424**, 99-103 (2003).

CHAPTER 5

TARGET CANCER METASTASES WITH THE MRCS AS THERAPEUTICS IN VIVO

5.1 ABSTRACT

Despite decades of effort, little progress has been made to improve the treatment of the cancer metastases. Here, we present a mechanoresponsive cell system (MRCS) to selectively identify and treat cancer metastases by targeting the unique biophysical cues in the tumor niche *in vivo*. Our MRCS selectively homes to and targets cancer metastases in response to specific mechanical cues to deliver therapeutics to effectively kill cancer cells as demonstrated in a metastatic breast cancer mouse model. MRCS demonstrates significantly reduced deleterious effects compared to MSCs constitutively expressing therapeutics. MRCS may represent a new paradigm for cancer treatment as biophysical cues, specifically matrix stiffness, is an appealing target due to its long half-life (measured in years), making it refractory to development of resistance.

Keywords: mesenchymal stem cell; tumor homing; cancer treatment; metastasis; murine model; side effect; chemotherapy; tissue damage

5.2 INTRODUCTION

A prospective clinical application of MSC lies in their intrinsic property to migrate toward tumors and metastases[1]. This is, actually, not a property unique to MSC, but rather is shared by many stem cells. For instance, in the circumstance of brain tumors, neural stem cells[2-4], and umbilical cord stem cells[5] have all been reported to migrate toward brain neoplasm. However, MSCs possess the added advantage for cancer gene therapy in that isolation of MSC is generally free of ethical issues: harvesting of these cells is less invasive than, for instance, the neural stem cells.

MSCs are reported to be recruited to pulmonary metastases incorporate into metastases[6-8]. It is possible that MSC homing to tumors involves interaction between active recruitment via chemokines and inflammatory processes as well as passive entrapment in the vasculature. Exogenously delivered MSCs are physically and molecularly non-specifically entrapped in locations with small blood vessels, including "filtering organs" including the lungs, liver, and spleen[9, 10]. Intriguingly, use of a vasodilator concomitant with administration of exogenous MSCs led to a noticeably altered biodistribution of MSCs, with a substantial decrease in entrapment in the lungs[9]. Moreover, treatment of exogenous MSCs with an integrin α4 blocking antibody results in entrapment of significantly fewer cells in the lung following intravenous injection[11]. Thus, we reason that the physical parameters of MSCs collaborate with molecular determinants to ultimately dictate homing and engraftment. Unraveling the relative contributions of molecular signals and physical parameters in MSC homing to tumors will reveal both new biology and novel targets for therapeutic intervention.

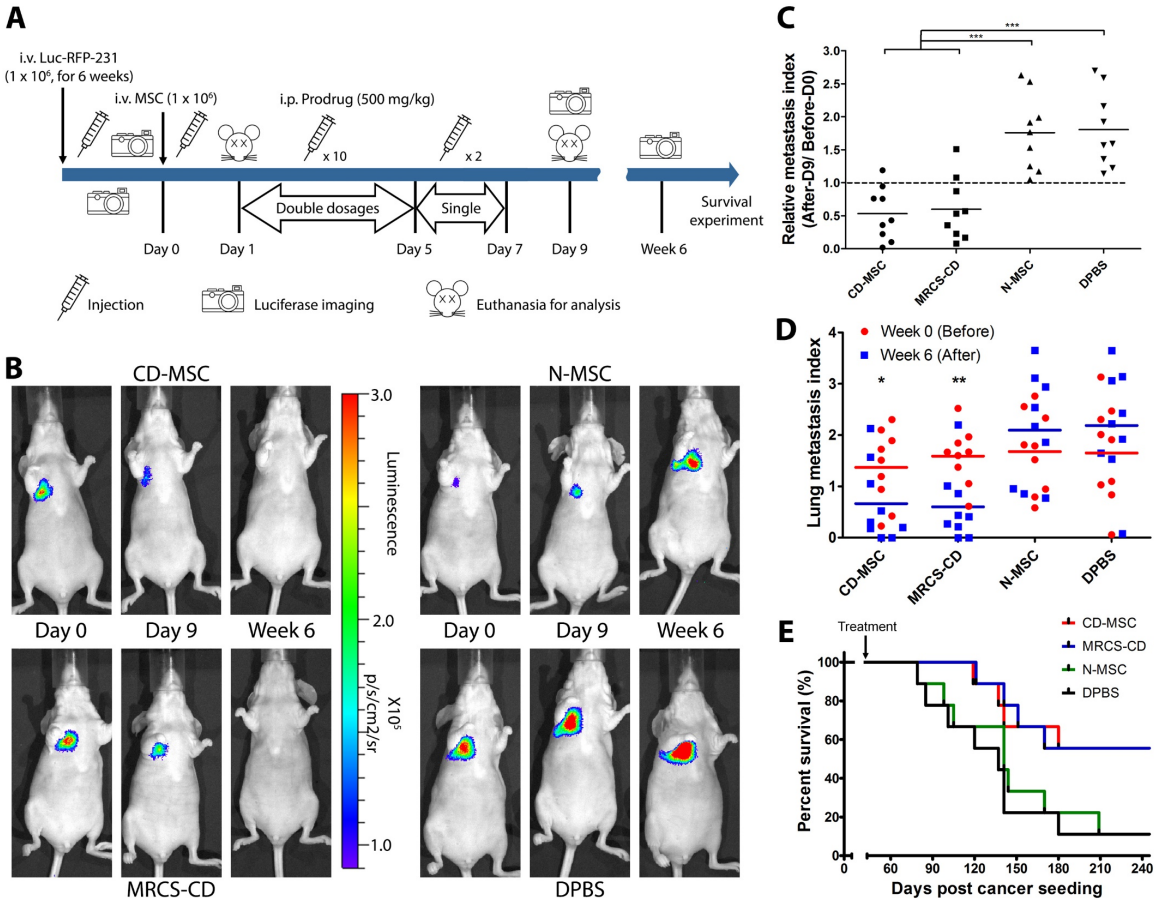

Figure 5.1. MRCS-CD killing cancer cells *in vivo*. (**A**) Design and timeline of animal experiment to test MRCS-CD with 5-FC *in vivo*. (**B**) Representative pictures of nude mice that received MRCS-CD treatments show that MRCS-CD decrease lung metastasis signals *in vivo*. Luciferase imaging was taken before (D0, left panels) and after 5-FC treatment short-term (D9, middle panels), as well as long-term (6 weeks, right panels). Quantification of luciferase signals that are proportional to cancer mass in the lungs shows that MRCS-CD are able to decrease lung metastasis signals *in vivo* both for (**C**) short-term and (**D**) long-term and (**E**) increase mice survival (Kaplan-Meier curve). In panel **C**, Relative Metastasis Index (RMI) = Luciferase read on D9 (after) / Luciferase read on D0 (before). In panel **D**, Lung Metastasis Index (LMI) = Log_{10} [(Luciferase read of the tested mouse) / (Luciferase read of tumor-free mice average)]. *i.e.*, the LMI of tumor-free mice = 0. The differences between "week 0" groups are not statistically significant. $n = 9$ for each group. $*P < 0.05$, $**P < 0.01$ and $***P < 0.001$. Error bar: mean ± S.D.. In panel **E**, *P* value: *CD-MSC vs. DPBS = 0.0382; *MRCS-CD vs. N-MSC = 0.0429; *MRCS-CD vs. DPBS = 0.0211. Median survival (Days): CD-MSC: 260; MRCS-CD: 260; N-MSC: 141; DPBS: 137. CD-MSC: Constitutive positive control; N-MSC: Native MSCs.

We utilized the reporter most specifically and robustly activated at the metastatic niche (MRCS-CD, described in Chapter 3) to locally activate a pro-drug *in vivo*. As intravenous

delivery of MSCs, used in most clinical trials, leads to initial entrapment of large numbers of MSCs in the pulmonary vasculature, localized activation of a pro-drug, rather than constitutively expressing a drug, at only the metastatic niche is desirable to avoid potential adverse toxicity in the pulmonary and other organ systems[6, 8]. To these ends, we used the pro-drug convertase, CD, engineered to be expressed by our MRCS (MRCS-CD) coupled with systemic 5-fluorocytosine (5-FC) infusion[12, 13], hence treating breast cancer lung metastasis in murine models.

5.3 RESULTS

5.3.1 Establishment of murine models bearing breast cancer metastases

As a model of breast cancer metastasis to the lung, we utilized an MDA-MB-231 xenotransplantation model in mice. We chose MDA-MB-231 cells because they secrete large amounts of LOX which leads to increased crosslinking of collagen fibrils in the lung that is essential for metastasis[14, 15] (see details in Chapter 6). In addition, inhibition of LOX is sufficient to prevent breast cancer metastasis of MDA-MB-231 cells[16]. MDA-MB-231 cells were engineered to express reporters including eGFP (eGFP-231) or firefly luciferase plus RFP (Luc-RFP-231) and seeded via tail vein injection in immune-compromised mice to first establish the metastases in the lung (4-6 weeks following cancer infusion) (Figure 5.1A, 5.1B, animals on Day 0) prior to MSC infusion. In this study, we utilized two sets of immune-compromised mice: *Foxn1*^{nu} (nude) and Nonobese diabetic/severe combined immunodeficiency gamma (NSG). We primarily focused on the nude mice system as it is partially immune-compromised and therefore more likely recapitulates the clinical setting than NSG. They also have better health conditions than NSG mice after cancer seeding so it allowed us to monitor the course of treatment for a longer period[17]. On the other hand, NSG mice are more robust and rapid in establishing the

tumor, and therefore were also used when we examined MRCS tumor-homing and correlation between collagen crosslinking, tumor cells and MRCS activation in *ex vivo* immunofluorescence and second harmonic generation (SHG) experiments (Chapter 6)[17, 18].

Moreover, testing in a spontaneous metastasis model such as an orthotopic model, would further strengthen translational as well as overall impact by better demonstrating how the cell-based system is broadly applicable. We still utilized the MDA-MB-231 xenotransplantation model due to the reasons abovementioned. Briefly, MDA-MB-231 cells are stably transduced with luciferase and 10^7 tumor cells suspended in Matrigel orthotopically implanted into adult female nude mice[19-21]. Six to seven weeks post-injection, we monitored luciferase expression from metastasized cancer cells in the lung with an IVIS Imaging System. Upon noting significant increases in luciferase activity, compared to control group which was injected with only Matrigel (Figure 5.S1A, 5.S1B), we then sacrificed the mouse and collected lung tissue, observing obviously growing RFP signal from metastasized cancer cells (data not shown). Moreover, because the metastasis efficiency in orthotopical model was relatively low, we also tried NSG mice and we observed strong luciferase signal in lung 6 weeks post injection (Figure 5.S1C). The above-mentioned data shows that we have successfully established the *in vivo* MDA-MB-231 xenotransplantation orthotopic model (Figure 5.S1).

Besides, testing in a patient derived xenograft (PDX) model, which would faithfully resemble the original tumor from which they were developed with similarity maintained across passages would also boost translational and whole impact by enhanced indicating how our MRCS is sketchily valid. It can confirm whether our MRCS are constrained only to the cancer lines (*e.g.*, MDA-MB-231) exanimated[22]. Adult female NSG mice were ordered from the Jackson Laboratory (JAX) and allowed to form lung metastases with *i.v.* injection of dissociated

cells from tumor fragments (0.5-1 x 10^6 in PBS, tail vein injection after tumor dissociation and lentiviral labeling with Luc-RFP)[23] or orthotopic implantation (*in vivo* passage, a tissue fragment <5mm inserted) of a highly metastatic HCI-010 line (triple negative breast cancer line as MDA-MB-231; clinical metastatic sites: lung and lymph nodes) derived from patient breast tumors [24, 25] into the mammary fat pad. From data in Figure 5.S2, it shows that 6 weeks post tumor *i.v.* implantation of Luc-RFP labeled dissociated cells from HCI-010 fragments into female NSG mice, luciferase signal was shown in the tumor-bearing mice with *in vivo* IVIS imaging and the signals from the tumor-bearing lungs were also observed in *ex vivo* IVIS imaging. Those data suggests that our PDX model of beast cancer lung metastasis has been successfully established.

5.3.2 MRCS homing to and specifically activated at the metastatic niche *in vivo*

We and others have previously shown that MSCs home to both primary tumor and metastatic sites including breast cancers[26-28]. In this study, we first examined whether MSCs engineered to constitutively express firefly luciferase (Luc-MSC) are able to home to metastatic sites in the lungs. We systemically infused Luc-MSC to mice hosting human eGFP-231 breast cancer cells in the lung and tumor-free controls. We found that Luc-MSC homed to and persisted in lung metastatic sites (Figure. 5.S3). Next, we investigated whether MRCS can home to and be specifically activated at the tumor sites using MRCS-Luc which serves as a surrogate for MRCS-CD and allows us to readily track transplanted MRCS and monitor their activation using induced luciferase *in vivo*. We demonstrated that systemically infused MRCS-Luc homed to and were induced to express luciferase only in the tumor sites in the lung of eGFP-231 tumor-bearing mice (Figure 5.S4A, 5.S4B). The observed luciferase signal, which reflects the collective functional outcome of MRCS homing and activation at tumor sites, persisted in tumor-bearing mice for up to 1-2 days (Figure 5.S4B). Given that previous studies including ours have consistently

demonstrated that systemically transplanted MSCs can persist in tumor sites for up to a week, we suspect that some residue MRCS might exist in tumor after 2 days following transplantation but become undetectable due to the limited sensitivity of *in vivo* luciferase imaging[28]. Finally, we confirmed the *in vivo* homing and activation of MRCS-CD in Luc-RFP-231 tumor-bearing mice using *ex vivo* immunohistochemistry (IHC). We demonstrated MRCS-CD were co-localized with and locally activated to express CD at cancer sites in lung sections of tumor-bearing (but not tumor-free) mice (Figure 5.S4C, 5.S4D). Similar results were observed with the infusion of MRCS-eGFP (Figure 5.S5). Collectively, these data suggest that MRCS selectively home to and are specifically activated at the metastatic niche *in vivo*. This set of experiments also allowed us to identify time points at which MRCS are persisted and activated in tumor *in vivo* to guide later treatment (5-FC) schedule.

As we intended to use MSCs as passive sensors and vectors of the mechano-environment, we also investigated, such as, MRCS-eGFP activation at multiple time points to determine the earliest time point at which the MRCSs are specifically and robustly activated to minimize any potential biological effects (*e.g.*, secretion of proteases and ECM components[27, 29, 30]) that MSCs exert to modify their local environment in metastases. Mice were sacrificed 1, 2, 3, and 7 days following injection to investigate the clearance of the MRCS in the lung and activation status of our reporters assayed by confocal microscopy as described in the following subtask. We additionally stained for makers of metastasis and the metastatic niche to determine if areas of reporter activation correlate with metastases and LOX (Chapter 6).

We have characterized the activity of our reporters at the metastatic niche, and determined the optimal promoter for specific activation in the lung metastatic niche. Although several organs, including muscle (12 kPa)[31] and bone (25-40 kPa)[32], approach or exceed the

tissue stiffness of invasive breast cancer and may promote activation of our MRCS, we anticipate this will not be a major issue due to the inherent homing ability of MSCs to cancer and metastases and their rapid clearance from non-inflamed or injured tissues[33, 34]. Although MSCs will encounter blood vessel endothelial cells, basement membrane and ECM components, each with their own characteristic stiffness, while in transit to the metastatic niche, we do not expect this to permanently influence reporter activity[35, 36]. Previous studies have established that expression of mechano-responsive genes is rapidly reversible, which we will additionally characterize in Chapter 3[32].

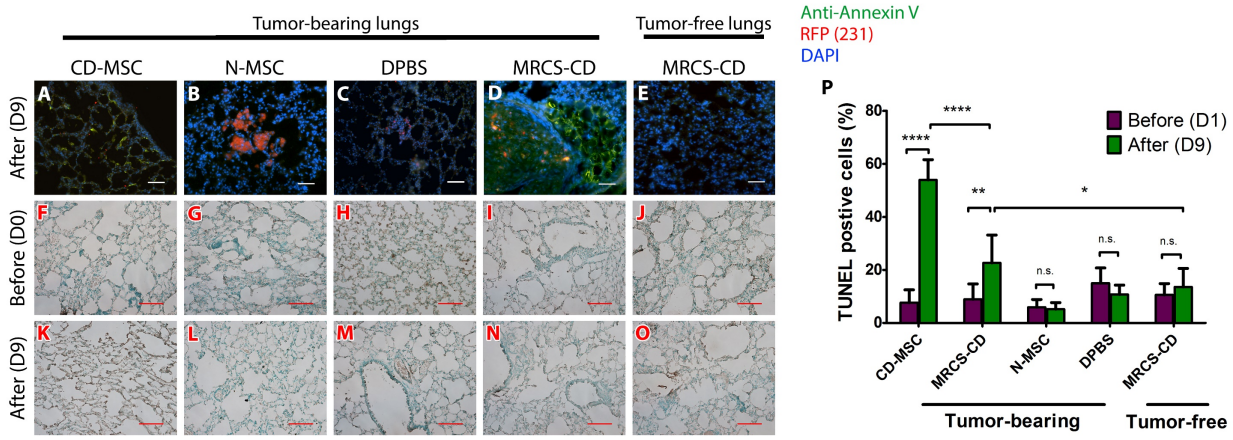

Figure 5.2. MRCS-CD killing cancer cells *in vivo* with minimal side effects. (**A** to **E**) Frozen sections of lungs of Luc-RFP-231 tumor-bearing and tumor-free nude mice sacrificed 24 hours following CD-MSC, MRCS-CD, N-MSC or DPBS infusion were stained with anti-Annexin V (green) and DAPI (blue). RFP signal (red) indicates the presence of lung metastasis. Scale bar = 100 μm. (**F** to **O**) Representative pictures of frozen section samples of tumor-bearing lungs and tumor-free lungs from nude mice treated by CD-MSC, MRCS-CD, N-MSC or DPBS before and after 5-FC injections by TUNEL assays. Horseradish Peroxidase (HRP) signals (brown) stand for damaged nuclei and green signals are methyl green counterstain of normal nuclei. Scale bar = 100 μm. (**P**) Quantification of TUNEL assay data indicate that MRCS-CD caused minimal lung tissue damage *in vivo*. n.s., not significant, $*P < 0.05$, $**P < 0.01$ and $****P < 0.0001$. Error bar: mean ± S.D.. CD-MSC: Constitutive positive control; N-MSC: Native MSCs.

5.3.3 MRCS-CD killing cancer specifically and with minimal side effects *in vivo*

We again made use of the MDA-MB-231 xenograft model described above to explore the effects of our localized therapy on disseminated breast cancer. To evaluate the efficacy of MRCS-CD for treating breast cancer lung metastasis, mice seeded with Luc-RFP-231 cancer for 6 weeks were given MRCS-CD (defined as Day 0) and subsequently prodrug 5-FC (500 mg/kg) and monitored for therapeutic outcomes (Figure 5.1A). Important controls include tumor-free mice and xenotransplanted mice injected with un-transduced MSCs and with MSCs constitutively expressing CD. MRCS-CD were administered 1 day prior to the start of prodrug treatment to allow time for co-localization with tumors in the lungs. 5-FC was given in multiple doses for 7 days, which is consistent to the typical MSC persistence period in the tumor. The amount of cancer within the lungs was quantified by measuring cancer luciferase signal using *in vivo* imaging (Figure 5.1B). Compared to initial values prior to prodrug treatment, luciferase signals were significantly decreased (and often disappeared) in mice treated with MRCS-CD and MSCs engineered to constitutively express CD (CD-MSC), both shortly after treatment (Day 9) and at 6 weeks after treatment. N-MSC and DPBS control groups failed to decrease lung metastasis signals, and in fact showed increase of cancer mass over time as cancer continued to grow, as expected. Cancer signals from after prodrug treatment (Day 9) were normalized to cancer signals before treatment (Day 0) for each mouse, which quantitatively demonstrated that CD-MSC and MRCS-CD significantly decreased the amount of cancer compared to N-MSC and DPBS groups that showed an increase in cancer burden (Figure 5.1C). In a longer term (6 weeks following treatment), CD-MSC and MRCS-CD treated groups maintained a lower amount of lung metastasis compared to the Day 0 baseline values and in fact, some mice appeared to have been “cured”, whereas N-MSC and DPBS groups saw an overall increase in cancer signals over

time (Figure 5.1D). Survival outcomes were also significantly improved by CD-MSC and MRCS-CD treatment compared to N-MSC and DPBS groups (Figure 5.1E). It should be noted that without 5-FC injection, MRCS-CD cannot attenuate cancer growth *in vivo* (Figure 5.S6). The data suggest that MRCS therapy can not only kill cancer rapidly *in vivo* but also have potential to prevent recurrence of cancer long-term. Note that, starting from Day 120 (Week 18), the survival rate of the MRCS treated group started to decline (Figure 5.1E), suggesting that in some animals, metastasis were decreased rather than totally cleared out by a single MRCS treatment. This demonstrates the potential need for repeated cell infusion together with prodrug administration in future work[37].

As intravenous delivery of MSCs, used in most clinical trials, leads to initial entrapment of large numbers of MSCs in the pulmonary vasculature, localized activation of a prodrug, rather than constitutively expressing a drug, at only the metastatic niche is desirable to avoid potential adverse toxicity in the pulmonary and other organ systems[8, 34]. Though CD-MSC and MRCS-CD had similar treatment outcomes in terms of efficacy, constitutively expressing CD would convert systemically infused 5-FC indiscriminately on tumor-bearing and tumor-free tissue alike. MRCS-CD, however, would only express CD to activate 5-FC conversion at sites of metastasis with the unique mechano-property and therefore have less damaging systemic side effects. To examine the side effects of MRCS-CD and compare it to CD-MSC, we used immunostaining of Annexin V and Terminal deoxynucleotidyl transferase dUTP Nick End Labeling (TUNEL) assay (Figure 5.2A-5.2E). Staining for Annexin V to measure apoptosis showed the specific activation of MRCS-CD at metastatic sites (Figure 5.2D), whereas no comparable Annexin V signal could be seen on tumor-free tissue (Figure 5.2E). CD-MSC treated group stained positive for Annexin V non-specifically indicating extensive tissue damage (Figure 5.2A). Mice treated with N-MSC

or DPBS stained positive for tumor but not for Annexin V (Figure 5.2B, 5.2C), indicating either native MSC or DPBS infusion does not cause cytotoxicity. TUNEL analysis for damaged DNA further confirmed higher lung tissue damage in CD-MSC group than for any other group after treatment, including MRCS-CD (Figure 5.2F-5.2O for representative images, and Figure 5.2P for quantification). Specifically, MRCS-CD caused localized cell apoptosis only at the tumor sites with minimal lung tissue damage compared to constitutively CD-expressing control. In tumor-free mice, there was no significant increase in tissue damage after treatment with MRCS-CD, demonstrating specificity of activation only at tumor sites. Collectively, our data suggest that MRCS-CD kill cancer specifically with minimized side effects *in vivo* compared to MSC constitutively expressing therapeutics.

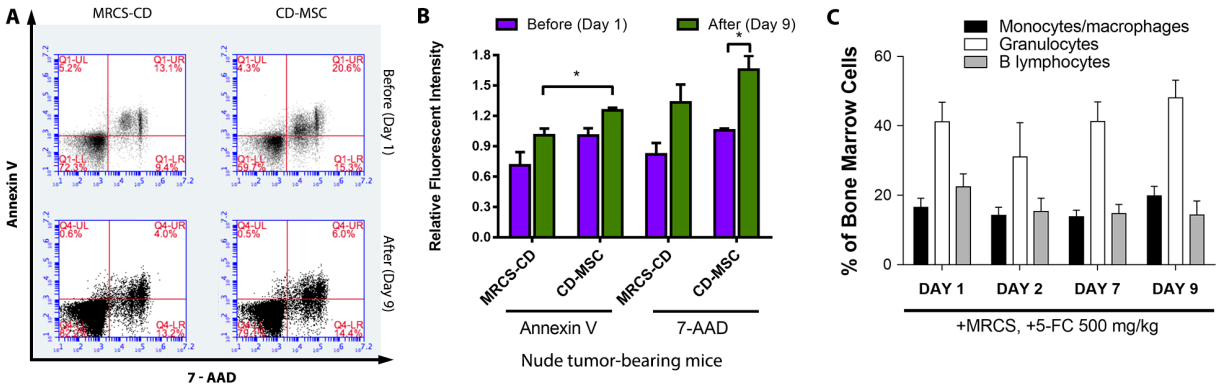

Figure 5.3. MRCS-CD causing minimal side effects *in vivo* in bones. (**A**) Luc-RFP-231 tumor-bearing and tumor-free nude mice treated by CD-MSC or MRCS-CD were sacrificed before (Day 1) and after (Day 9) 5-FC injections. Bones were harvested and bone marrow was flushed and stained with Annexin V and 7-AAD for FACS. (**B**) Quantification of FACS data indicate that MRCS-CD caused minimal bone marrow damage *in vivo*. (**C**) FACS show no significant difference on bone marrow cell population during the MRCS-CD treatment in the presence of 5-FC (Day 1, Day 2, Day 7 and Day 9 as indicated), showing minimal side effects on bone marrows from MRCS. *$P < 0.05$. Error bar: mean ± S.D.. CD-MSC: Constitutive positive control.

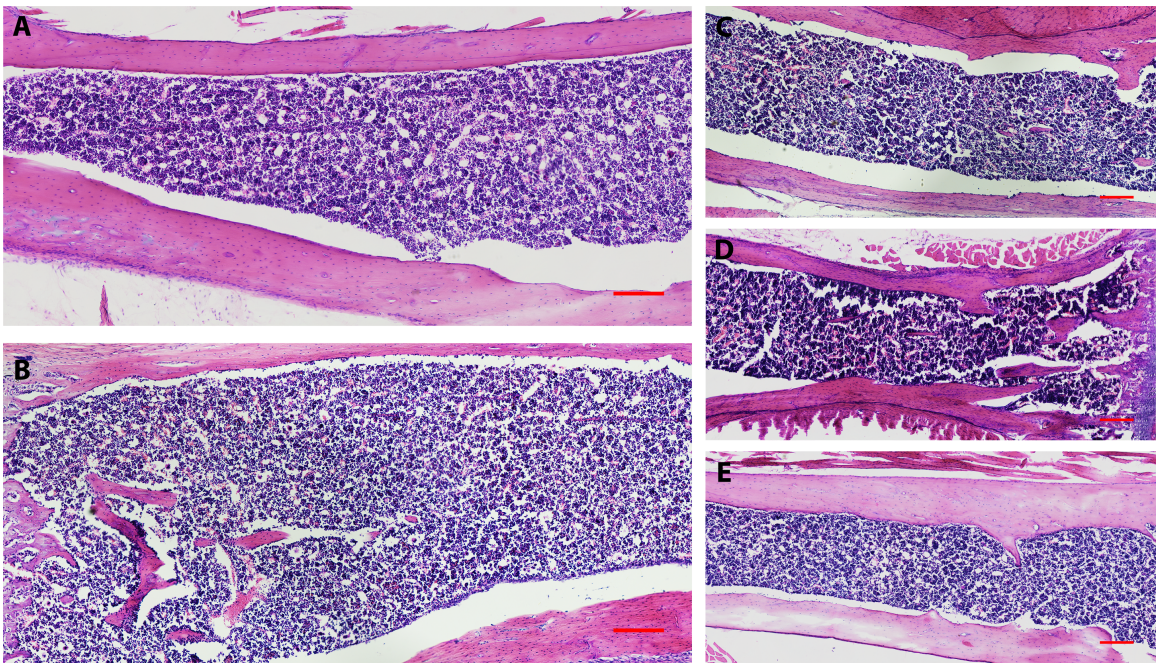

Figure 5.4. MRCS-CD causing minimal side effects *in vivo* in bone marrow. Representative pictures of sectioned bones with H&E staining indicate minimal tissue damage in bone marrow of tumor-bearing mice treated with, (**A**) CD-MSC or (**B**) MRCS-CD or tumor-free mice treated with (**C**) CD-MSC or (**D**) MRCS-CD or (**E**) that of tumor-bearing mice treated with native MSCs, accompanied with 5-FC treatment as indicated. Scale bar = 200 μm. CD-MSC: Constitutive positive control.

We briefly mention that other stiff regions of tissue are not targets where MSCs home, but stronger evidence would be showing the lack of MSCs and apoptosis in the animal models used. In order to rule out the potential off-target effects in other stiff tissues in the body, we performed experiments and collected new data to show the minimal systemic side effects of MRCS in some other tissues where the cells may home (Figure 5.3, 5.4 and 5.S7-5.S9). In particular we focused on potential deleterious effects to the bone marrow, since our MSCs are bone marrow-derived. We used flow cytometry for bone marrow cells and showed no significant increase in apoptosis or necrosis after treatment for both MRCS-CD and CD-MSC groups in nude (Figure 5.3A, 5.3B) and NSG (Figure 5.S7) mice. There was also no significant change in the bone marrow cell population after treatment (Figure 5.3C), showing that the bone marrow was not depleted by the MRCS-CD treatment compared to conventional chemotherapy [38]. In

other organs (paraffin embedded and H&E stained), we observed no significant tissue damage for either treatment group in bone marrow (Figure 5.4), liver (Figure 5.S8) or brain (Figure 5.S9). This is likely due to the lack of metastasis, as well as the lack of MSC homing to these other organs. The toxicity to the lungs, which is where both the tumors as well as the MSCs are localized, is our focus for this current study.

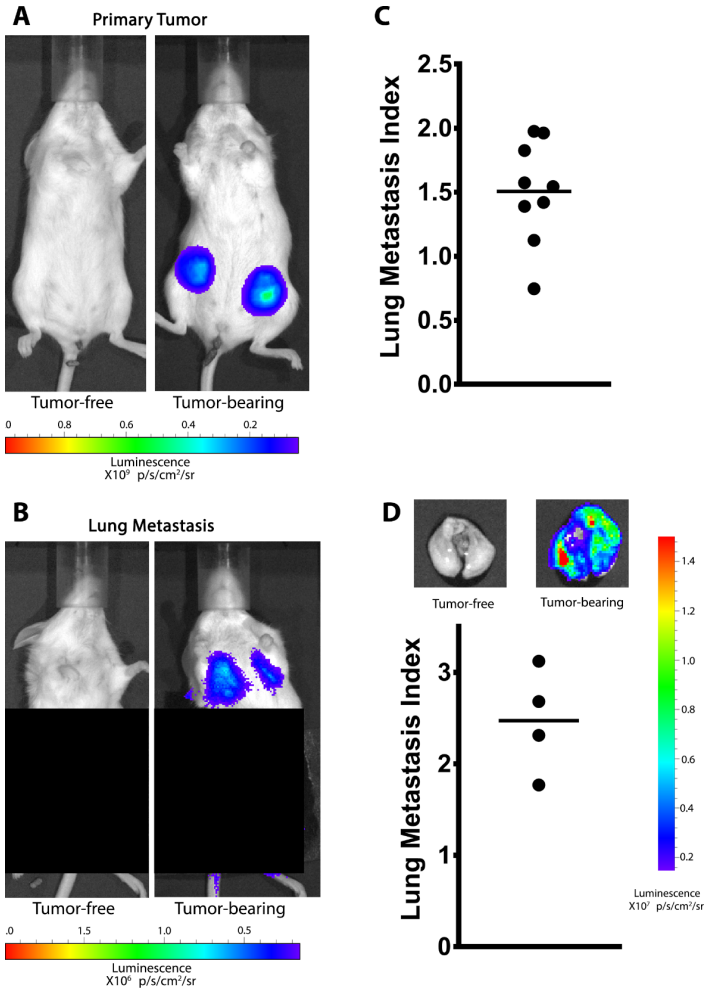

Figure 5.5. Spontaneous lung metastasis model establishment. (**A** to **C**) 6 weeks after subcutaneous implantation of Luc-RFP-231 into fat pad of female NSG mice, *in vivo* luciferase imaging was performed with an IVIS Lumina. Representative pictures of *in vivo* luciferase imaging of (**A**) primary tumors and (**B**) lung metastasis. (**C**) Quantification of luciferase activity of Luc-RFP-231 in the lungs of tumor-bearing NSG mice 6 weeks after Luc-RFP-231 implantation. (**D**) 6 weeks after Luc-RFP-231 implantation, tumor-bearing NSG mice were sacrificed and lungs were imaged with an IVIS Lumina. Lung Metastasis Index = Log_{10} [(Luciferase read of the tested tumor-bearing mouse/lung) / (Luciferase read of tumor-free mice/lungs average)]. *i.e.*, the LMI of tumor-free mice/lungs = 0.

5.4 DISCUSSION AND FUTURE DIRECTION

To demonstrate translatability, efficacy needs to be shown for a patient-derived xenograft (PDX) lung cancer line at a minimum. To address the issue of translatability of our MRCS platform, we have considered several more clinically relevant models: 1) A spontaneous model of breast cancer metastasis in the lungs 2) a spontaneous transgenic model and 3) two PDX models using orthotopic implantation or tail vein infusion of highly metastatic HCI-010 cells [24] derived from patient breast tumors that have been passaged in mice. The establishment of the spontaneous model is shown in Figure 5.5, which shows that lung metastasis does occur in the mice 6 weeks after implantation of cancer cells to the mouse fat pads. Though we were able to establish the PDX model, due to the long time it takes for tumors to grow and metastasize after implantation (4+ months), as well as current logistical problems of tracking unlabeled cancer cells, we will include this data for PDX in a future publication.

As for testing cancer xenograft outside the lung in other sites of metastasis, we focused on lung metastasis in this study for many reasons. Logistically, the animal models we used establishing cancer through tail vein injections or subcutaneous implantations will mainly result in lung metastasis [39]. These models were the easiest to establish and still achieve consistent metastasis with which to test our MRCS. Biologically, the metastasis of breast cancer to the lungs is prevalent and deadly, as addressed in the introduction, and for the scope of this paper we have made this type of metastasis our primary goal. For these reasons we chose these models of cancer to demonstrate a novel, proof-of-concept study of MRCS.

Future studies will be conducted to test the translatability of MRCS to metastasis in other sites. We could establish different animal models to ensure metastasis in other sites, for example

using portal vein injections of HCI-010 (0.5 x 10^6 in PBS) into adult female mice will result in PDX liver metastasis. Though it is true that MSCs do experience initial entrapment in the lungs, there is evidence in the literature that suggest MSCs are still capable of homing to primary tumor [40, 41] or metastatic sites other than lungs, including liver [42, 43], which we will be able to show for our MRCS in future work.

An important goal of our platform is to develop a method to selectively deliver therapeutic agents to the metastatic lung mechano-environment. To determine which reporter construct(s) (*e.g.*, *TUBB3*, *MYOD1,* or *RUNX2*) is most suited to this platform, we will perform image-based analysis of lung sections[44, 45]. Briefly, we will 1) quantify the integrated fluorescent intensity of each of the GFP reporters in the lung, 2) bin the intensities into "no", "low" and "high" groups, and 3) quantify average distance between metastases and/or LOX accumulation and reporter intensity in the "high" bin. The reporter with the shortest distance between "high" reporter activity and metastases/LOX accumulation will be selected as the metastatic niche specific promoter for targeted delivery of future therapeutics. We will also perform this analysis on lung tissue extracted at the time points described in the previous subtask to determine the optimal time following injection of our MRCS that produces robust and specific signal at the metastatic niche.

These abovementioned experiments will determine the specificity and degree of activation of, for instance, the MRCS-Luc and MRCS-GFP, and MRCS-High reporters in adult female PDX mice with lung metastases. In these experiments, the MRCS will express a GFP or Luc reporter under the control of aforementioned promoters. Model characterization will be performed to determine the time points for MRCS injection. Then, mice will be injected intravenously (tail vein) with 1 x 10^6 MRCS cells (either expressing GFP or Luc). At multiple

time points following injection (6, 24, 48, 72 hours and 7 days post-injection), mice will be imaged via IVIS Lumina (MRCS-Luc) or sacrificed via CO_2 inhalation and organs harvested for later analysis (MRCS-GFP).

Moreover, we will test the cell system in a spontaneous transgenic model (FVB/N-Tg(MMTV-PyVT)634Mul/J), which is the most commonly used model for the study of mammary tumor progression and metastasis. MMTV-PyMT is the model of breast cancer lung metastasis (80-94% in female tumor-bearing mice), in which MMTV-LTR is used to drive the expression of mammary gland specific polyoma virus middle T-antigen, leading to a rapid development of highly metastatic tumors[46, 47]. More importantly, a heterogonous stiffness profile of malignant tissues including lungs of MMTV-PyTM mice was reported[48]. This experiment will determine the specificity and degree of activation of the MRCS-Luc and MRCS-GFP, and MRCS-High reporters in adult female MMTV-PyMT mice with lung metastases. In these experiments, the MRCS will express a GFP or Luc reporter under the control of the promoters abovementioned. Adult female MMTV-PyMT mice (breeder pair ordered from JAX) will be allowed to form spontaneous lung metastases. Model characterization will be performed to determine the time points for MRCS injection. Then, mice will be injected intravenously (tail vein) with 1 x 10^6 MRCS cells (either expressing GFP or Luc). At multiple time points following injection (6, 24, 48, 72 hours and 7 days post-injection), mice will be imaged via IVIS Lumina (MRCS-Luc) or sacrificed via CO_2 inhalation and organs harvested for later analysis (MRCS-GFP).

Recruitment from the bone marrow and other organs represents the first key step in MSC homing to tumors[49]. It is reported that endogenous MSCs can mobilize from the bone marrow and other tissues to the peripheral blood under both normoxia and hypoxia, inflammation, and

injury conditions[50-52]. Moreover, this process is tightly regulated, with endogenous MSC-like cells only being isolated and cultured from the blood of mice subjected to femoral artery injury, but not from the blood of uninjured mice[51]. In addition, the field of MSC in cancer gene therapy has not advanced to the clinical setting primarily because of concerns that MSC might support tumor growth. While this is an important question to address, it is equally important to delineate the factor(s) and pathways that are responsible for the tumor tropism of MSC. The precise mechanism governing the migratory activities of MSC is not fully understood and may be dependent on different types of pathological insults.

As we intend to use MSCs as passive sensors and vectors of the mechano-environment, we will investigate MRCS activation at multiple time points to determine the earliest time point at which the MRCSs are specifically and robustly activated to minimize any potential biological effects (*e.g.*, secretion of proteases and ECM components[27, 29, 30]) that MSCs exert to modify their local environment in metastases. Mice will be sacrificed 1, 2, 3, and 7 days following injection to investigate the clearance of the MRCS in the lung and activation status of our reporters assayed by confocal microscopy as described in the following subtask. We will additionally stain for makers of metastasis and the metastatic niche in Chapter 6 to determine if areas of reporter activation correlate with metastases and LOX.

The novelty of this platform is in the use of the mechano-sensing promoter to drive facultative expression of CD in MSCs (MRCS), as opposed to the constitutively expressed CD system that has previously been shown in literature (CD-MSC). While the latter is used *in vivo* as a positive control, identical *in vivo* survival results are achieved. It is surprising that identical survival curves were achieved for the CD-MSC and MRCS-CD. It seems unlikely that every MRCS-CD cell would fully express the CD protein. This suggests that the MRCS-CD treatment

would deliver a less of the 5-FU therapeutic agent compared to CD-MRSC that should correlate with a slightly reduced survival. It is indeed intriguing to see similar survival curves for MRCS-CD and CD-MSC in Figure 5.1E. There are many factors in an *in vivo* setting as complicated as the cancer microenvironment which could lead to compound events that complicate the overall outcome. Survival is only measured as live or dead, and is an all or nothing collective measure of many beneficial and detrimental factors from the cell treatments. We did include more quantitative measurements of *in vivo* efficacy, in the amount of cancer signal remaining, in Figure 5.1C (short term) and Figure 5.1D (long term). The data was able to demonstrate that both MRCS-CD and CD-MSC treatment groups attenuated cancer signals significantly when compared to native controls, though the difference between these two treatment groups was not large enough to be significant.

One possible explanation for this phenomenon is that both MRCS-CD and CD-MSC were able to reach a threshold level of cancer killing, below which point the mice have levels of cancer below the limit of detection and thus reached similar cancer signals and survival. The survival curves shown in the current text cover a very long period of time, particularly in terms of the total mouse lifespan. It is unlikely, therefore, that one cell treatment course would have such long-lasting (lifelong) effects in these animals. To potentially see the difference between the MRCS-CD and CD-MSC groups, in the future we will fine tune a few parameters such as the initial tumor burden in the mice, the timing of MSC treatment, and the dosage of cells to more precisely compare treatment efficacy. It is also important to note that the MRCS-CD treatment has other advantages over the CD-MSC. Mice treated with CD-MSC exhibited overall signs of worse health: they had lower body weight, signs of inflammation, and abnormal behaviors. One potential explanation for this is that this *in vivo* imaging assay only detects the amount of cancer

being killed, but cannot detect the non-specific killing of other healthy tissue. However, we would like to emphasize the goal of the study is to demonstrate the efficacy of MRCS-CD in attenuating cancer, which we believe the data presented show. Future studies will be conducted to go beyond this proof of concept and better isolate and emphasize the effects of MRCS-CD.

In vitro data shown in Figure 4.3B indicates that CD-MSCs kill cancer cells quite effectively (10% survive) and *in vivo* AFM data provided a tissue stiffness of 17 kPa for tumor-bearing lung. *In vitro* assays performed on matrix with similar stiffness, 10 kPa, showed 40% of the cancer cells survive. This suggests that CD-MSC killing would be 4-fold more effective. We do agree that CD-MSC should be more effective at killing cancer compared to MRCS-CD, as reflected in our *in vitro* data. CD-MSC consistently show greater attenuation of cancer cell proliferation (Figure 5.1B), and higher conversion of pro-drug to active drug (Figure 5.1C) when compared to MRCS-CD. I*n vitro* and *in vivo* results may not exactly correspond because *in vitro* 2D gels cannot fully replicate the complex 3D cancer environment *in vivo* [53].

It is difficult to rectify how the MRCS system manages to both reduce toxicity yet still kills tumors and extends survival with the same effectiveness as the constitutive CD-MSC system. Presumably the reduced toxicity occurs because the 5-FU drug is turned off quickly. Our data shows gene expression drops to negligible levels within 48 hours. Certainly the prolongation of 5-FU production from 2 to 7 days would translate to more effective killing, yet could also explain the increased toxicity. Though the persistence of Luc-MSC in the homing experiment showed that some cells remained over a period of days, most of the cells do seem to clear out of the lungs by the end of 2 days (Figure 5.S3). This suggests that the amount of cells remaining after this period is negligible and cannot produce any significant amount of therapeutic. However, in transwell co-culture experiments, MRCS-CD on stiff substrate were able to kill

MDA-MB-231 cells in the presence of 5-FC to a significant level as compared to native MSC controls at starting at Day 2 (Figure 5.S10). This suggests that, despite the relatively short lifespan *in vivo*, they would still be able to noticeably attenuate cancer growth. In future studies we will be able to tune parameters such as cell dosage, number of injections, treatment timing, and initial cancer burden of the mice to better demonstrate any differences between the therapeutic benefits and side effects of MRCS-CD and CD-MSC.

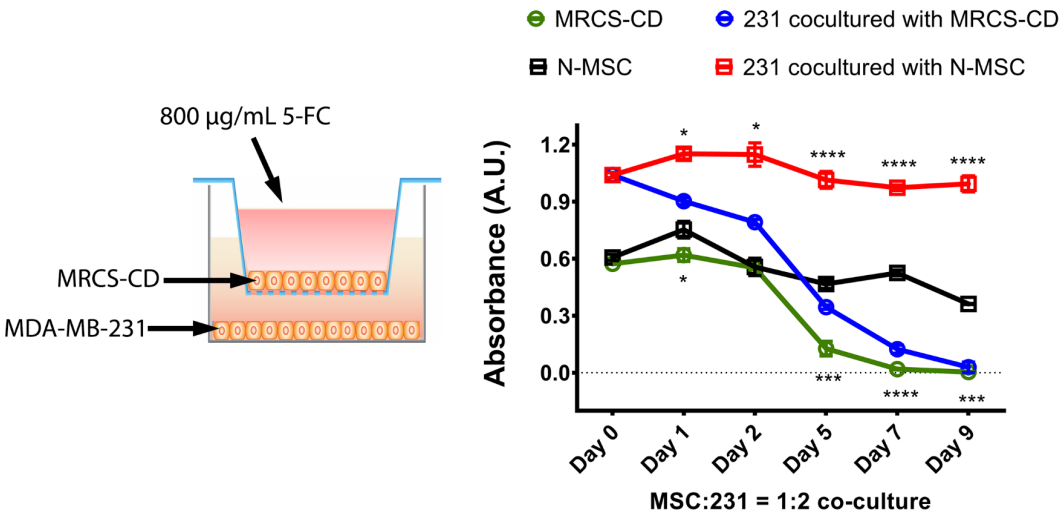

Figure 5.6. Bystander effect from MRCS-CD starting early *in vitro* on stiff substrate. Coculture of MRCS-CD (upper chamber) and MDA-MB-231 (bottom chamber) was performed using Transwell (MSC: 231=1:2) in the presence of 800 µg/ml 5-FC. On day 0 (cell seeding), day 1, day 2, day 5, day 7 and day 9, XTT assay was performed to measure the proliferation of cells. 231 proliferation started to significantly decrease from day 1 whereas that of MSCs was postponed, implicating that 231 cells are more sensitive than MSCs to 5-FU treatment. Error bar: mean ± S.D.. *$P < 0.05$, ***$P < 0.001$ and ****$P < 0.0001$. N-MSC: Native MSCs.

The accumulation of DNA damage with the prodrug and CD-MSCs or MRCS-CD suggests further damage with time and additional dosing. We have performed transwell experiments to determine the timing of cell killing for both cancer cells and MRCS-CD, shown in Figure 5.6. The data show that MDA-MB-231 cancer cells cultured with MRCS-CD begin to die off quickly between Day 2 and Day 5 (blue line), though a small decline can be seen as early as Day 1, whereas cancer cells cultured with native MSC do not cease proliferation (red line).

The MRCS-CD themselves also begin to die off within the same timeframe (green line) whereas the native MSC do not (black line).

We have 1) generated an MRCS for specifically converting 5-FC to its active form under stiff matrix conditions, 2) applied our MRCS to treatment of lung metastases in a mouse model of breast cancer, and 3) compared the efficacy and lung toxicity of our MRCS to other MSC-based systems. A potential pitfall is that the bystander effect of the CD/5-FC system may be too strong or weak to effectively treat metastases while sparing the normal lung. Multiple alternative methods exist to locally delivery therapeutics via transcriptional regulation of a promoter, including thymidine kinase[54], TRAIL[55], and IFN-β[6], which we will explore. In the future we are very interested in exploring the idea that our MRCS can be used to prevent metastases from forming by targeting the increased stiffness associated with the pre-metastatic niche as well. Experiments applying our system in autochthonous models of breast cancer and using mouse MSCs will also be informative in the future[46, 56]. Increased matrix stiffness is also associated with local invasion of the primary tumor and derangement of the vasculature; targeting these stiff areas of the primary tumor may both target the most invasive areas of the tumor and renormalize the vasculature for subsequent treatments[57-60]. We anticipate that in the future our MRCS will serve as a platform technology for targeting of specific tissue stiffness in multiple tissues and disease states.

5.5 MATERIALS AND METHODS

Transwell co-culture assays

MSCs (MRCS-CD or N-MSC) were plated on type I collagen (BD Biosciences)-coated 6.5 mm transwell culture inserts with pore size of 0.45 μm (Corning Life Sciences), while Luc-

RFP-231 cancer cells were plated on the lower chamber. After cell seeding, both of them were allowed to grow for 24 hours in MSC growth medium separately before the transwell got assembled. Then the MSCs and cancer cells started to be co-cultured with 800 μg/ml of 5-FC in MSC growth medium (Day 0). (Figure 5.6) On Day 0, 1, 2, 5, 7 and 9, respectively, XTT assays were performed to measure the cell viability. Procedures were similar to the above XTT section, except XTT reagents were collected after the incubation of the reagents, and redistributed to a new 96-well plate for measurement. XTT reagent was washed off with sterile PBS and MSC growth medium after each measurement. Cells were then re-incubated in growth medium until next time point of measurement. (Figure 5.S10) Inserts with MSCs were removed on Day 1, 2, 7 and 9, respectively, and an XTT assay was performed on Day 9. Served as controls, the readings from cancer cells without co-culture at the same time point were used for normalization.

Breast cancer lung metastasis animal models

0.5 x 10^6 (2.5 x 10^6/ml in Dulbecco's Phosphate-Buffered Saline (DPBS, Lonza)) LV-*CMV*::Luc-RFP MDA-MB-231 (Luc-RFP-231) or LV-*CMV*::eGFP MDA-MB-231 (eGFP-231) breast cancer cells were infused intravenously (*i.v.*) into immunocompromised female nude mice (8 weeks, #088, Charles River Laboratories) or NOD-SCID gamma (NSG) mice (8 weeks, #005557, The Jackson Laboratory). For the spontaneous metastasis model, 1 x 10^6 Luc-RFP-231 cells were implanted subcutaneously (*s.c.*) into the fat pads of female NSG mice (8 weeks). All animals injected with cancer cells or DPBS as healthy controls were picked randomly. All animal experiments and procedures were performed after the approval from the University of California-Irvine (UCI) Institution of Animal Care and Use Committee (IACUC protocol number 2012-3062) and conducted according to the Animal Welfare Assurance (#A3416.01).

Cell dissociation and patient-derived xenograft model establishment

Whole HCI-010 tumors were extracted and cut finely. 5 ml collagenase (Sigma) solution per gram of tissue was added to the cut tumors. Tumors were then incubated on a rotary shaker for 60 minutes at 37°C before spin down and washed with Hank's Balanced Salt Solution (HBSS, Thermo Fisher Scientific). Pellets were resuspeneded in primary growth medium and cultivated at 37°C with 5% CO_2. Primary cells were than transduced with Luc-RFP lentivirus as described in Chapter 2 and 3. Transduced cells were implanted *i.v.* into female NSG mice after overnight recovery. All animal experiments and procedures were performed after the approval from the University of California-Irvine (UCI) Institution of Animal Care and Use Committee (IACUC protocol number 2012-3062) and conducted according to the Animal Welfare Assurance (#A3416.01).

MSC transplantation and prodrug treatment

4 (NSG *i.v.* model) or 6 (nude *i.v.* model or NSG *s.c.* model) weeks after Luc-RFP-231 cell transplantation, 1 x 10^6 LV-*CMV*::eGFP MSCs co-transduced with MRCS-CD (eGFP-MRCS-CD), LV-MRCS-eGFP MSCs (MRCS-eGFP), CD-MSC, MRCS-CD, N-MSC (5 x 10^6 /ml in DPBS) or DPBS were *i.v.* infused into the mice harboring of breast cancer cells and into tumor-free control mice (Day 0) through tail vain. For second harmonic generation (SHG) imaging and immunohistochemistry (IHC) (*ex vivo*), animals infused with eGFP-MRCS-CD or MRCS-eGFP were euthanized *(n* = 3 for each group) 24 hours later (Day 1) and lungs were harvested. For cancer treatment experiment, Luc-RFP-231 tumor-bearing or tumor-free mice infused with CD-MSC, MRCS-CD, N-MSC or DPBS were intraperitoneal (*i.p.*) administered with 5-FC (500 mg/kg in DPBS) for 7 days (two doses/day for Day 1-Day 5 and one dose/day

for Day 6-Day 7). Representative mice (n = 3 for each group) were euthanized on Day 1 and Day 9 respectively for *ex vivo* assays (Figure 5.1A). For survival experiment, the endpoint of mice was defined as "found dead" or euthanasia criteria stated in UCI IACUC protocol 2012-3062.

In vivo and ex vivo bioluminescence imaging

4 (NSG *i.v.* model) or 6 (nude *i.v.* model or NSG *s.c.* model) weeks after Luc-RFP-231 cell transplantation, *in vivo* Luc activity from Luc-RFP-231 cells was measured (Day 0) as previously described[61]. Briefly, *in vivo* Luc signal was imaged with an IVIS Lumina (Caliper LifeSciences, MA) 10 minutes after intraperitoneal (*i.p.*) injection of D-luciferin (150 mg/kg in DPBS) into mice. Mice were anesthetized with 2-3% of isoflurane (Western Medical Supply, CA) and *in vivo* Luc activity was measured at the indicated time points. Before cancer treatment, nude mice with Luc signals in the lungs were imaged and grouped randomly and minimal adjustment was performed to keep the differences between "week 0" groups (red spots) not statistically significant (Figure 5.1D). After the cancer treatment experiments, *in vivo* Luc activity from Luc-RFP-231 cells was measured on Day 9 and 6 weeks after treatment (Figure 5.1A).

4 (NSG) or 6 (nude) weeks after eGFP-231 cell transplantation, 1 x 10^6 Luc-MSC, MRCS-Luc, N-MSC (5 x 10^6 /ml in DPBS) or DPBS were systemically infused into the mice harboring of breast cancer cells and into tumor-free control mice (Day 0). *In vivo* Luc activity was measured at the indicated time points.

6 weeks after *s.c.* Luc-RFP-231 cell transplantation, mice were sacrificed and lungs were harvested. 150 μg/ml D-luciferin was added onto the lungs and *ex vivo* Luc activity from Luc-RFP-231 cells in the lungs was measured with an IVIS Lumina.

Tissue processing, Histology and TUNEL assays

Lungs, livers and brains were collected from tumor-bearing or tumor-free nude mice (Day 0 or Day 9) and flash frozen in Tissue-Tek® O.C.T™ Compound (Sakura Finetek, CA), with overnight fixation in 4% PFA, and with overnight incubation in 30% sucrose solution (Amresco, OH). Frozen sections 8 μm thick were taken using a Reichert-Jung Cryocut 1800 microtome (Leica Instruments, Germany) onto UltraClear positively charged slides (Denville, 25 x 75 x 1 mm). Bones were fixed overnight in 4% PFA, then decalcified for 10 days in a 14% EDTA solution with 0.2% PFA in PBS prior to embedding in paraffin and sectioning with a Leica microtome.

Masson's trichrome staining was performed to assess extent of tissue crosslinking and fibrosis (Day 0). Slides were fixed in Bouin's solution (Sigma) overnight at room temperature, then briefly rinsed in tap water before further washing in water on a shaker for 20 minutes. Slides were stained in a working solution of Weigert's hematoxylin (1: 1 ratio of solution A and solution B, Sigma) for 8 minutes and washed thoroughly in running tap water. Slides were then stained in Biebrich scarlet-acid fuchsin solution (Sigma) for 5 minutes and washed in water. Slides were differentiated in a 1: 1 phosphomolybdic-phosphotungstic acid solution (Sigma) for 5 minutes. Slides were then stained in aniline blue solution (Sigma) for 5 minutes and differentiated in a 1% acetic acid (Sigma) solution for 2 minutes. Finally, slides were rinsed in water, then dehydrated with a few dips each in 70%, 90% and 100% ethanol and cleared for 1 minute in Histoclear (Thermo Fisher Scientific) before mounting with Permount (Thermo Fisher Scientific).

Terminal deoxynucleotidyl transferase dUTP Nick End Labeling (TUNEL) assay was performed to further assess tissue damage (Day 0 and Day 9). The ApoBrdU-IHC DNA Fragmentation Assay Kit (Biovision) was used with the included protocol. Data were analyzed with ImageJ (http://imagej.nih.gov/, NIH, MD).

Hematoxylin and eosin (H&E) was performed to assess systemic tissue damage in lung, liver, brain and bone. Slides were stained with Harris hematoxylin (Sigma) for 10 minutes, followed by acid alcohol (1% HCl in 70% ethanol), Scott's bluing reagent (Sigma) for 1 minute and Eosin Y (Sigma) for 5 minutes. Slides were dehydrated and mounted as previously described.

Ex vivo Immunohistochemistry

Lung tissues were harvested from tumor-bearing or tumor-free nude or NSG mice (Day 0 for LOX staining, Day 1 for MRCS homing and activation and Day 9 for Annexin V) and processed as abovementioned. Frozen slides (8 µm) were thawed and rehydrated in dH_2O for 5 minutes, then fixed in chilled acetone (Thermo Fisher Scientific) at -20°C for 10 minutes, permeabilized in 0.1% Triton X-100 for 10 minutes, and blocked in 0.1% Triton X-100 with 5% normal donkey serum for 1 hour. Primary antibodies (see Table 3.1) were diluted 1: 100 from the stock solution and applied overnight at 4°C. Slides were washed in 1X PBS. Then, secondary antibodies (see Table 3.2) were diluted 1: 500 from the stock solution and were applied for 30 minutes at room temperature. Slides were stained for nuclei with DAPI (1 µg/ml), then washed in PBS and mounted with Fluoromount-G. Slides were imaged with Nikon Eclipse Ti inverted microscope.

Bone marrow flushing and flow cytometry

1 day, 2 days, 7 days or 9 days after MSC infusion with 5-FC treatment as above mentioned, respectively, nude or NSG mice were sacrificed and bones, specifically femurs from both legs, were harvested with muscle tissue removed carefully. Bone marrow was then flushed with PBS and treated with red blood cell lysing buffer (Lonza). Blood cells left were then washed twice with PBS and diluted into 1 x 10^5 cells/ml. 300 µl of cells in suspension was then stained with (Figure 5.3A, 5.3B and 5.S7) anti-B220, anti-CD11b, anti-CD3e and anti-Gr1-PE-Cy7 or (Figure 5.3C) Annexin V-FITC (BioLegend, CA) and 7-Aminoactinomycin D dye (7-AAD, Thermo Fisher Scientific) after washing for 2 times. Finally, the resuspended cells were analysed with a BD Accuri™ C6 flow cytometry machine (BD Biosciences). Compensation and unstained controls were also prepared for the analysis.

Statistical Analysis

Data were analyzed by Student's *t* test when comparing 2 groups and by ANOVA when comparing more than 2 groups. Log-rank (Mantel-Cox) test was performed for animal survival data analysis by two-way ANOVA. Data were expressed as mean ± S. D. or mean ± S. E. M., and differences were considered significant at $P < 0.05$.

5.6 SUPPLEMENTAL MATERIAL

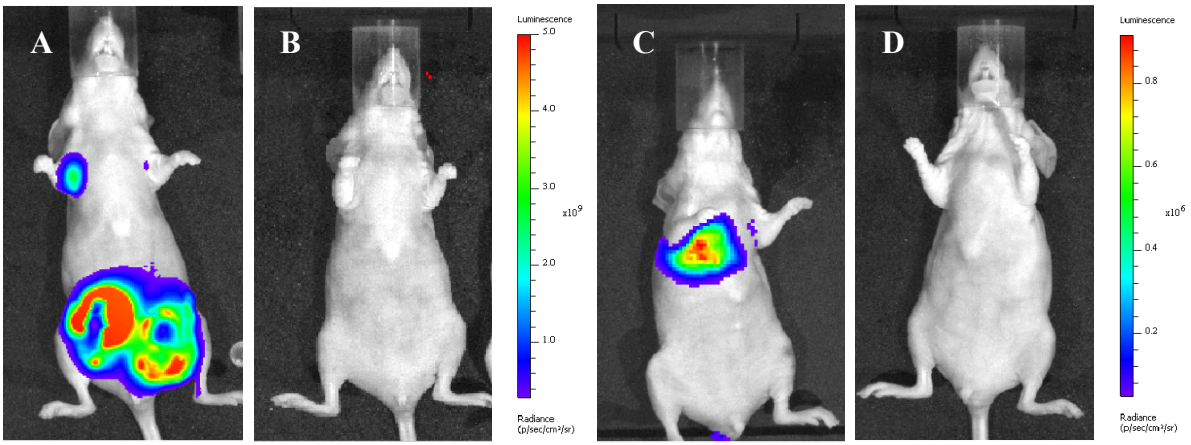

Figure 5.S1. *In vivo* luciferase imaging of MDA-MB-231 xenograft tumors in mice. (A) Nude mice developed large breast cancer tumors 7 weeks after orthotopic injections of luciferase expressing MDA-MB-231 cells with metastases in the lymph nodes and lungs as compared to Matrigel injected mice **(B)**. Nude mice developed robust tumors in the lungs 4 weeks after intravenous injections of luciferase expressing MDA-MB-231 cells **(C)** as compared to the PBS injected mice **(D)**. Luciferin – 15mg/kg.

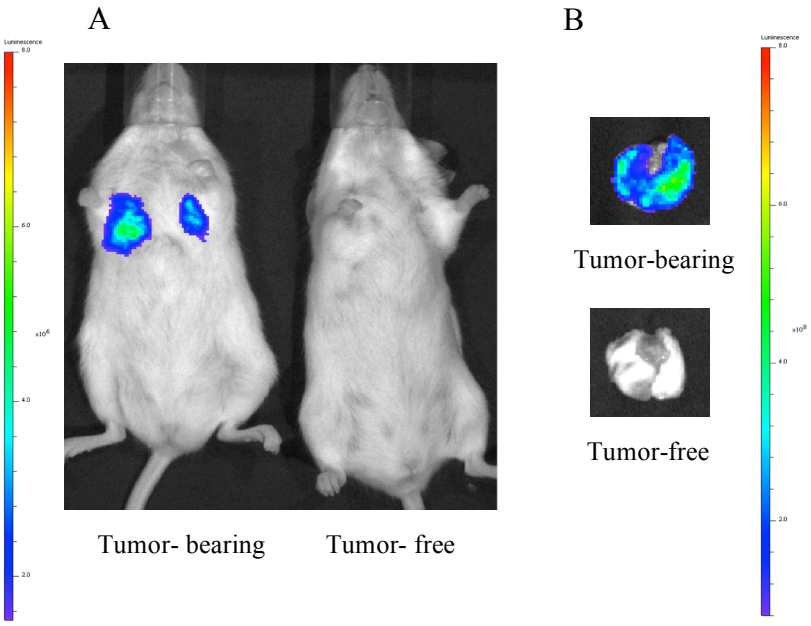

Figure 5.S2. A patient-derived xenograft (PDX) model has been established. (A) NSG female mice developed lung metastases 6 weeks after *i.v.* injection of 1 x 10^6 Fluc-RFP labeled dissociated cells from UCI-010 fragments. **(B)** Lungs were harvested after *in vivo* luciferase imaging and *ex vivo* IVIS imaging was performed to confirm the lung metastasis of PDX model.

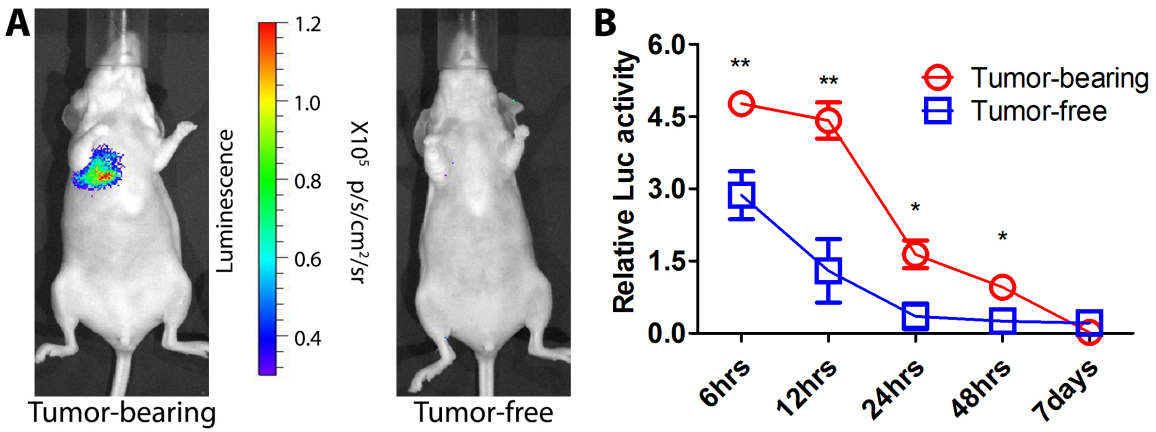

Figure 5.S3. Luc-MSC homing to the metastatic niche *in vivo*. (**A**) shows the representative pictures of *in vivo* luciferase imaging of systemically infused Luc-MSC 12 hours after MSC infusion. (**B**) Quantification of luciferase activity of Luc-MSC in the lungs of eGFP-231 tumor-bearing and tumor-free nude mice at different time points following systemic infusion. MSC persisted longer in tumor-bearing mice than in tumor-free mice until they were cleared out in approximately 1 week. The *in vivo* luciferase imaging was performed with an IVIS Lumina at the indicated time points. Relative Luc Activity = Log_2 [(Luciferase read of the tested mouse infused with Luc-MSC) / (Luciferase read of control mice average injected with DPBS)]. *i.e.*, the RLA of mice injected with DPBS = 0. $n = 4$ for tumor-bearing and $n = 3$ for tumor-free nude mice. Error bar: mean ± S.E.M.. * $P < 0.05$, ** $P < 0.01$.

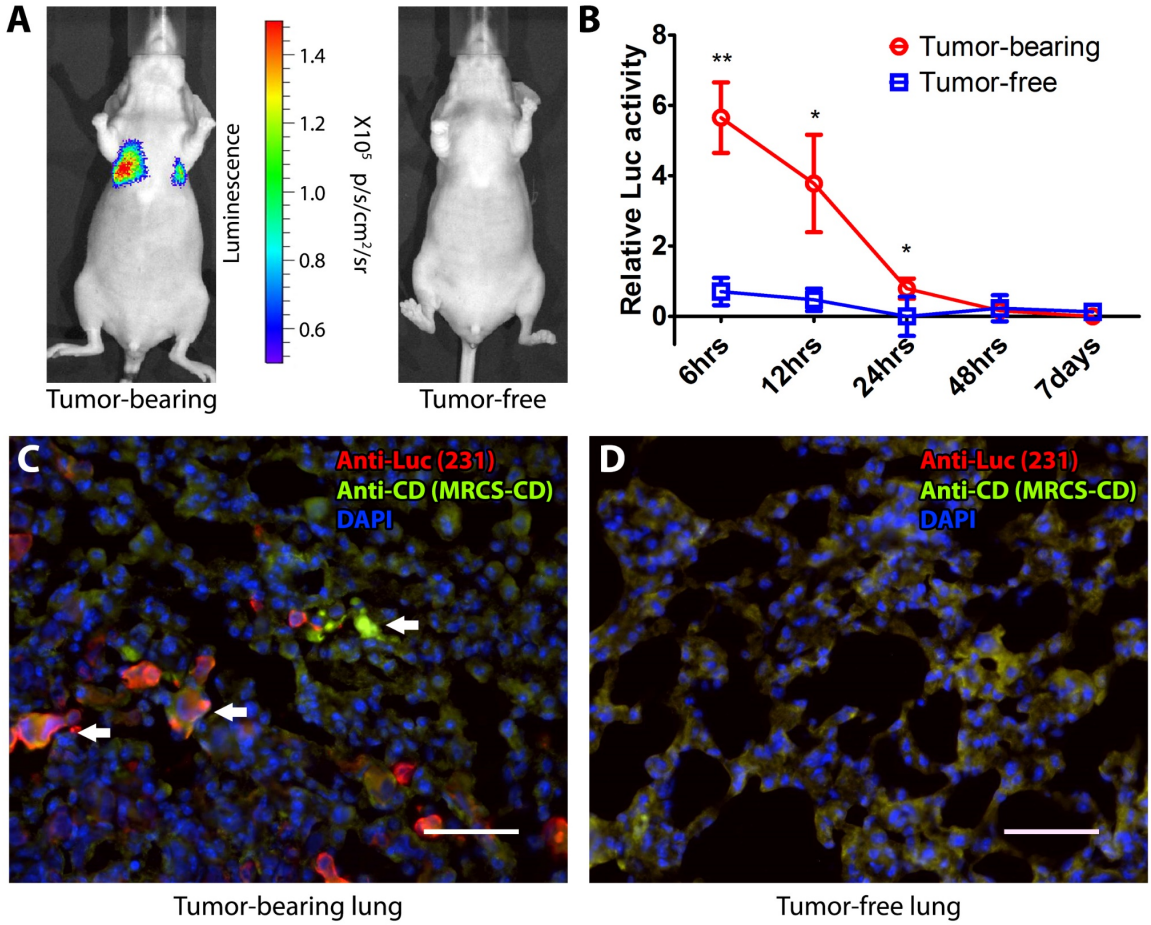

Figure 5.S4. MRCS homing and specific activation in response to the metastatic niche *in vivo*. (**A**) Representative pictures of *in vivo* luciferase imaging of systemically infused MRCS-Luc 12 hours after infusion. (**B**) Systemically infused MRCS-Luc were turned on in the lungs of eGFP-231 tumor-bearing nude mice but not tumor-free mice. Relative Luc Activity (RLA) = Log_2 [(Luciferase read of the mouse infused with MRCS-Luc) / (Luciferase read of control mice average injected with DPBS)]. *i.e.*, the RLA of mice injected with DPBS = 0. RLA were measured and plotted for tumor-bearing and tumor-free mice at different time points following systemic infusion of MRCS-Luc. $n = 4$ for tumor-bearing and n = 3 for tumor-free nude mice. Error bar: mean ± S.E.M.. * $P < 0.05$ and ** $P < 0.01$. (**C** and **D**) Frozen sections of lungs of Luc-RFP-231 tumor-bearing NSG mice and tumor-free NSG mice, respectively, sacrificed 24 hours after MRCS-CD infusion were stained with anti-Luc (red) for lung metastasis, anti-CD (green) for cytosine deaminase expressed by MRCS-CD and DAPI (blue). MRCS-CD were observed to home to and specifically activated to express CD at tumor sites. White arrows indicate the co-localization of lung metastatic sites and MRCS-CD expressing CD (turned on). Scale bar = 50 μm.

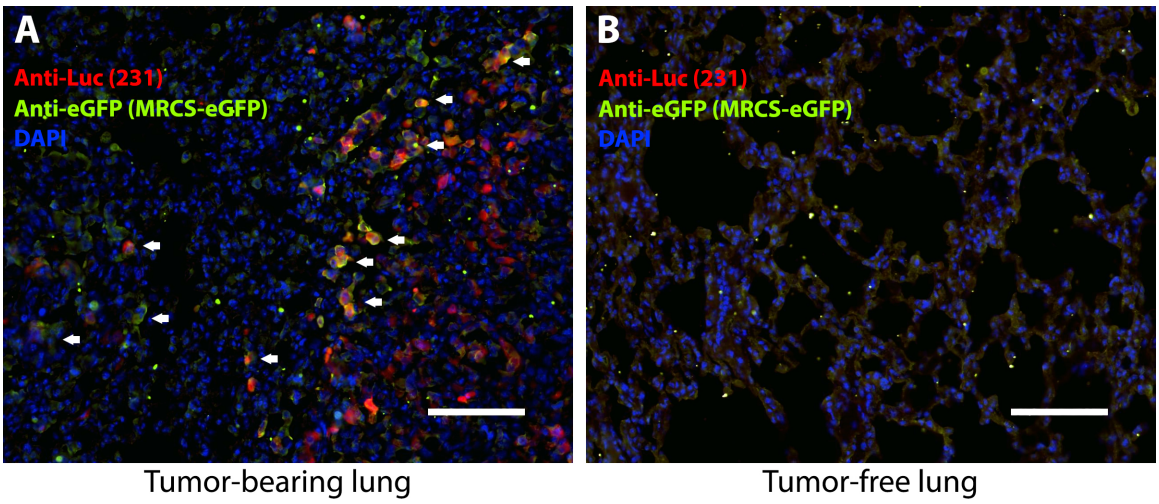

Figure 5.S5. Specific activation of MRCS-eGFP in response to the metastatic niche *in vivo.* MRCS-eGFP were observed to home to and specifically turned on at tumor sites in NSG mice. Frozen sections of lungs of (**A**) Luc-RFP-231 tumor-bearing mice and (**B**) tumor-free mice sacrificed 24 hours after MRCS-eGFP infusion were stained with anti-Luc (red) for lung metastasis, anti-eGFP for eGFP expressed by MRCS-eGFP (green) and DAPI (blue). White arrows indicate the co-localization of lung metastatic sites and MRCS-eGFP expressing eGFP (turned on). Scale bar = 100 μm.

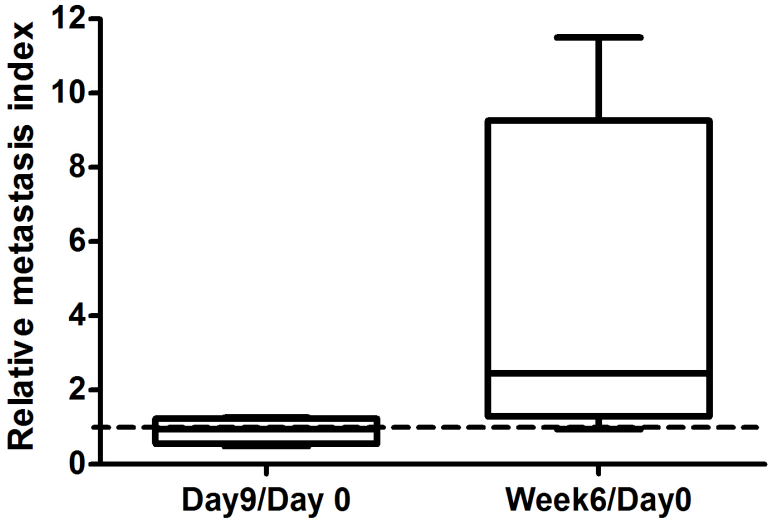

Figure 5.S6. MRCS-CD not able to attenuate cancer growth in the absence of 5-FC *in vivo.* 6 weeks after Luc-RFP-231 were seeded i.v. into nude mice, 10^6 MRCS-CD were administered systemically into tumor-bearing mice without 5-FC injection. *In vivo* luciferase activity was measured at different time points (before (Day 0), 9 days (Day 9) and 6 weeks (Week 6) after MRCS infusion) with an IVIS Lumina. These data show that MRCS-CD cannot kill cancer without the presence of 5-FC *in vivo*. Relative Metastasis Index (RMI) = Luciferase read on Day 9 or Week 6 (after) / Luciferase read on Day 0 (before). $n = 4$ for each group.

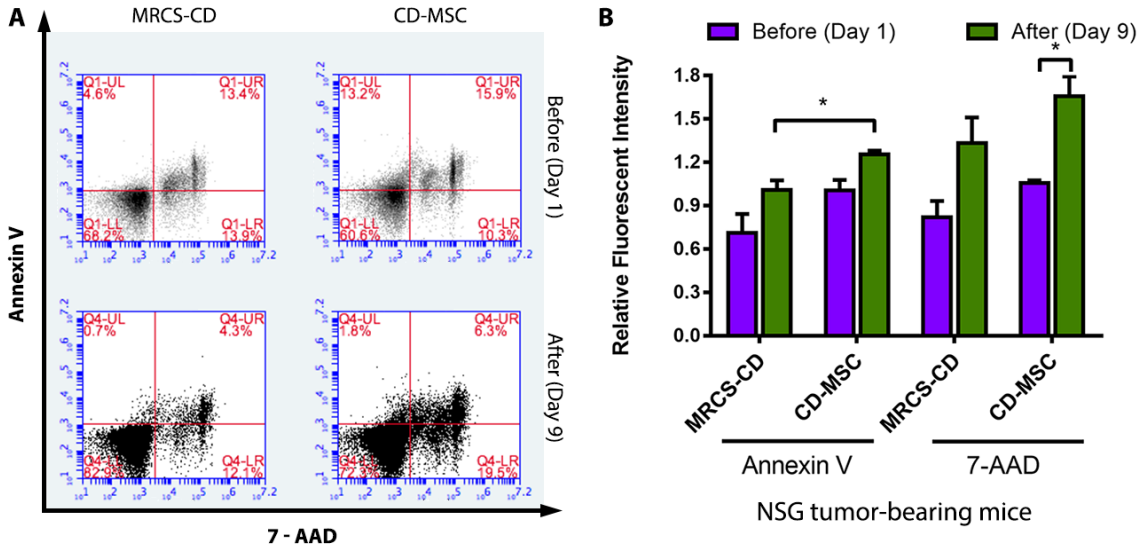

Figure 5.S7. MRCS-CD causing minimal side effects *in vivo* in bones. (**A**) Luc-RFP-231 tumor-bearing and tumor-free NSG mice treated by CD-MSC or MRCS-CD were sacrificed before (Day 1) and after (Day 9) 5-FC injections. Bones were harvested and bone marrow was flushed and stained with Annexin V and 7-AAD for FACS. (**B**) Quantification of FACS data indicate that MRCS-CD caused minimal bone marrow damage *in vivo*. *$P < 0.05$. Error bar: mean ± S.D.. CD-MSC: Constitutive positive control.

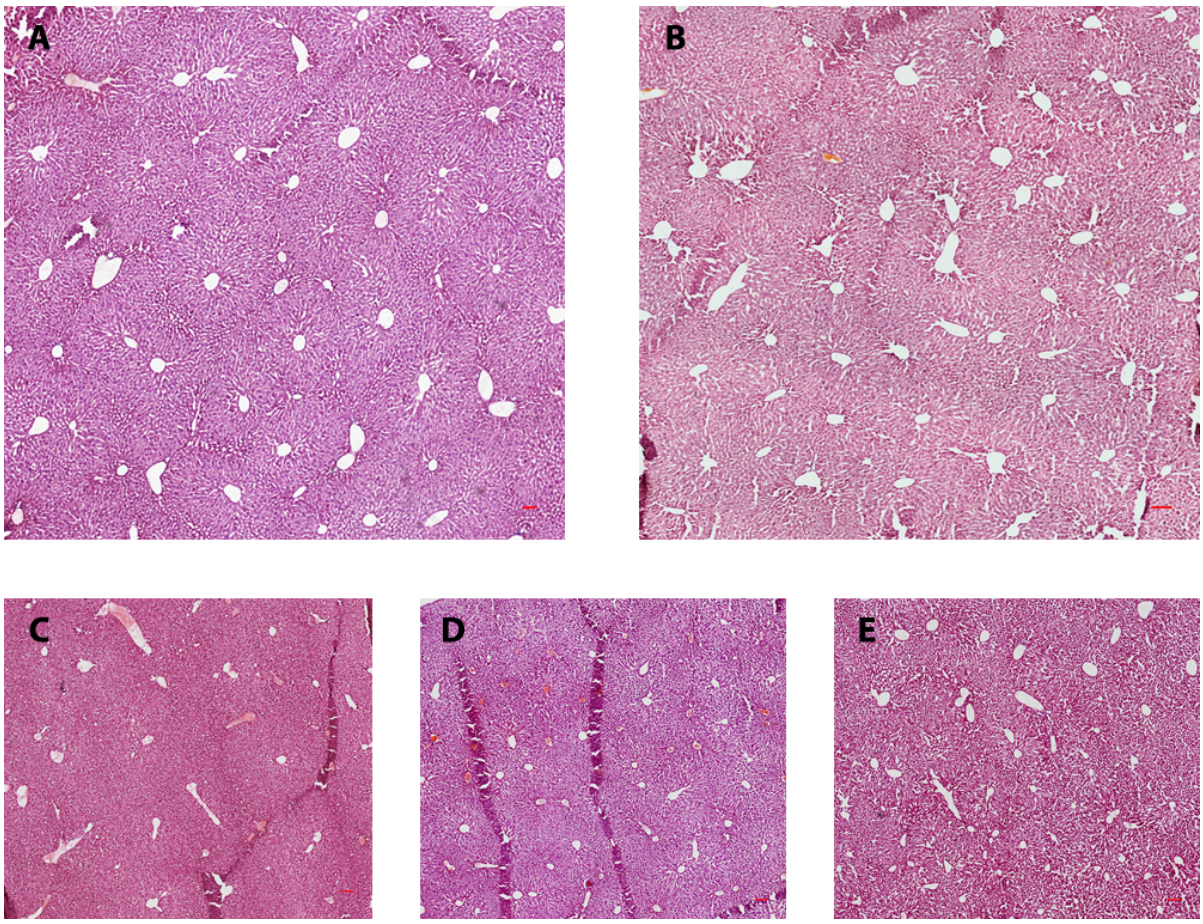

Figure 5.S8. MRCS-CD causing minimal side effects *in vivo* in livers. Representative pictures of sectioned bones with H&E staining indicate minimal tissue damage in livers of tumor-bearing mice treated with, (**A**) CD-MSC or (**B**) MRCS-CD or tumor-free mice treated with (**C**) CD-MSC or (**D**) MRCS-CD or (**E**) those of tumor-bearing mice treated with native MSCs, accompanied with 5-FC treatment as indicated. Scale bar = 100 μm.

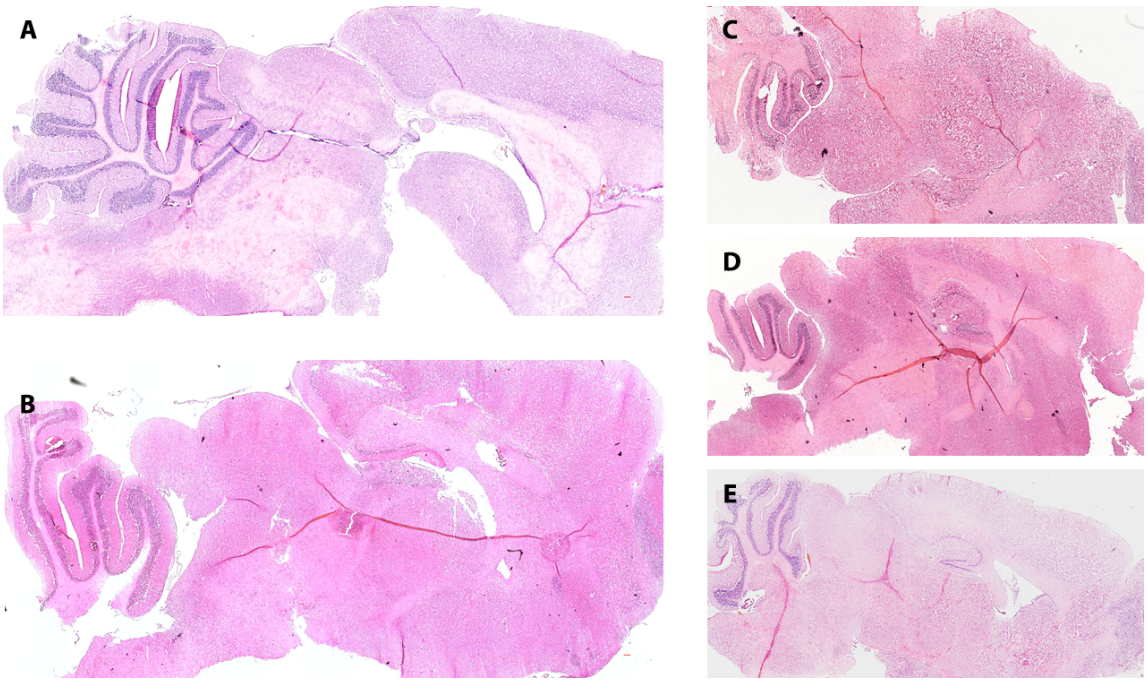

Figure 5.S9. MRCS-CD causing minimal side effects *in vivo* in brains. Representative pictures of sectioned bones with H&E staining indicate minimal tissue damage in brains of tumor-bearing mice treated with, (**A**) CD-MSC or (**B**) MRCS-CD or tumor-free mice treated with (**C**) CD-MSC or (**D**) MRCS-CD or (**E**) those of tumor-bearing mice treated with native MSCs, accompanied with 5-FC treatment as indicated. Scale bar = 100 μm.

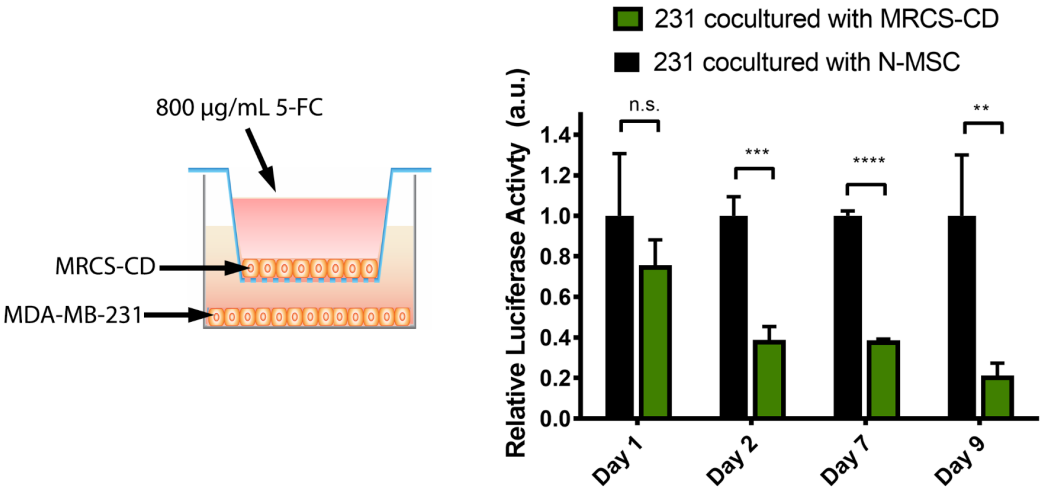

Figure 5.S10. Bystander effect from MRCS-CD lasting after MSC removal *in vitro* on stiff substrate. Coculture of MRCS-CD (upper chamber) and MDA-MB-231 (bottom chamber) was performed using Transwell (MSC: 231=1:2) in the presence of 800 μg/ml 5-FC. MSCs were removed on day 1, day 2, day 7 and day 9 and XTT assay was performed on day 9 to measure the proliferation of MSCs. 231 proliferation significantly decreased even when MRCS-CD were removed on day 2, indicating that the bystander effect may last after the clear out of MRCS-CD. n.s., not significant, $^{**}P < 0.01$, $^{***}P < 0.001$ and $^{****}P < 0.0001$. Error bar: mean ± S.D.. N-MSC: Native MSCs.

5.7 REFERENCES

1. Shah, K. Stem cell therapeutics for cancer. (John Wiley & Sons, Hoboken, N.J.; 2013).
2. Aboody, K.S. et al. Neural stem cells display extensive tropism for pathology in adult brain: evidence from intracranial gliomas. *Proceedings of the National Academy of Sciences of the United States of America* **97**, 12846-12851 (2000).
3. Aboody, K.S. et al. Neural Stem Cell–Mediated Enzyme/Prodrug Therapy for Glioma: Preclinical Studies. *Science translational medicine* **5**, 184ra159 (2013).
4. Shah, K. et al. Glioma therapy and real-time imaging of neural precursor cell migration and tumor regression. *Ann Neurol* **57**, 34-41 (2005).
5. Kim, S.M. et al. Gene therapy using TRAIL-secreting human umbilical cord blood-derived mesenchymal stem cells against intracranial glioma. *Cancer research* **68**, 9614-9623 (2008).
6. Studeny, M. et al. Bone marrow-derived mesenchymal stem cells as vehicles for interferon-beta delivery into tumors. *Cancer research* **62**, 3603-3608 (2002).
7. Studeny, M. et al. Mesenchymal stem cells: potential precursors for tumor stroma and targeted-delivery vehicles for anticancer agents. *Journal of the National Cancer Institute* **96**, 1593-1603 (2004).
8. Wang, H. et al. Trafficking mesenchymal stem cell engraftment and differentiation in tumor-bearing mice by bioluminescence imaging. *Stem Cells* **27**, 1548-1558 (2009).
9. Gao, J., Dennis, J.E., Muzic, R.F., Lundberg, M. & Caplan, A.I. The dynamic in vivo distribution of bone marrow-derived mesenchymal stem cells after infusion. *Cells Tissues Organs* **169**, 12-20 (2001).
10. Furlani, D. et al. Is the intravascular administration of mesenchymal stem cells safe? Mesenchymal stem cells and intravital microscopy. *Microvasc Res* **77**, 370-376 (2009).
11. Fischer, U.M. et al. Pulmonary passage is a major obstacle for intravenous stem cell delivery: the pulmonary first-pass effect. *Stem Cells Dev* **18**, 683-692 (2009).
12. Aboody, K.S. et al. Targeting of melanoma brain metastases using engineered neural stem/progenitor cells. *Neuro-oncology* **8**, 119-126 (2006).
13. Joo, K.M. et al. Human neural stem cells can target and deliver therapeutic genes to breast cancer brain metastases. *Molecular therapy : the journal of the American Society of Gene Therapy* **17**, 570-575 (2009).
14. Wong, C.C. et al. Hypoxia-inducible factor 1 is a master regulator of breast cancer metastatic niche formation. *Proceedings of the National Academy of Sciences of the United States of America* **108**, 16369-16374 (2011).
15. Xiao, Q. & Ge, G. Lysyl oxidase, extracellular matrix remodeling and cancer metastasis. *Cancer microenvironment : official journal of the International Cancer Microenvironment Society* **5**, 261-273 (2012).
16. Bondareva, A. et al. The lysyl oxidase inhibitor, beta-aminopropionitrile, diminishes the metastatic colonization potential of circulating breast cancer cells. *PloS one* **4**, e5620 (2009).
17. Fidler, I.J. Rationale and methods for the use of nude mice to study the biology and therapy of human cancer metastasis. *Cancer Metastasis Rev* **5**, 29-49 (1986).
18. Xie, X. et al. Comparative studies between nude and scid mice on the growth and metastatic behavior of xenografted human tumors. *Clin Exp Metastasis* **10**, 201-210 (1992).
19. Bandyopadhyay, A. et al. Doxorubicin in combination with a small TGFbeta inhibitor: a potential novel therapy for metastatic breast cancer in mouse models. *PloS one* **5**, e10365 (2010).
20. Tester, A.M. et al. Pro-matrix metalloproteinase-2 transfection increases orthotopic primary growth and experimental metastasis of MDA-MB-231 human breast cancer cells in nude mice. *Cancer research* **64**, 652-658 (2004).
21. Tekedereli, I. et al. Targeted silencing of elongation factor 2 kinase suppresses growth and sensitizes tumors to doxorubicin in an orthotopic model of breast cancer. *PloS one* **7**, e41171 (2012).
22. Aparicio, S., Hidalgo, M. & Kung, A.L. Examining the utility of patient-derived xenograft mouse models. *Nature reviews. Cancer* **15**, 311-316 (2015).
23. Chen, H.J. et al. Comprehensive models of human primary and metastatic colorectal tumors in immunodeficient and immunocompetent mice by chemokine targeting. *Nature biotechnology* **33**, 656-660 (2015).
24. Lawson, D.A. et al. Single-cell analysis reveals a stem-cell program in human metastatic breast cancer cells. *Nature* **526**, 131-135 (2015).
25. DeRose, Y.S. et al. Tumor grafts derived from women with breast cancer authentically reflect tumor pathology, growth, metastasis and disease outcomes. *Nat Med* **17**, 1514-1520 (2011).

26. Kidd, S. et al. Direct evidence of mesenchymal stem cell tropism for tumor and wounding microenvironments using in vivo bioluminescent imaging. *Stem Cells* **27**, 2614-2623 (2009).
27. Reagan, M.R. & Kaplan, D.L. Concise review: Mesenchymal stem cell tumor-homing: detection methods in disease model systems. *Stem Cells* **29**, 920-927 (2011).
28. Liu, L. et al. Exogenous marker-engineered mesenchymal stem cells detect cancer and metastases in a simple blood assay. *Stem Cell Res Ther* **6**, 181 (2015).
29. Potapova, I.A. et al. Mesenchymal stem cells support migration, extracellular matrix invasion, proliferation, and survival of endothelial cells in vitro. *Stem Cells* **25**, 1761-1768 (2007).
30. Ries, C. et al. MMP-2, MT1-MMP, and TIMP-2 are essential for the invasive capacity of human mesenchymal stem cells: differential regulation by inflammatory cytokines. *Blood* **109**, 4055-4063 (2007).
31. Engler, A.J. et al. Myotubes differentiate optimally on substrates with tissue-like stiffness: pathological implications for soft or stiff microenvironments. *The Journal of cell biology* **166**, 877-887 (2004).
32. Engler, A.J., Sen, S., Sweeney, H.L. & Discher, D.E. Matrix elasticity directs stem cell lineage specification. *Cell* **126**, 677-689 (2006).
33. Karp, J.M. & Leng Teo, G.S. Mesenchymal stem cell homing: the devil is in the details. *Cell stem cell* **4**, 206-216 (2009).
34. Ankrum, J. & Karp, J.M. Mesenchymal stem cell therapy: Two steps forward, one step back. *Trends in molecular medicine* **16**, 203-209 (2010).
35. Soofi, S.S., Last, J.A., Liliensiek, S.J., Nealey, P.F. & Murphy, C.J. The elastic modulus of Matrigel as determined by atomic force microscopy. *Journal of structural biology* **167**, 216-219 (2009).
36. Cox, T.R. & Erler, J.T. Remodeling and homeostasis of the extracellular matrix: implications for fibrotic diseases and cancer. *Disease models & mechanisms* **4**, 165-178 (2011).
37. Aboody, K.S. et al. Neural stem cell-mediated enzyme/prodrug therapy for glioma: preclinical studies. *Science translational medicine* **5**, 184ra159 (2013).
38. Shaikh, A., Bhartiya, D., Kapoor, S. & Nimkar, H. Delineating the effects of 5-fluorouracil and follicle-stimulating hormone on mouse bone marrow stem/progenitor cells. *Stem cell research & therapy* **7**, 59 (2016).
39. Fantozzi, A. & Christofori, G. Mouse models of breast cancer metastasis. *Breast Cancer Research* **8**, 212 (2006).
40. Dwyer, R.M. et al. Mesenchymal Stem Cell-Mediated Delivery of the Sodium Iodide Symporter Supports Radionuclide Imaging and Treatment of Breast Cancer. *STEM CELLS* **29**, 1149-1157 (2011).
41. Kanehira, M. et al. Targeted delivery of NK4 to multiple lung tumors by bone marrow-derived mesenchymal stem cells. *Cancer Gene Ther* **14**, 894-903 (2007).
42. Zielske, S.P., Livant, D.L. & Lawrence, T.S. Radiation Increases Invasion of Gene-Modified Mesenchymal Stem Cells into Tumors. *International Journal of Radiation Oncology*Biology*Physics* **75**, 843-853 (2009).
43. Li, G.-C. et al. Human mesenchymal stem cells inhibit metastasis of a hepatocellular carcinoma model using the MHCC97-H cell line. *Cancer Science* **101**, 2546-2553 (2010).
44. Kaneko, K. et al. Detection of peritoneal micrometastases of gastric carcinoma with green fluorescent protein and carcinoembryonic antigen promoter. *Cancer research* **61**, 5570-5574 (2001).
45. Contag, C.H., Jenkins, D., Contag, P.R. & Negrin, R.S. Use of reporter genes for optical measurements of neoplastic disease in vivo. *Neoplasia* **2**, 41-52 (2000).
46. Fantozzi, A. & Christofori, G. Mouse models of breast cancer metastasis. *Breast cancer research : BCR* **8**, 212 (2006).
47. Guy, C.T., Cardiff, R.D. & Muller, W.J. Induction of mammary tumors by expression of polyomavirus middle T oncogene: a transgenic mouse model for metastatic disease. *Mol Cell Biol* **12**, 954-961 (1992).
48. Plodinec, M. et al. The nanomechanical signature of breast cancer. *Nature nanotechnology* **7**, 757-765 (2012).
49. Droujinine, I.A., Eckert, M.A. & Zhao, W. To grab the stroma by the horns: from biology to cancer therapy with mesenchymal stem cells. *Oncotarget* **4**, 651-664 (2013).
50. Hong, H.S. et al. A new role of substance P as an injury-inducible messenger for mobilization of CD29(+) stromal-like cells. *Nat Med* **15**, 425-435 (2009).
51. Wang, C.H. et al. Late-outgrowth endothelial cells attenuate intimal hyperplasia contributed by mesenchymal stem cells after vascular injury. *Arterioscler Thromb Vasc Biol* **28**, 54-60 (2008).
52. He, Q., Wan, C. & Li, G. Concise review: multipotent mesenchymal stromal cells in blood. *Stem Cells* **25**, 69-77 (2007).

53. Shah, K. Mesenchymal stem cells engineered for cancer therapy. *Advanced Drug Delivery Reviews* **64**, 739-748 (2012).
54. Song, C. et al. Thymidine kinase gene modified bone marrow mesenchymal stem cells as vehicles for antitumor therapy. *Human gene therapy* **22**, 439-449 (2011).
55. Loebinger, M.R., Eddaoudi, A., Davies, D. & Janes, S.M. Mesenchymal stem cell delivery of TRAIL can eliminate metastatic cancer. *Cancer research* **69**, 4134-4142 (2009).
56. Soleimani, M. & Nadri, S. A protocol for isolation and culture of mesenchymal stem cells from mouse bone marrow. *Nature protocols* **4**, 102-106 (2009).
57. Byfield, F.J., Reen, R.K., Shentu, T.P., Levitan, I. & Gooch, K.J. Endothelial actin and cell stiffness is modulated by substrate stiffness in 2D and 3D. *Journal of biomechanics* **42**, 1114-1119 (2009).
58. Provenzano, P.P. et al. Enzymatic targeting of the stroma ablates physical barriers to treatment of pancreatic ductal adenocarcinoma. *Cancer cell* **21**, 418-429 (2012).
59. Levental, K.R. et al. Matrix crosslinking forces tumor progression by enhancing integrin signaling. *Cell* **139**, 891-906 (2009).
60. Ng, M.R. & Brugge, J.S. A stiff blow from the stroma: collagen crosslinking drives tumor progression. *Cancer cell* **16**, 455-457 (2009).
61. Liu, L. et al. Exogenous marker-engineered mesenchymal stem cells detect cancer and metastases in a simple blood assay. *Stem Cell Res Ther* **6**, 181 (2015).

CHAPTER 6

MECHANISM STUDY OF THE MRCS IN METASTATIC NICHE

6.1 ABSTRACT

In order to enhance the treatment of the cancer metastases, by leveraging the central role of the mechanoenvironment in cancer metastasis, we present a mechanoresponsive cell system (MRCS) to selectively identify and treat cancer metastases by targeting the unique biophysical cues in the tumor niche *in vivo*. Our MRCS targets cancer metastases in response to specific mechanical cues to deliver therapeutics to effectively kill cancer cells as demonstrated in a metastatic breast cancer mouse model. Our data suggests a strong correlation between collagen crosslinking and tissue-stiffness elevation at the metastatic sites where our MRCS are specifically activated by the unique, cancer associated mechano-cues. Finally, our MRCS will serve as a platform for future diagnostics and therapies targeting aberrant tissue stiffness including cancer and fibrotic diseases, and generate an entirely new technique to elucidate mechanobiology and to reveal what cells "feel" in their native environment *in vivo*.

Keywords: mesenchymal stem cell; lysyl oxidase; collagen crosslinking; stiffness; AFM; SHG; tissue apoptosis

6.2 INTRODUCTION

In the recent years, it has become less shadowy that mechanical and biophysical cues play a vital role in sustaining stem cell activities and functions[1]. Mechanical signals received by the local extracellular matrix (ECM), including particularly firmness, have been shown to regulate short and long-tern cellular activities, including morphological change and cell differentiation[2]. Specifically multiple recent publications have established that tissue and matrix stiffness is sufficient to drive expression of genes involved in MSC differentiation[2-6]. MSC differentiation is inherently a transcriptional program with each lineage defined by expression of characteristic transcription factors. This therefore allows us to use promoters regulating genes involved in MSC differentiation to drive expression of matrix stiffness-responsive reporters or therapeutics.

Intriguingly it is shown matrix stiffness directs 3-Dimension MSC differentiation in a similar manner to what was observed on 2-Dimension environments, but by altering integrin clustering rather than cell morphology[7]. In a covalently crosslinked hyaluronic acid hydrogel, however, it was shown that MSCs are differentiated into adipocytes independently of matrix stiffness, and once matrix is degraded, MSCs spread and undergo osteogenesis[8]. Whether this latter finding is related to the changes in hydrogel mechanical properties resulting from degradation is unclear, but combining these studies with a recent finding that the stress relaxation of gels regulates spreading, proliferation, and differentiation of MSCs[9, 10] suggests that matrix-stiffness-driven differentiation in 3-Dimension requires a labile environment where cells can generate traction forces and reorganize ligand binding.

It suggests that force can be transmitted from the matrix to the nucleus through physical connections between cytoskeletal and nucleoskeletal proteins, but how matrix stiffness influences long-term gene expression and cell fate is just beginning to be understood at the molecular level. Yes-associated protein (YAP) and transcriptional coactivator with PDZ-binding motif (TAZ) were shown to play a functional role in MSC differentiation by promoting expression of mechanosensitive genes upon matrix stiffening[11].

In spite of the abovementioned studies on stem cell and mechanobiology *in vitro*, more exploration should be performed to show how mechanotransduction plays a role *in vivo*[12, 13]. Cells constantly interact with their surrounding niche, which includes an array of complex biochemical and biophysical signals from the surrounding ECM. Although not appreciated historically, it has recently become evident that the physical and mechanical properties of cellular microenvironments (the so-called "mechano-niche") regulate important cell functions[14-18]. Important roles for matrix stiffness in driving breast cancer metastasis have been elucidated[19, 20]. Specifically, increased matrix stiffness, which is primarily driven by increased collagen deposition and crosslinking by lysyl oxidase (LOX) proteins, promotes breast cancer migration, invasion, cell plasticity, and eventual metastasis, primarily through regulation of integrin signaling[21]. Interestingly, LOX accumulation spatially correlates with the presence of metastases in both mouse models of metastasis and human patients[22]. In mouse models of breast cancer metastasis, secretion of LOX by the primary breast tumor leads to collagen crosslinking in discrete areas of the lung that promote formation of metastases[22-26]. Deposition of LOX at the metastatic niche correlates with both collagen linearization and formation of collagen-collagen covalent bonds in the lung parenchyma, both of which dramatically increase matrix stiffness[21]. Therefore, we reasoned that the unique mechanical properties of the metastatic niche might offer

a legitimate target for the development of diagnostics and therapeutics specifically targeting metastases.

We hypothesize that a cell-based system, specifically, mesenchymal stem cells (MSCs) can be used for such an approach to generate a mechano-responsive cell system (MRCS) that responds specifically to mechanoenvironmental cues to target breast cancer metastases (Figure 3.1). In light of the tight correlation between tissue stiffness and breast cancer metastasis and mechanotransduction-mediated MSC differentiation, we have developed a MRCS to directly target the mechanoenvironmental cues of breast cancer metastases for specific delivery of an anti-tumor agent, cytosine deaminase (CD) that locally activates prodrug 5-fluocytosine (5-FC) to kill cancer. Our study demonstrates that the MRCS specifically responds to matrix stiffness *in vitro*, and can selectively target and kill cancer metastases with minimal side effect *in vivo* that is mediated by biophysical and mechanical properties in the tumor microenvironment.

6.3 RESULTS

Secretion of LOX by the primary breast tumor leads to increased linearization and crosslinking of collagen at the metastatic niche associated with increased matrix stiffness[22, 24, 27]. We theorize that LOX accumulation correlates with increased matrix stiffness at the metastatic niche. This is supported by previous reports that 1) collagen linearization and crosslinking are robust surrogate markers of matrix stiffness[21, 28] and 2) that exogenous MSCs recruited to the metastatic lung assume an osteogenic differentiation profile associated with increased matrix stiffness not observed in the normal lung[29-31].

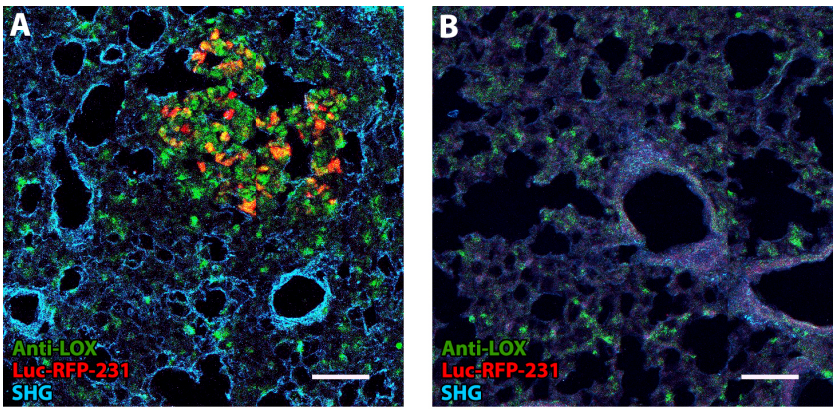

Figure 6.1. Lysyl Oxidase (LOX) expression upregulated and increased collagen expression in metastatic niche. (A and **B)** Representative frozen sections of lungs of Luc-RFP-231 tumor-bearing NSG mice and tumor-free NSG mice sacrificed before MRCS infusion, respectively, stained with anti-LOX (green), lung metastases (RFP, red) as well as second harmonic generation (SHG) imaging of collagen networks (cyan). The data indicate that the LOX expression was co-localized with lung metastatic sites and collagen crosslinking. Scale bar = 100 μm. (**C** and **D**) Trichrome staining assay was performed to show the degree of collagen expression in the lungs of tumor-bearing and tumor-free nude mice, respectively. Scale bar = 100 μm.

6.3.1 Characterization of the mechano-environment of the metastatic niche *in vivo*

It has been demonstrated that secretion of LOX by the primary breast tumor leads to increased linearization and crosslinking of collagen at the metastatic niche resulting in increased matrix stiffness[24]. Therefore, collagen linearization and crosslinking are robust surrogate markers of matrix stiffness. In addition, it has been reported that exogenous MSCs recruited to the metastatic lung assume an osteogenic differentiation profile but not observed in the normal lung[30], although whether this is mediated by matrix stiffness is unclear. To mechanistically

elucidate the activation and function of MRCS in metastatic niche *in vivo*, we first validated the correlation between LOX expression and collagen expression in metastatic tissues. A significant upregulation of LOX expression was observed in tumor-bearing lungs (Day 0) and correlated to the location of tumor cells, compared to that in tumor-free lungs (Figure 6.1A, 6.1B and 6.S1). Tumor-bearing lungs (Day 0) had higher collagen expression than tumor-free lungs by Masson's trichrome staining (Figure 6.1C, 6.1D), which is consistent to previous study[19]. In order to further explore the correlation between collagen crosslinking and metastatic niche, we performed second harmonic generation (SHG) imaging to co-localize collagen and lung metastases. SHG microscopy is a powerful modality for imaging collagen fibers (fibrillar network and linearization) relating to tissue environment with high specificity[21]. In close collaboration with Dr. Michelle A. Digman and the Laboratory for Fluorescence Dynamics at University of California-Irvine, we utilized the SHG two-photon microscopy coupled with immunofluorescence for, including LOX and metastatic cells to understand changes in stiffness that occur during metastasis. Briefly, SHG allows visualization of unlabeled collagen fibrils; the density and degree of linearization of collagen fibrils correlates tightly with mechanical stiffness and degree of crosslinking of the collagen[26, 32]. With SHG imaging high collagen expression was observed to co-localize with cancer metastasis (Figure 6.1A, 6.1B and 6.S2) and LOX expression (Day 0, Figure 6.1A, 6.1B). Intriguingly, we also observed that the collagen networks are significantly more linearized in cancer-specific region of tumor-bearing lungs than that in non-cancer region of tumor bearing lungs and tumor-free lungs (Day 0, Figure 6.2A to 6.2D and 6.S2A to 6.S2F (see Methods for collagen linearization quantification), which indicates that the metastatic niches in the lungs possess unique mechano-microenvironment. Tumor-bearing lungs (Day 0) were also confirmed to have higher stiffness compared to tumor-free lungs by atomic

force microscopy (AFM) (Figure 6.2E to 6.2H). To test our hypothesis that local accumulation of LOX in the lung parenchyma induces increases in matrix stiffness, we employed AFM microindentation to directly assay the stiffness of the metastatic niche. Briefly, unfixed lungs from mice with metastases were flash frozen, sectioned, and analyzed with AFM microindentation[33, 34] to generate a high-resolution force map (performed at the California NanoSystems Institute (CNSI) at University of California-Los Angeles). Force maps of tissue sections showed that, besides having higher overall Young's modulus (17.68 ± 25.63 kPa), tumor-bearing lungs are more heterogeneous in stiffness as compared to tumor-free lungs that were less stiff (1.61 ± 3.97 kPa) (Figure 6.2G, 6.2H). Together, this set of data suggests a strong correlation between metastasis, LOX expression, increased collagen expression/crosslinking/linearization, and elevated stiffness at the metastatic sites.

6.3.2 The activation and tumor-killing functions of MRCS *in vivo* mediated by tumor mechano-cues

In order to further study how our MRCS interacts with the metastatic niche with the unique mechano-property, we co-transduced the MRCS-CD to constitutively express eGFP as a cell tracker. We then performed SHG imaging with *ex vivo* IHC staining 24 hours after the systemic infusion of MRCS to tumor-bearing (Figure 6.2A, 6.2B) and tumor-free (Figure 6.2C) mice (Day 1). As observed on the SHG-IHC overlaid images, significantly more MRCS (characterized by the constitutively expressed eGFP) was observed in tumor-bearing lungs. Importantly, CD of eGFP-labeled MRCS-CD is preferentially activated in the cancer regions that are associated with more linearized collagen crosslinking (Figure 6.2A). By contrast, few MRCS was activated to express CD in less linearized non-cancer regions (Figure 6.2B) or in tumor-free lungs (Figure 6.2C). Collectively, this set of data, together with our previous MRCS tumor

homing data (Figure 5.S4, 5.S5) and MRCS-CD induced cell apoptosis at the metastatic sites (Figure 5.2D), strongly suggest that the activation and tumor-killing functions of MRCS *in vivo* are specifically mediated by the unique, cancer associated mechano-cues.

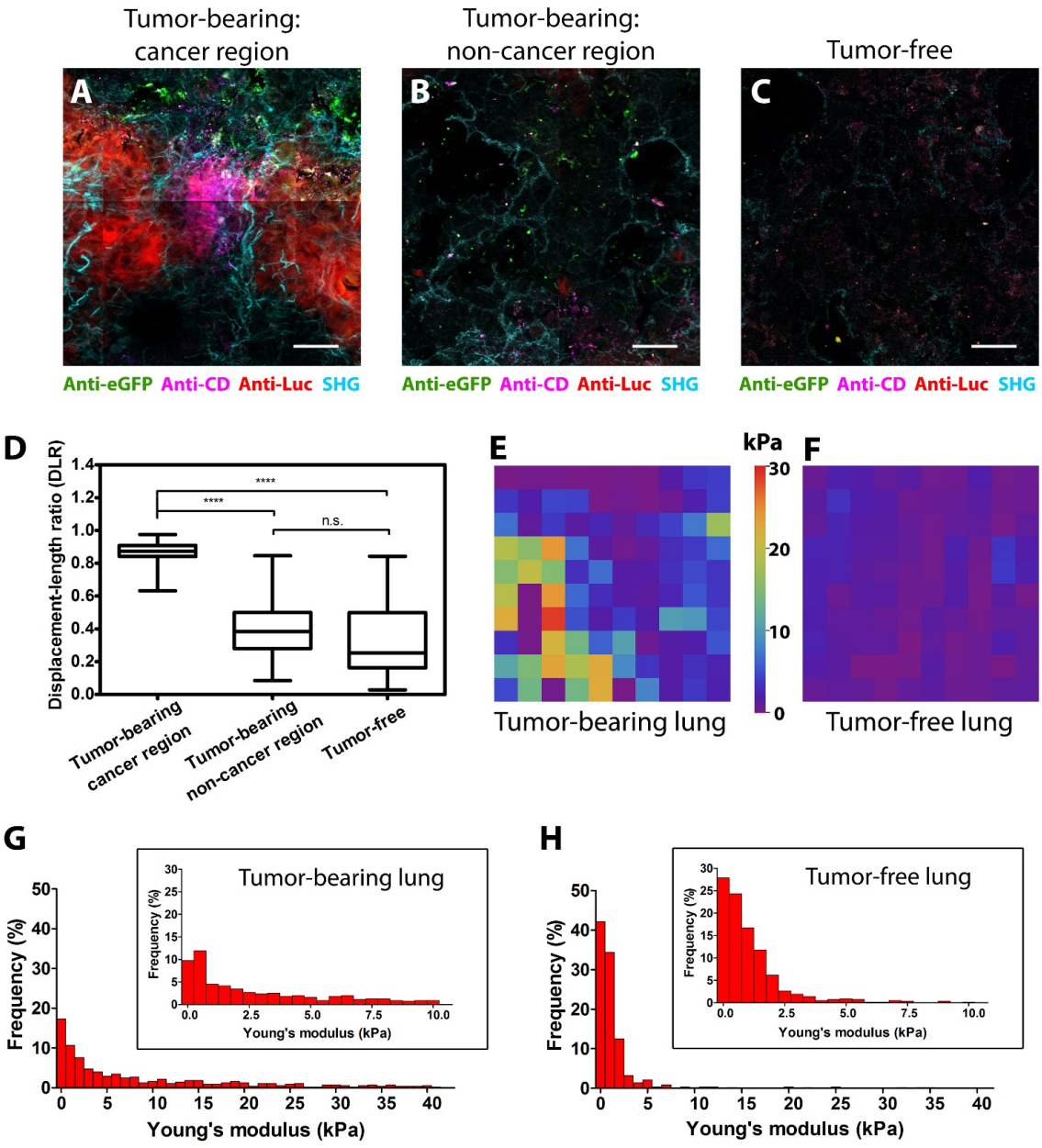

Figure 6.2. Specific activation of MRCS in response to mechano-cues in the metastatic niche *in vivo*. (**A** to **C**) Frozen sections of lungs of Luc-RFP-231 tumor-bearing NSG mice and tumor-free NSG mice sacrificed 24 hours after eGFP co-transfected MRCS-CD infusion were stained with anti-Luc (red) for lung metastasis, anti-CD (magenta) for cytosine (*continued*)

(*continued*) deaminase expressed by MRCS-CD and anti-eGFP (green) for MRCS-CD tracking. Second harmonic generation (SHG) imaging of collagen networks (cyan) was also presented and overlaid with IHC imaging. The data indicates that the MRCS-CD and its specific activation were co-localized with lung metastatic sites and collagen crosslinking and linearized networks. Scale bar = 50 μm. Multiple high quality images were generated and processed with ImageJ and Matlab, and then tiled into a large, stitched image. Each representative picture was then extracted from the tiled image. (see Methods) (**D**) Quantification of collagen linearization using displacement to length ratio (DLR) of collagen fibers in SHG images. Briefly, when the ratio = 1, it is a line while the ratio < 1, it is curved. The data shows that the collagen networks in cancer regions of tumor-bearing lungs of NSG mice are significantly more linearized than those in non-cancer regions of tumor-bearing lungs and in tumor-free lungs. Representative pictures are displayed in Figure 6.S2. n.s., not significant. ****$P < 0.0001$. (**E** and **F**) Representative Atomic Force Microscopy (AFM) stiffness maps (50 μm x 50 μm) of tumor-bearing and tumor-free lungs. (**G** and **H**) display the frequency of young modules values of tumor-bearing and tumor-free lungs from AFM micro-indentation fell into the range 0 ~ 40 kPa (bin size = 1 kPa) while the inset graphs show the frequency within the range 0 ~10 kPa (bin size = 0.5 kPa). AFM micro-indentation data show that the stiffness of tumor-bearing and tumor-free lungs from nude mice is heterogeneous and higher compared to that of tumor-free lungs from nude mice. ***$P <$ 0.001 (Young modulus of tumor-bearing lungs vs. tumor-free lungs).

Moreover, we have new data (Figure 6.3, 6.S3) to show the activation of death pathways in tumor cells within the lung tissue via PARP p85. The tumor-bearing: cancer region image shows higher crosslinking (SHG) signals as well as cancer signals (RFP), and also have higher expression of PARP (Figure 6.3A). The tumor-bearing: non-cancer region image shows parts of the lung from mice with cancer but without cancer in that particular section of the lungs. These regions have less crosslinking than the cancer regions of the lung and display less or no PARP (Figure 6.3B). The tumor-free image is from a healthy control mouse, with low crosslinking and no PARP signals (Figure 6.3C). Similar results were observed in a tail vein model, images for which are shown in Figure 6.4. In summary, with MRCS-CD, the apoptosis is correlated with cancer and increased crosslinked collagen. In CD-MSC there is apoptosis regardless of the tissue environment, with PARP signals present in highly crosslinked regions (Figure 6.S3C) but also in healthy controls (Figure 6.S3D).

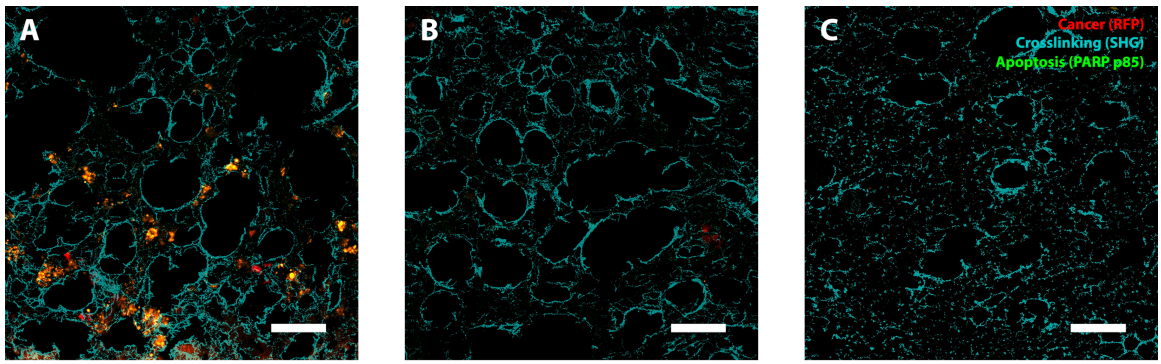

Figure 6.3. Crosslinking-specific tissue damage by MRCS in response to mechano-cues in the metastatic niche *in vivo*. Frozen sections of lungs of Luc-RFP-231 metastasis from primary tumors (tumor-bearing) NSG mice and tumor-free NSG mice sacrificed after MRCS-CD infusion and 5-FC treatment as indicated (Day 9) were stained with anti-PARP p85 (green) for tissue apoptosis. RFP signal (red) indicates the presence of lung metastasis. SHG imaging of collagen networks (cyan) was presented and overlaid with IHC imaging. (**A**) Tissue damage was only observed in lung metastatic sites with crosslinked collagen network but not in less crosslinked (**B**) non-cancer or (**C**) tumor free regions, indicating that the MRCS-CD and its specific tissue damage were co-localized (indicated as yellow) with lung metastatic sites and collagen crosslinking and linearized networks. Scale bar = 100 μm.

6.4 DISCUSSION AND FUTURE DIRECTION

Thus we have characterized changes in the lung metastatic niche that occur during metastasis. Furthermore, using well-established image analysis methods, we will quantify the density and linearity of collagen fibrils and examine its correlation with LOX accumulation and the presence of disseminated tumor cells (*e.g.*, RFP if the cancer cells are engineered, or cytokeratin (CK))[35, 36]. Performing a systemic analysis of the lung mechano-environment in this manner will allow us to better understand the dynamics of stiffness that occur in lung metastases within the established time points.

Also, as microindentation is non-destructive, we will subsequently fix lung sections and stain for LOX and cancer markers such as CK to determine if areas of increased lung tissue

stiffness correlate with LOX accumulation or metastases[34]. We can also try to merge the IHC imaging (such as MRCS activation or stiffness-specific tissue damage from the MRCS) together with the AFM force map. However, optimization of protocol will be necessary as the data-collecting layers (*e.g.*, upper surface of tissue samples would be scanned with AFM microindentation whereas two-photo microscopy will imaging the deeper layer of the stained tissue samples without fixation.) can be distinct from methods used.

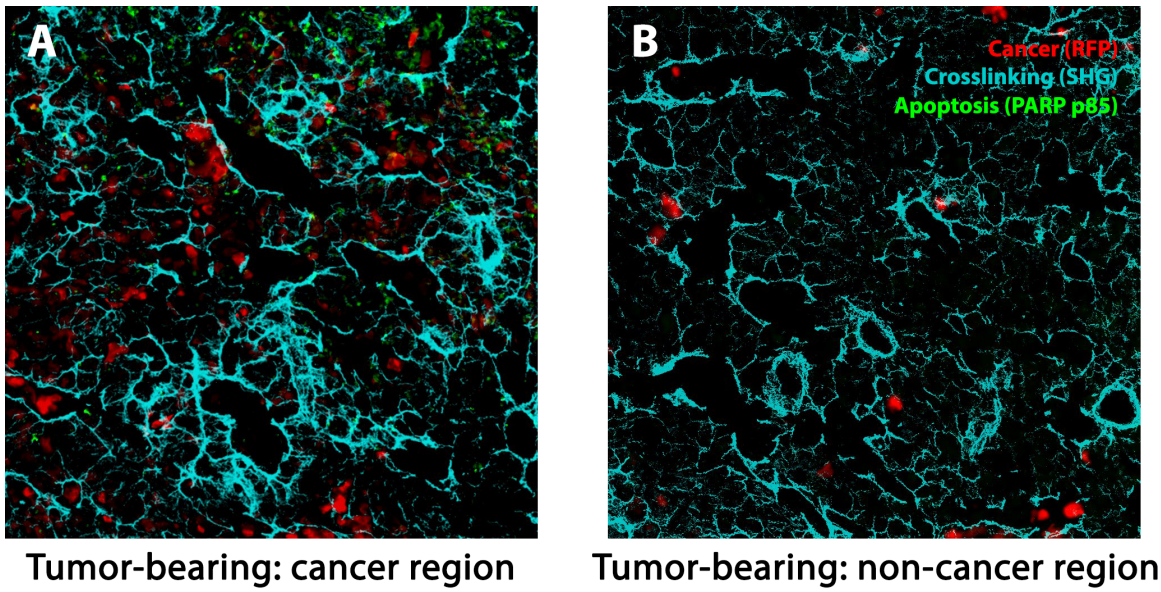

Figure 6.4. Crosslinking-specific tissue damage by MRCS in response to mechano-cues in the metastatic niche *in vivo*. Frozen sections of lungs of Luc-RFP-231 tumor-bearing NSG mice sacrificed after MRCS-CD infusion and 5-FC treatment as indicated (Day 9) were stained with anti-PARP p85 (green) for tissue apoptosis. RFP signal (red) indicates the presence of lung metastasis. SHG imaging of collagen networks (cyan) was presented and overlaid with IHC imaging. (**A**) Tissue damage was only observed in lung metastatic sites with crosslinked collagen network but not in less crosslinked (**B**) regions, indicating that the MRCS-CD and its specific tissue damage were co-localized with lung metastatic sites and collagen crosslinking and linearized networks. Scale bar = 100 μm.

Since with AFM stiffness measurement will be location-sensitive (*e.g.*, stiffness will vary from core to periphery in human primary tumor[37]), alternative stiffness measurements will be necessary to confirm the AFM results of the *in vivo* model. Therefore we will collaborate with

Dr. Wendy F. Liu[38] from the Edwards Lifesciences Center and conduct MTS indentation test and rheometry assay[21, 39] to measure the stiffness of the metastatic niche. Briefly, unfixed lung sample will be prepared as above-mentioned and analyzed with MTS indentation machine and rheometer. Fat tissue from mice fat pad (stiffness negative control), primary tumor (stiffness positive control) and lung tissue from healthy mice (negative control) will be measured as well.

MRCS demonstrates significantly reduced deleterious effects compared to MSCs constitutively expressing therapeutics. Nonetheless it is difficult to rectify how the MRCS system manages to both reduce toxicity yet still kills tumors and extends survival with the same effectiveness as the constitutive CD-MSC system. Presumably the reduced toxicity occurs because the 5-FU drug is turned off quickly. Figure 5.S4B shows gene expression drops to negligible levels within 48 hours, suggesting 5-FU therapy will also cease at this time point. Although this would reduce toxicity compared to a constitutive CD/5-FU production, how 48 hours of therapy can work as efficiently as continuous drug production (therapy) for 1 week (the duration of stem cell persistence shown in Figure 5.6). Certainly the prolongation of 5-FU production from 2 to 7 days would translate to more effective killing, yet could also explain the increased toxicity. How the MRCS can achieve both reduced toxicity yet maintain the same level of killing as the CD-MSC therapy has to be addressed in detail in the future.

The MRCS system can manage to reduce toxicity and still kill tumors because of the biophysical properties of the pre-metastatic niche as well as the tumor sites themselves [40]. In tail vein model which is a model of proof-of-concept, tumors for the most part correlate to higher crosslinking and stiffness and there are relatively few tumor regions without this biophysical change, therefore the MRCS cells will still be able to kill the cancer in these regions (but without off-target activation in softer, healthy regions). In the lungs, our data show that MRCS-CD had

lower toxicity to the tissue after treatment, as compared to CD-MSC, and this has been quantified via TUNEL assay (Figure 5.2P). In spontaneous model which is more relevant to mimicking the premetastatic niche, apoptosis is correlated to highly crosslinked areas with disseminated tumors, showing high specificity targeting metastases (Figure 6.3A).

6.5 MATERIALS AND METHODS

Breast cancer lung metastasis animal models

0.5 x 10^6 (2.5 x 10^6/ml in Dulbecco's Phosphate-Buffered Saline (DPBS, Lonza)) LV-*CMV*::Luc-RFP MDA-MB-231 (Luc-RFP-231) or LV-*CMV*::eGFP MDA-MB-231 (eGFP-231) breast cancer cells were infused intravenously (*i.v.*) into immunocompromised female nude mice (8 weeks, #088, Charles River Laboratories) or NOD-SCID gamma (NSG) mice (8 weeks, #005557, The Jackson Laboratory). For the spontaneous metastasis model, 1 x 10^6 Luc-RFP-231 cells were implanted subcutaneously (*s.c.*) into the fat pads of female NSG mice (8 weeks). All animals injected with cancer cells or DPBS as healthy controls were picked randomly. All animal experiments and procedures were performed after the approval from the University of California-Irvine (UCI) Institution of Animal Care and Use Committee (IACUC protocol number 2012-3062) and conducted according to the Animal Welfare Assurance (#A3416.01).

MSC transplantation and prodrug treatment

4 (NSG *i.v.* model) or 6 (nude *i.v.* model or NSG *s.c.* model) weeks after Luc-RFP-231 cell transplantation, 1 x 10^6 LV-*CMV*::eGFP MSCs co-transduced with MRCS-CD (eGFP-MRCS-CD), LV-MRCS-eGFP MSCs (MRCS-eGFP), CD-MSC, MRCS-CD, N-MSC (5 x 10^6 /ml in DPBS) or DPBS were *i.v.* infused into the mice harboring of breast cancer cells and into tumor-free control mice (Day 0) through tail vain. For second harmonic generation (SHG)

imaging and immunohistochemistry (IHC) (*ex vivo*), animals infused with eGFP-MRCS-CD or MRCS-eGFP were euthanized *(n* = 3 for each group) 24 hours later (Day 1) and lungs were harvested. For cancer treatment experiment, Luc-RFP-231 tumor-bearing or tumor-free mice infused with CD-MSC, MRCS-CD, N-MSC or DPBS were intraperitoneal (*i.p.*) administered with 5-FC (500 mg/kg in DPBS) for 7 days (two doses/day for Day 1-Day 5 and one dose/day for Day 6-Day 7). Representative mice (*n* = 3 for each group) were euthanized on Day 1 and Day 9 respectively for *ex vivo* assays (Figure 5.1A). For survival experiment, the endpoint of mice was defined as "found dead" or euthanasia criteria stated in UCI IACUC protocol 2012-3062.

In vivo and ex vivo bioluminescence imaging

4 (NSG *i.v.* model) or 6 (nude *i.v.* model or NSG *s.c.* model) weeks after Luc-RFP-231 cell transplantation, *in vivo* Luc activity from Luc-RFP-231 cells was measured (Day 0) as previously described[41]. Briefly, *in vivo* Luc signal was imaged with an IVIS Lumina (Caliper LifeSciences, MA) 10 minutes after intraperitoneal (*i.p.*) injection of D-luciferin (150 mg/kg in DPBS) into mice. Mice were anesthetized with 2-3% of isoflurane (Western Medical Supply, CA) and *in vivo* Luc activity was measured at the indicated time points. Before cancer treatment, nude mice with Luc signals in the lungs were imaged and grouped randomly and minimal adjustment was performed to keep the differences between "week 0" groups (red spots) not statistically significant (Figure 5.1D). After the cancer treatment experiments, *in vivo* Luc activity from Luc-RFP-231 cells was measured on Day 9 and 6 weeks after treatment (Figure 5.1A).

4 (NSG) or 6 (nude) weeks after eGFP-231 cell transplantation, 1 x 10^6 Luc-MSC, MRCS-Luc, N-MSC (5 x 10^6 /ml in DPBS) or DPBS were systemically infused into the mice

harboring of breast cancer cells and into tumor-free control mice (Day 0). *In vivo* Luc activity was measured at the indicated time points.

6 weeks after *s.c.* Luc-RFP-231 cell transplantation, mice were sacrificed and lungs were harvested. 150 µg/ml D-luciferin was added onto the lungs and *ex vivo* Luc activity from Luc-RFP-231 cells in the lungs was measured with an IVIS Lumina.

Tissue processing, Histology and TUNEL assays

Lungs, livers and brains were collected from tumor-bearing or tumor-free nude mice (Day 0 or Day 9) and flash frozen in Tissue-Tek® O.C.T™ Compound (Sakura Finetek, CA), with overnight fixation in 4% PFA, and with overnight incubation in 30% sucrose solution (Amresco, OH). Frozen sections 8 µm thick were taken using a Reichert-Jung Cryocut 1800 microtome (Leica Instruments, Germany) onto UltraClear positively charged slides (Denville, 25 x 75 x 1 mm). Bones were fixed overnight in 4% PFA, then decalcified for 10 days in a 14% EDTA solution with 0.2% PFA in PBS prior to embedding in paraffin and sectioning with a Leica microtome.

Masson's trichrome staining was performed to assess extent of tissue crosslinking and fibrosis (Day 0). Slides were fixed in Bouin's solution (Sigma) overnight at room temperature, then briefly rinsed in tap water before further washing in water on a shaker for 20 minutes. Slides were stained in a working solution of Weigert's hematoxylin (1: 1 ratio of solution A and solution B, Sigma) for 8 minutes and washed thoroughly in running tap water. Slides were then stained in Biebrich scarlet-acid fuchsin solution (Sigma) for 5 minutes and washed in water. Slides were differentiated in a 1: 1 phosphomolybdic-phosphotungstic acid solution (Sigma) for 5 minutes. Slides were then stained in aniline blue solution (Sigma) for 5 minutes and

differentiated in a 1% acetic acid (Sigma) solution for 2 minutes. Finally, slides were rinsed in water, then dehydrated with a few dips each in 70%, 90% and 100% ethanol and cleared for 1 minute in Histoclear (Thermo Fisher Scientific) before mounting with Permount (Thermo Fisher Scientific).

Terminal deoxynucleotidyl transferase dUTP Nick End Labeling (TUNEL) assay was performed to further assess tissue damage (Day 0 and Day 9). The ApoBrdU-IHC DNA Fragmentation Assay Kit (Biovision) was used with the included protocol. Data were analyzed with ImageJ (http://imagej.nih.gov/, NIH, MD).

Hematoxylin and eosin (H&E) was performed to assess systemic tissue damage in lung, liver, brain and bone. Slides were stained with Harris hematoxylin (Sigma) for 10 minutes, followed by acid alcohol (1% HCl in 70% ethanol), Scott's bluing reagent (Sigma) for 1 minute and Eosin Y (Sigma) for 5 minutes. Slides were dehydrated and mounted as previously described.

Ex vivo Immunohistochemistry

Lung tissues were harvested from tumor-bearing or tumor-free nude or NSG mice (Day 0 for LOX staining, Day 1 for MRCS homing and activation and Day 9 for Annexin V) and processed as abovementioned. Frozen slides (8 μm) were thawed and rehydrated in dH_2O for 5 minutes, then fixed in chilled acetone (Thermo Fisher Scientific) at -20°C for 10 minutes, permeabilized in 0.1% Triton X-100 for 10 minutes, and blocked in 0.1% Triton X-100 with 5% normal donkey serum for 1 hour. Primary antibodies (see Table 3.1) were diluted 1: 100 from the stock solution and applied overnight at 4°C. Slides were washed in 1X PBS. Then, secondary antibodies (see Table 3.2) were diluted 1: 500 from the stock solution and were applied for 30

minutes at room temperature. Slides were stained for nuclei with DAPI (1 μg/ml), then washed in PBS and mounted with Fluoromount-G. Slides were imaged with Nikon Eclipse Ti inverted microscope.

Second harmonic generation (SHG) imaging and analysis

For SHG imaging, frozen 40 μm sections of fixed (for LOX-SHG co-localization) or unfixed (for MRCS-SHG co-localization and SHG quantification), OCT mounted, mouse lungs (Day 0 for LOX-SHG co-localization and Day 1 for MRCS-SHG co-localization) were taken as abovementioned and dried overnight, in the dark, at room temperature on slides. Slides were then prepared similarly as described in the "*Ex vivo* Immunohistochemistry" session. The fluorescent signals from antibody stained slides were imaged using a Zeiss LSM710 Multiphoton/Confocal microscope (Zeiss, Germany) with a 40x W1.2NA objective (Zeiss, Germany). Slides were sequentially imaged in order of increasing fluorescent wavelength to reduce photo bleaching. SHG was performed at an 840 nm excitation wavelength and narrow bandpass detection, with a spectral window of 420/20 nm[42-44]. Images were processed with ImageJ and Matlab (MathWorks Inc., MA). For MRCS-SHG co-localization and representative images for SHG quantification, multiple high quality pictures were generated per sample and tiled into a giant image to cover an immense session of the sample, where the representative pictures were selected. For SHG quantification, collagen fibers imaged by SHG were automatically or manually selected and the ratio of displacement and length of the collagen fibers was analyzed and plotted. In order to minimize artifacts caused by collagen bundles close to blood vessels, the fibrillar length and curvature of collagen were extracted and adjusted by quasi manual selection of fibrillar structures.

For SHG-PARP p85 colocalization, large lung tissue scans of fluorescent channels 594 nm (for cancer) and 640 nm (for PARP p85) were taken on a Nikon (insert model) at 20x magnification. The sample was then scanned in the same approximate area using above mentioned Zeiss LSM710. The SHG scan was then overlaid upon the fluorescent scan, using ImageJ, to get a high definition fluorescence and SHG combined image for analysis. The overlaid large scans were then divided into sections using a grid of approximately 500 x 500 μm. Each section of the grid was treated as a separate data point for SHG-PARP p85 colocalization.

Bone marrow flushing and flow cytometry

1 day, 2 days, 7 days or 9 days after MSC infusion with 5-FC treatment as above mentioned, respectively, nude or NSG mice were sacrificed and bones, specifically femurs from both legs, were harvested with muscle tissue removed carefully. Bone marrow was then flushed with PBS and treated with red blood cell lysing buffer (Lonza). Blood cells left were then washed twice with PBS and diluted into 1 x 10^5 cells/ml. 300 μl of cells in suspension was then stained with (Figure 5.3A, 5.3B and 5.S7) anti-B220, anti-CD11b, anti-CD3e and anti-Gr1-PE-Cy7 or (Figure 5.3C) Annexin V-FITC (BioLegend, CA) and 7-Aminoactinomycin D dye (7-AAD, Thermo Fisher Scientific) after washing for 2 times. Finally, the resuspended cells were analysed with a BD Accuri™ C6 flow cytometry machine (BD Biosciences). Compensation and unstained controls were also prepared for the analysis.

Atomic force microscopy (AFM)

Six weeks after *i.v.* infusion of Luc-RFP-231 cancer cells or DPBS administration as tumor-free control, nude mice (Day 0) were euthanized and lungs were immediately harvested and kept in ice-cold Ringer solution (Thermo Fisher Scientific). All the AFM assays were

performed within 48 hours after mice euthanasia. Lung samples were cut into 500 μm thick slices using a rat heart slicer matrix (Zivic Instruments, PA) and mounted to a 60 mm plastic petri dish using epoxy glue (Devcon, MA). Samples were measured using Bruker BioScope Catalyst Atomic Force/ Zeiss LSM5 Confocal Fluorescence Microscope (Bruker, MA/ Zeiss, Germany) using contact mode in fluid, using MLCT C Triangular cantilevers (spring constant = 0.01 N/m, Bruker). Data points were taken 5 μm apart on 50 x 50 μm scans. Data was analyzed with Nanoscope Analysis v1.5 software, using a Sneddon conical model with Poisson ratio 0.4[33, 37].

Statistical Analysis

Data were analyzed by Student's *t* test when comparing 2 groups and by ANOVA when comparing more than 2 groups. Mann Whitney test was used for AFM data analysis. Outliers in AFM data were removed by Grubb's test ($P < 0.05$). Data were expressed as mean ± S. D. or mean ± S. E. M., and differences were considered significant at $P < 0.05$.

6.6 SUPPLEMENTAL MATERIAL

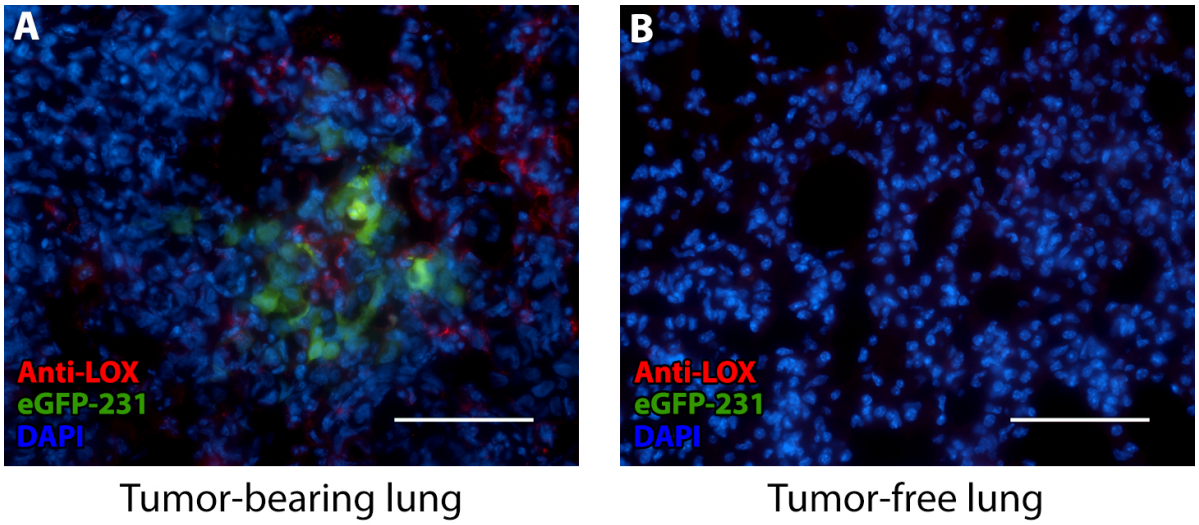

Figure 6.S1. Upregulation and co-localization with tumor of lysyl Oxidase (LOX) expression in tumor-bearing lungs. Representative frozen sections of lungs of (**A**) eGFP-231 tumor-bearing NSG mice and (**B**) tumor-free NSG mice sacrificed before MRCS infusion (Day 0) were stained with anti-LOX (red) and DAPI (blue). eGFP (green) stands for lung metastasis. The data indicates that LOX was highly expressed in tumor-bearing lungs. Scale bar = 50 μm.

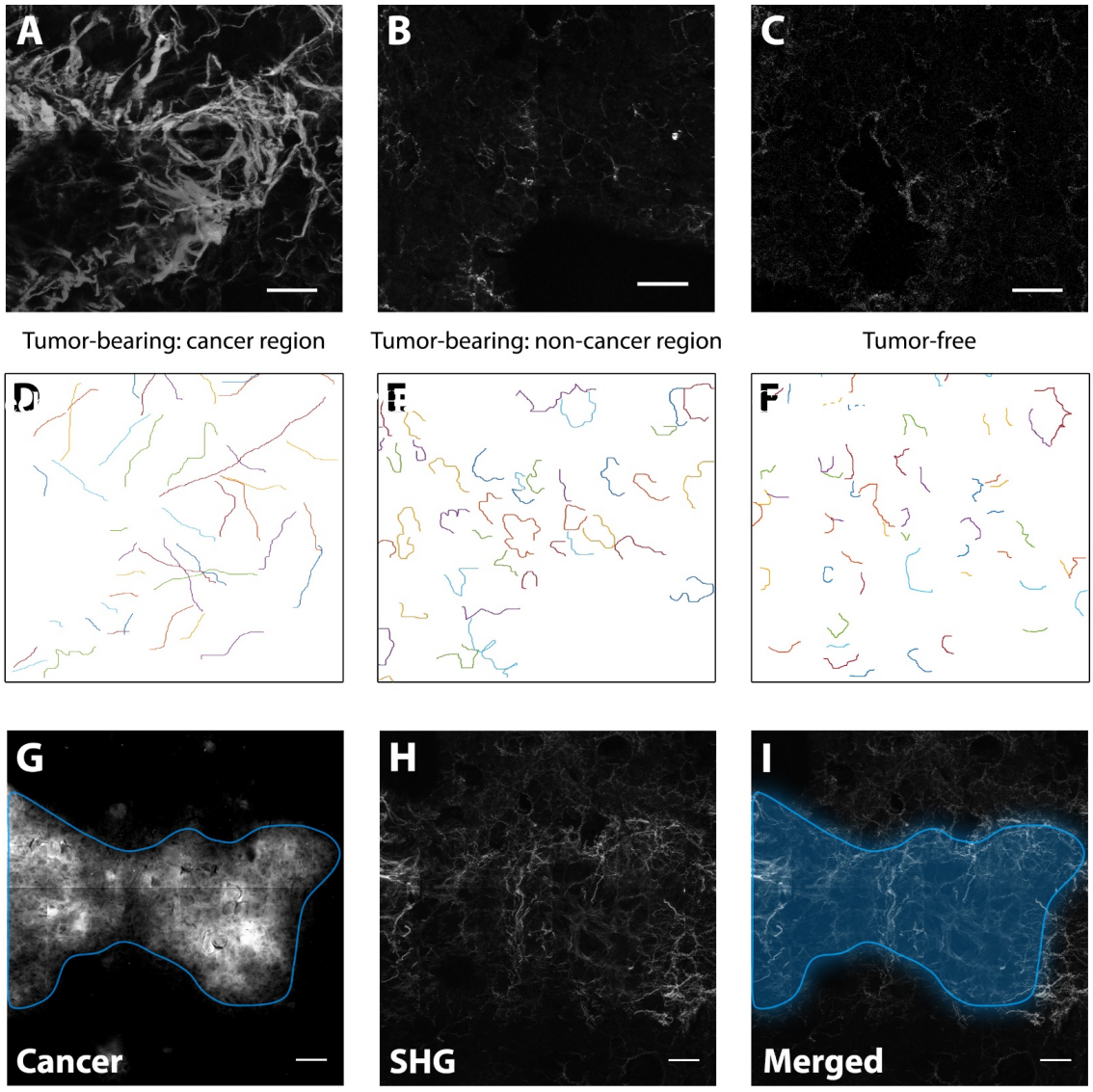

Figure 6.S2. Second Harmonic Generation (SHG) imaging showing upregulated and more linearized collagen network in tumor-bearing lungs. (**A** to **C**) Representative SHG pictures of cancer (Luc-RFP-231) region and non-cancer region of tumor-bearing lungs as well as tumor-free lungs of NSG mice show that the collagens are upregulated and more linearized at cancer regions. Scale bar = 50 μm. (**D**, **E** and **F**) are corresponding images of selected fibrillar structures of (**A**, **B** and **C**) respectively (see Methods). They were used for quantification of collagen linearization. The areas with no cancer have more curved structures while there are more linear structures near cancer. (**G**) The regions of cancer expressing RFP were imaged with confocal microscopy and highlighted in blue line. (**H**) SHG imaging of the corresponding area of panel **G**. (**I**) Co-localization of cancer signal and collagen network by merging panels **G** and **H**. The highlighted areas are defined as "cancer regions". Scale bar = 50 μm.

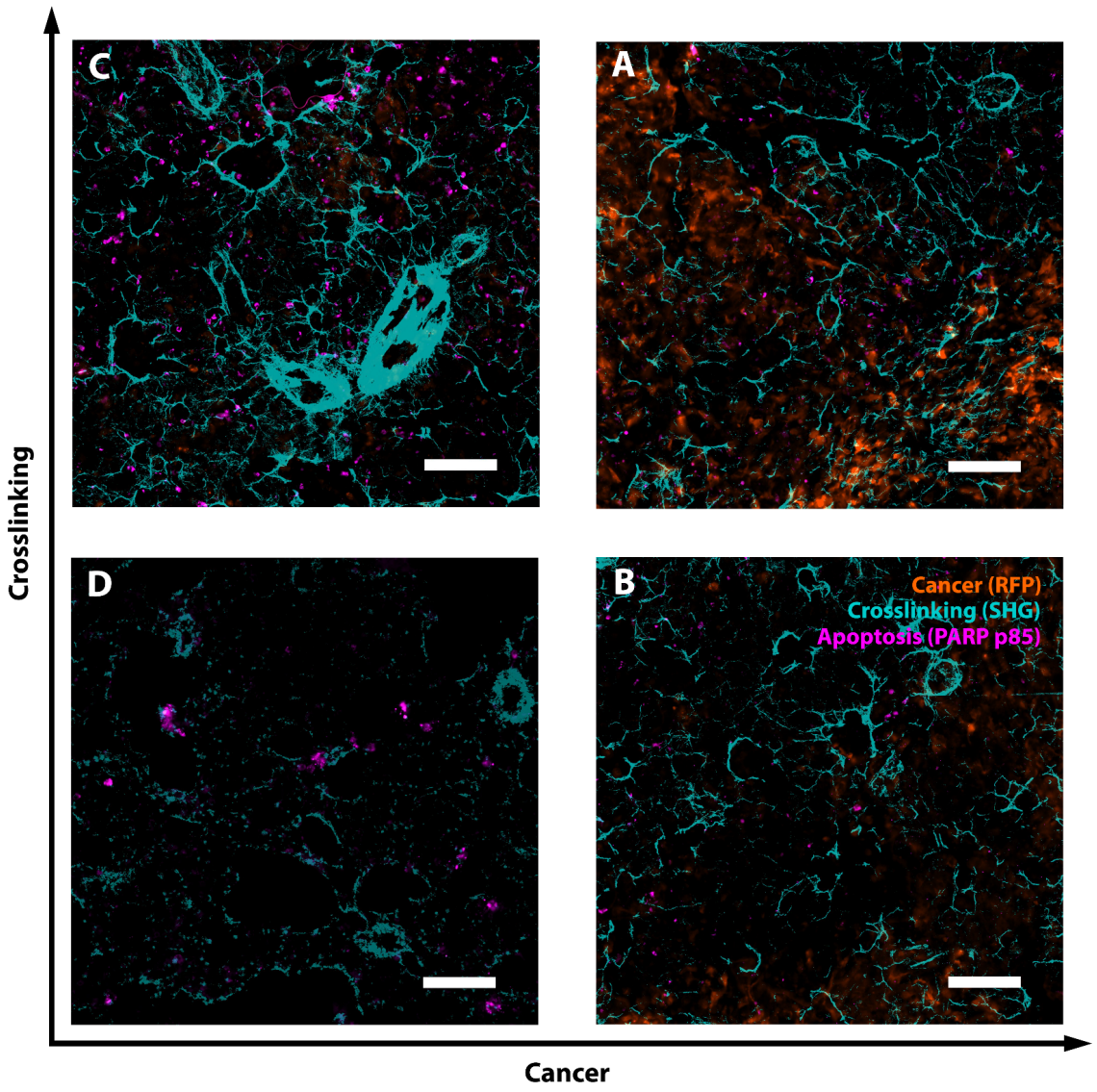

Figure 6.S3. Constitutively CD-expressing MSCs causing non-specific tissue damage *in vivo*. Frozen sections of lungs of Luc-RFP-231 tumor-bearing NSG mice and tumor-free NSG mice sacrificed after CD-MSC infusion and 5-FC treatment as indicated (Day 9) were stained with anti-PARP p85 (magenta) for tissue apoptosis. RFP signal (orange) indicates the presence of lung metastasis. SHG imaging of collagen networks (cyan) was presented and overlaid with IHC imaging. Non-specific tissue damage was observed in both (**A** to **C**) tumor bearing and (**D**) tumor free lungs regardless of the extent of collagen crosslinking. Scale bar = 100 μm.

6.7 REFERENCES

1. Shin, J.W. & Mooney, D.J. Improving Stem Cell Therapeutics with Mechanobiology. *Cell stem cell* **18**, 16-19 (2016).
2. Engler, A.J., Sen, S., Sweeney, H.L. & Discher, D.E. Matrix elasticity directs stem cell lineage specification. *Cell* **126**, 677-689 (2006).
3. Rowlands, A.S., George, P.A. & Cooper-White, J.J. Directing osteogenic and myogenic differentiation of MSCs: interplay of stiffness and adhesive ligand presentation. *American journal of physiology. Cell physiology* **295**, C1037-1044 (2008).
4. Pek, Y.S., Wan, A.C. & Ying, J.Y. The effect of matrix stiffness on mesenchymal stem cell differentiation in a 3D thixotropic gel. *Biomaterials* **31**, 385-391 (2010).
5. Park, J.S. et al. The effect of matrix stiffness on the differentiation of mesenchymal stem cells in response to TGF-beta. *Biomaterials* **32**, 3921-3930 (2011).
6. Tse, J.R. & Engler, A.J. Stiffness gradients mimicking in vivo tissue variation regulate mesenchymal stem cell fate. *PloS one* **6**, e15978 (2011).
7. Huebsch, N. et al. Harnessing traction-mediated manipulation of the cell/matrix interface to control stem-cell fate. *Nat Mater* **9**, 518-526 (2010).
8. Khetan, S. et al. Degradation-mediated cellular traction directs stem cell fate in covalently crosslinked three-dimensional hydrogels. *Nat Mater* **12**, 458-465 (2013).
9. Chaudhuri, O. et al. Substrate stress relaxation regulates cell spreading. *Nat Commun* **6**, 6364 (2015).
10. Chaudhuri, O. et al. Hydrogels with tunable stress relaxation regulate stem cell fate and activity. *Nat Mater* **15**, 326-334 (2016).
11. Dupont, S. et al. Role of YAP/TAZ in mechanotransduction. *Nature* **474**, 179-183 (2011).
12. Swift, J. et al. Nuclear lamin-A scales with tissue stiffness and enhances matrix-directed differentiation. *Science* **341**, 1240104 (2013).
13. Seo, B.R. et al. Obesity-dependent changes in interstitial ECM mechanics promote breast tumorigenesis. *Science translational medicine* **7**, 301ra130 (2015).
14. Butcher, D.T., Alliston, T. & Weaver, V.M. A tense situation: forcing tumour progression. *Nat Rev Cancer* **9**, 108-122 (2009).
15. Jaalouk, D.E. & Lammerding, J. Mechanotransduction gone awry. *Nat Rev Mol Cell Biol* **10**, 63-73 (2009).
16. Wirtz, D., Konstantopoulos, K. & Searson, P.C. The physics of cancer: the role of physical interactions and mechanical forces in metastasis. *Nat Rev Cancer* **11**, 512-522 (2011).
17. Humphrey, J.D., Dufresne, E.R. & Schwartz, M.A. Mechanotransduction and extracellular matrix homeostasis. *Nat Rev Mol Cell Biol* **15**, 802-812 (2014).
18. Downing, T.L. et al. Biophysical regulation of epigenetic state and cell reprogramming. *Nat Mater* **12**, 1154-1162 (2013).
19. Cox, T.R. et al. LOX-mediated collagen crosslinking is responsible for fibrosis-enhanced metastasis. *Cancer research* **73**, 1721-1732 (2013).
20. Cox, T.R. & Erler, J.T. Remodeling and homeostasis of the extracellular matrix: implications for fibrotic diseases and cancer. *Disease models & mechanisms* **4**, 165-178 (2011).
21. Levental, K.R. et al. Matrix crosslinking forces tumor progression by enhancing integrin signaling. *Cell* **139**, 891-906 (2009).
22. Wong, C.C. et al. Hypoxia-inducible factor 1 is a master regulator of breast cancer metastatic niche formation. *Proceedings of the National Academy of Sciences of the United States of America* **108**, 16369-16374 (2011).
23. Erler, J.T. et al. Lysyl oxidase is essential for hypoxia-induced metastasis. *Nature* **440**, 1222-1226 (2006).
24. Erler, J.T. et al. Hypoxia-induced lysyl oxidase is a critical mediator of bone marrow cell recruitment to form the premetastatic niche. *Cancer cell* **15**, 35-44 (2009).
25. Bondareva, A. et al. The lysyl oxidase inhibitor, beta-aminopropionitrile, diminishes the metastatic colonization potential of circulating breast cancer cells. *PloS one* **4**, e5620 (2009).
26. Wong, C.C. et al. Inhibitors of hypoxia-inducible factor 1 block breast cancer metastatic niche formation and lung metastasis. *J Mol Med (Berl)* **90**, 803-815 (2012).
27. Barker, H.E., Cox, T.R. & Erler, J.T. The rationale for targeting the LOX family in cancer. *Nature reviews. Cancer* **12**, 540-552 (2012).

28. Lopez, B. et al. Impact of treatment on myocardial lysyl oxidase expression and collagen cross-linking in patients with heart failure. *Hypertension* **53**, 236-242 (2009).
29. Studeny, M. et al. Bone marrow-derived mesenchymal stem cells as vehicles for interferon-beta delivery into tumors. *Cancer research* **62**, 3603-3608 (2002).
30. Wang, H. et al. Trafficking mesenchymal stem cell engraftment and differentiation in tumor-bearing mice by bioluminescence imaging. *Stem Cells* **27**, 1548-1558 (2009).
31. Studeny, M. et al. Mesenchymal stem cells: potential precursors for tumor stroma and targeted-delivery vehicles for anticancer agents. *Journal of the National Cancer Institute* **96**, 1593-1603 (2004).
32. Chen, X., Nadiarynkh, O., Plotnikov, S. & Campagnola, P.J. Second harmonic generation microscopy for quantitative analysis of collagen fibrillar structure. *Nature protocols* **7**, 654-669 (2012).
33. Liu, F. & Tschumperlin, D.J. Micro-mechanical characterization of lung tissue using atomic force microscopy. *Journal of visualized experiments : JoVE* (2011).
34. Lopez, J.I., Kang, I., You, W.K., McDonald, D.M. & Weaver, V.M. In situ force mapping of mammary gland transformation. *Integrative biology : quantitative biosciences from nano to macro* **3**, 910-921 (2011).
35. Chandler, E.M. et al. Implanted adipose progenitor cells as physicochemical regulators of breast cancer. *Proceedings of the National Academy of Sciences of the United States of America* **109**, 9786-9791 (2012).
36. Kakkad, S.M. et al. Hypoxic tumor microenvironments reduce collagen I fiber density. *Neoplasia* **12**, 608-617 (2010).
37. Plodinec, M. et al. The nanomechanical signature of breast cancer. *Nature nanotechnology* **7**, 757-765 (2012).
38. McWhorter, F.Y., Wang, T., Nguyen, P., Chung, T. & Liu, W.F. Modulation of macrophage phenotype by cell shape. *Proceedings of the National Academy of Sciences of the United States of America* **110**, 17253-17258 (2013).
39. Paszek, M.J. et al. Tensional homeostasis and the malignant phenotype. *Cancer cell* **8**, 241-254 (2005).
40. Erler, J.T. et al. Hypoxia-induced lysyl oxidase is a critical mediator of bone marrow cell recruitment to form the pre-metastatic niche. *Cancer cell* **15**, 35-44 (2009).
41. Liu, L. et al. Exogenous marker-engineered mesenchymal stem cells detect cancer and metastases in a simple blood assay. *Stem Cell Res Ther* **6**, 181 (2015).
42. Bianchini, P. & Diaspro, A. Three-dimensional (3D) backward and forward second harmonic generation (SHG) microscopy of biological tissues. *J Biophotonics* **1**, 443-450 (2008).
43. Campagnola, P.J. et al. Three-dimensional high-resolution second-harmonic generation imaging of endogenous structural proteins in biological tissues. *Biophys J* **82**, 493-508 (2002).
44. Altendorf, H. et al. Imaging and 3D morphological analysis of collagen fibrils. *J Microsc* **247**, 161-175 (2012).

CHAPTER 7

CONCLUSION AND FUTURE DIRECTIONS

7.1 SUMMARY

Stem cell has been a hot and emerging area for years, especially for its applications as regenerative medicines and drug delivery systems. Some stem cell based medicines derived from adult cell lines (*e.g.,* mesenchymal stem cells (MSCs) and neural stem cells) have been approved or undergoing clinical trials[1, 2] with promising outcomes. Surprisingly, mechanical cues provide a link to MSCs as well: we can simply use certain stiffness to regulate MSC differentiation. Moreover, it is reported MSC has tumor tropism and is able to be entrapped in organs such as lung and liver with systemic administration, showing a perfect drug delivery vector targeting primary and metastatic tumor foci. Thus we establish mechano-responsive cell system (MRCS) sensing the stiffness of cancer foci, providing a second "security" for target specificity and further reducing the side effects from the prodrug-enzyme (Cytosine Deaminase (CD)-5-Fluorocytosine (5-FC)) therapy.

Despite decades of effort, little progress has been made to improve the diagnosis and treatment of the cancer metastases. In particular, due to the heterogeneity of cancer and its ability to develop resistance to current treatments that target biochemical markers, novel targeting strategies are urgently needed. Inspired by the tight correlation between tissue stiffness increase and breast cancer metastatic niche found in recent studies[3-7] and the fact that MSCs differentiate to specific lineages depending on the stiffness of the microenvironment[8], we have developed a new class of cancer therapeutics that directly target the mechanoenvironmental cues of cancer

metastases. The MRCS represents a first attempt to directly interrogate the unique mechano-niche *in vivo* and apply it for localized delivery of agents including imaging reporters and therapeutics.

Mechano-niches play vital roles in development, homeostasis and disease progression including many types of cancer, and therefore serve as an emerging target for next generation therapeutics[9, 10]. In particular, matrix stiffness is an enormously appealing target for cancer therapeutics due to its long half-life (measured in years), as compared to the much shorter half-life of biochemical markers, making it refractory to development of resistance[11, 12]. Given the enormous challenge in the search of unique cancer biomarkers, matrix stiffness may present a new opportunity, especially when used in combination with other chemical biomarkers, to improve the sensitivity and specificity in cancer targeting. In addition, the natural ability of MRCS to actively home to and integrate into tumors and metastases enables the efficient delivery of therapeutics to the target site. Together, our MRCS system could have major clinical implications in increasing the effectiveness of therapies for patients with metastatic cancer while also ameliorating the deleterious side effects associated with chemotherapy[13] or other, less specific cell-based delivery systems that are engineered to constitutively express therapeutics. In addition, our system could potentially be used to prevent metastasis by targeting lysyl oxidase (LOX)-mediated, stiff pre-metastatic niche[4, 6, 7] by, for example, engineering the MRCS to secrete matrix remodeling enzymes, such as metalloproteases, to reduce the stiffness of the niche.

MSCs have been proven safe for transplantation in humans in the clinic[14, 15], which paves the way for quick clinic translation of the proposed MRCS. Transplanted MSCs, themselves, have previously been proposed to regulate cancer progression, both positively and negatively[16-

[18]. We do not consider it as a major issue as MRCS only stays in tumors transiently (< 7 days) and would be eliminated by suicide genes (CD). Although several organs, including muscle (12 kPa) and bone (25-60 kPa)[8, 19], approach or exceed the tissue stiffness of invasive breast cancer and may promote activation of our MRCS, we anticipate this will not be a major issue due to the inherent homing ability of MSCs to cancer and metastases and their rapid clearance from non-inflamed or non-injured tissues[16, 20]. Although when in transit to the metastatic niche MSCs will encounter blood vessel endothelial cells, basement membrane and extracellular matrix (ECM) components, each with their own characteristic stiffness, we do not expect this to irreversibly influence MRCS activity[8]. In particular, many of these mechanical interactions involve shear stress, which does not regulate MSC differentiation. Previous studies have also established that expression of mechano-responsive genes is rapidly reversible[8, 21].

Our approach targeting the unique mechano-niche *in vivo* by MRCS represents a new paradigm for the treatment of cancer metastases and potentially other types of fibrotic diseases through, for example, delivery of metalloproteases. Moreover, by using cells engineered to respond to variations in matrix stiffness to drive expression of diagnostic reporters (*e.g.,* the herpes simplex virus type 1 thymidine kinase (HSV-1-tk) gene coupled with positron emission tomography imaging[22] with a sensitivity of $10^{-11} \sim 10^{-12}$ *M*), the MRCS could also be used to detect micrometastases at a higher resolution than current imaging techniques. Our system potentially has major advantages over current methods of identifying micrometastases in that it can amplify the signal from smaller numbers of cells by detecting the properties of the local microenvironment, and that it can be used *in vivo* without a need for biopsy or invasive techniques. Finally, our MRCS could also generate an entirely new technique to elucidate mechanobiology, specifically, the interplay of biomechanical cues[23] with cells in their native

environment *in vivo* in the context of cancer and other conditions (*e.g.,* inflammation and injury). Although previous studies have established that matrix stiffness is tightly linked to invasiveness and metastasis, current methods of measuring stiffness rely on elastography or *ex vivo* measurements with atomic force microscope (AFM) or compression devices[4, 9]. Unfortunately, these techniques lack the resolution to directly measure the stiffness of the ECM with which the cells interact; instead, it measures the average stiffness of larger regions encompassing both ECM and cellular components of the tissues of interest. A cell-based stiffness sensor will reveal what cells actually "feel" in their native environment and represent a paradigm-shifting method of dynamically interrogating the mechano-environment of primary tumors, metastases, and changes in matrix stiffness during disease progression and response to therapies at a cellular resolution *in vivo*.

7.2 DIRECTIONS FOR FURTHER RESEARCH

This thesis presents an engineered stem cell system that specifically targets the unique mechano-niche of the tumor microenvironment *in vivo*, which represents a powerful new tool to interrogate, detect and treat cancer.

Due to the heterogeneity of cancer and its ability to escape from current treatments, people are undergoing a hard time to efficiently and specifically report or cure cancer, especially cancer metastasis which accounts for 90% of cancer death and almost incurable nowadays. Therefore, novel cancer biomarkers and more powerful therapeutics and diagnostics that can specially target cancers and their metastases are urgently needed. During the past 20 years, when people studied biological process such as cancer progression and cell proliferation, they mostly focused on soluble factors. However, recently studies show that some mechanical cues such as

stiffness and shear stress also play very important roles and offer a totally novel dimension for researchers to look back into the "old story"[24]. Interestingly, it is reported that increased stiffness in tumor microenvironment promotes the progression of primary as well as invasive (*i.e.*, metastasis) cancers, showing that increased stiffness has potential as a cancer marker in lung and liver, for example.

7.2.1 Next step of MRCS development and its broader applications

As described in Chapter 5 and 6, it is well known that lysyl oxidase (LOX) and its related proteins[25] play critical roles in fibrosis formation and progression[4, 26] at tumor site as crosslinkers of extracellular matrix (*e.g.,* collagen I). Recently it was reported that LOX is an important mediator in breast cancer metastasis[3, 5], contributing to the formation of pre-metastatic niche[6] and of more significant, LOX mediated collagen crosslinking may be responsible to fibrosis-enhanced metastasis[7]. However, whether increased stiffness is a fundamental property of metastatic niche *in vivo* and can be utilized as a therapeutic target[9, 27] is still controversial although it is reported that cells tend to migrate to stiffer substrates *in vitro* with a durotaxis[28]. Our MRCS can sense certain stiffness and not only eliminate malignant cells but also report the stiffness at specific metastatic sites, thus help answer the unmet questions abovementioned.

In the future, after further optimization, MRCS will be applied to wider areas, targeting different kinds of stiffness-related diseases or symptoms such as organ fibrosis[9] (*e.g.,* heart, lung and liver) resulting from genetic, aging or other unknown reasons as well as wound healing and scar dissolving of skin and organs after injury or surgery. In one word, we aim to make our MRCS a specific, sufficient and safe platform ending up with clinical and translational applications and make true contributions to the real world.

7.2.2 Interdisciplinary impact from the study of the MRCS

The study of MRCS is a combination of, for example, cell engineering, mechanobiology, stem cell therapy, cancer biology and imaging techniques as described in previous chapters.

As mentioned in Chapter 3, we also have been working with Dr. Qing Nie and developed a mathematic model to mimic the process that the fate of certain cell types, including mesenchymal stem cells (MSCs), can be influenced by mechanical dosing and "mechanical memory". It has also been reported that stem cells possess "mechanical memory" and are able to "remember" past physical signals depending on previous culture time and the stiffness of substrates (*e.g.,* ECM)[21]. The actual mechanisms of how stem cells sense the surrounding ECM and the factors affecting the cell fates, including matrix stiffness, ligand types, proteins, tethering, and porosity, remain poorly defined[29, 30]. The stem cell/substrate interface is a complex and dynamic microenvironment in which cells and substrates cooperatively dictate one another's fate[30]. It is intriguing to point out that due to the mechanical memory, *in vitro* stem cell cultures can yield unpredictable, controversial and undesirable cell fate, some of which have been previously ignored in the scientific community. The mechanical memory also makes it very difficult to perform certain *in vitro* assays on substrates with extremely high or low stiffness or for very long or short periods of incubation time. For example, MSCs can be biased towards osteogenic differentiation, even on soft hydrogels, after a period of mechanical dosing on stiff tissue culture polystyrene plates (TCPS)[21]. Therefore, developing predictive models to understand mechano-mediated cell/substrate interplays may facilitate better design of biomaterials, cell-based therapeutics and engineered tissue constructs in regenerative medicine. However, in order to fully study and potentially find translational applications for the aforementioned mechanisms, it is necessary to cover a large range of experimental conditions,

which is technically challenging. For instance, experimentally knock-down of key genes (*e.g.,* Yes-associated protein (YAP)) involved in mechanotransduction can be lethal or highly toxic *in vitro* and *in vivo*[31, 32]. Thus, there is great need for a computer-based mathematical system that can simulate an extreme range of culture conditions (*e.g.,* stiffness of culture substrates and culture duration) and that can accurately predict mechano-cue induced cell differentiations.

7.2.3 Drug delivery systems based on engineered cells and their derivatives

Systemic administration of mesenchymal stem cells (MSCs) affords the potential to ameliorate the symptoms of Multiple Sclerosis (MS) in both preclinical and clinical studies. However, the efficacy of MSC-based therapy for MS likely depends on the number of cells that home to inflamed tissues and on the controlled production of paracrine and immunomodulatory factors. We evaluated whether targeted delivery of MSCs with triple PSGL1/SLeX/IL-10 engineering via mRNA transfection improves therapeutic outcomes in mouse experimental autoimmune encephalomyelitis (EAE), a murine model for human MS. We found PSGL-1/SLeX mRNA transfection significantly enhanced MSC homing to the inflamed spinal cord. *In vivo* treatment with MSCs engineered with PSGL-1/SLeX/IL-10 in EAE mice exhibited a superior therapeutic function over native (unmodified) MSCs, evidenced by significantly improved myelination and decreased lymphocytes infiltration into the white matter of the spinal cord. Our strategy of targeted delivery of performance-enhanced MSCs could potentially be utilized to increase the effectiveness of MSC-based therapy for MS and other central nervous system (CNS) disorders[33].

The delivery of therapeutics to the central nervous system remains a major challenge in part due to the presence of the blood–brain barrier (BBB). Recently, cell-derived vesicles,

particularly exosomes, have emerged as an attractive vehicle for targeting drugs to the brain, but whether or how they cross the BBB remains unclear. We investigated the interactions between exosomes and brain microvascular endothelial cells (BMECs) *in vitro* under conditions that mimic the healthy and inflamed BBB *in vivo*. Our results indicate that cell-derived exosomes can cross the BBB model under stroke-like conditions *in vitro*. This study encourages further development of engineered exosomes as drug delivery vehicles or tracking tools for treating or monitoring neurological diseases[34].

9.3 References

1. Aboody, K.S. et al. Neural stem cell-mediated enzyme/prodrug therapy for glioma: preclinical studies. *Science translational medicine* **5**, 184ra159 (2013).
2. Aboody, K.S. et al. Targeting of melanoma brain metastases using engineered neural stem/progenitor cells. *Neuro-oncology* **8**, 119-126 (2006).
3. Erler, J.T. & Giaccia, A.J. Lysyl oxidase mediates hypoxic control of metastasis. *Cancer research* **66**, 10238-10241 (2006).
4. Levental, K.R. et al. Matrix crosslinking forces tumor progression by enhancing integrin signaling. *Cell* **139**, 891-906 (2009).
5. Erler, J.T. et al. Lysyl oxidase is essential for hypoxia-induced metastasis. *Nature* **440**, 1222-1226 (2006).
6. Erler, J.T. et al. Hypoxia-induced lysyl oxidase is a critical mediator of bone marrow cell recruitment to form the premetastatic niche. *Cancer cell* **15**, 35-44 (2009).
7. Cox, T.R. et al. LOX-mediated collagen crosslinking is responsible for fibrosis-enhanced metastasis. *Cancer research* **73**, 1721-1732 (2013).
8. Engler, A.J., Sen, S., Sweeney, H.L. & Discher, D.E. Matrix elasticity directs stem cell lineage specification. *Cell* **126**, 677-689 (2006).
9. Cox, T.R. & Erler, J.T. Remodeling and homeostasis of the extracellular matrix: implications for fibrotic diseases and cancer. *Disease models & mechanisms* **4**, 165-178 (2011).
10. Gasiorowski, J.Z., Murphy, C.J. & Nealey, P.F. Biophysical cues and cell behavior: the big impact of little things. *Annu Rev Biomed Eng* **15**, 155-176 (2013).
11. Sherratt, M.J. Tissue elasticity and the ageing elastic fibre. *Age (Dordr)* **31**, 305-325 (2009).
12. McPherson, J.M., Sawamura, S.J. & Conti, A. Preparation of [3H]collagen for studies of the biologic fate of xenogenic collagen implants in vivo. *The Journal of investigative dermatology* **86**, 673-677 (1986).
13. Hall, J.M. et al. Activation of the aryl-hydrocarbon receptor inhibits invasive and metastatic features of human breast cancer cells and promotes breast cancer cell differentiation. *Mol Endocrinol* **24**, 359-369 (2010).
14. Trounson, A., Thakar, R.G., Lomax, G. & Gibbons, D. Clinical trials for stem cell therapies. *BMC medicine* **9**, 52 (2011).
15. Liu, L. et al. From blood to the brain: can systemically transplanted mesenchymal stem cells cross the blood-brain barrier? *Stem cells international* **2013**, 435093 (2013).
16. Ankrum, J. & Karp, J.M. Mesenchymal stem cell therapy: Two steps forward, one step back. *Trends in molecular medicine* **16**, 203-209 (2010).
17. Droujinine, I.A., Eckert, M.A. & Zhao, W. To grab the stroma by the horns: from biology to cancer therapy with mesenchymal stem cells. *Oncotarget* **4**, 651-664 (2013).
18. El-Haibi, C.P. et al. Critical role for lysyl oxidase in mesenchymal stem cell-driven breast cancer malignancy. *Proceedings of the National Academy of Sciences of the United States of America* **109**, 17460-17465 (2012).
19. Huebsch, N. et al. Matrix elasticity of void-forming hydrogels controls transplanted-stem-cell-mediated bone formation. *Nat Mater* **14**, 1269-1277 (2015).
20. Karp, J.M. & Leng Teo, G.S. Mesenchymal stem cell homing: the devil is in the details. *Cell stem cell* **4**, 206-216 (2009).
21. Yang, C., Tibbitt, M.W., Basta, L. & Anseth, K.S. Mechanical memory and dosing influence stem cell fate. *Nat Mater* **13**, 645-652 (2014).
22. Brader, P. et al. Imaging of lymph node micrometastases using an oncolytic herpes virus and [F]FEAU PET. *PloS one* **4**, e4789 (2009).
23. Singh, A.K., Upadhyay, R.C., Malakar, D., Kumar, S. & Singh, S.V. Effect of thermal stress on HSP70 expression in dermal fibroblast of zebu (Tharparkar) and crossbred (Karan-Fries) cattle. *J Therm Biol* **43**, 46-53 (2014).
24. Halder, G., Dupont, S. & Piccolo, S. Transduction of mechanical and cytoskeletal cues by YAP and TAZ. *Nature reviews. Molecular cell biology* **13**, 591-600 (2012).
25. Akiri, G. et al. Lysyl oxidase-related protein-1 promotes tumor fibrosis and tumor progression in vivo. *Cancer research* **63**, 1657-1666 (2003).
26. Paszek, M.J. et al. Tensional homeostasis and the malignant phenotype. *Cancer cell* **8**, 241-254 (2005).

27. Barker, H.E., Cox, T.R. & Erler, J.T. The rationale for targeting the LOX family in cancer. *Nature reviews. Cancer* **12**, 540-552 (2012).
28. Guilak, F. et al. Control of stem cell fate by physical interactions with the extracellular matrix. *Cell stem cell* **5**, 17-26 (2009).
29. Trappmann, B. et al. Extracellular-matrix tethering regulates stem-cell fate. *Nat Mater* **11**, 642-649 (2012).
30. Wen, J.H. et al. Interplay of matrix stiffness and protein tethering in stem cell differentiation. *Nat Mater* **13**, 979-987 (2014).
31. Azzolin, L. et al. YAP/TAZ incorporation in the beta-catenin destruction complex orchestrates the Wnt response. *Cell* **158**, 157-170 (2014).
32. Raghunathan, V.K. et al. Role of substratum stiffness in modulating genes associated with extracellular matrix and mechanotransducers YAP and TAZ. *Invest Ophthalmol Vis Sci* **54**, 378-386 (2013).
33. Liao, W. et al. Mesenchymal stem cells engineered to express selectin ligands and IL-10 exert enhanced therapeutic efficacy in murine experimental autoimmune encephalomyelitis. *Biomaterials* **77**, 87-97 (2016).
34. Chen, C.C. et al. Elucidation of Exosome Migration Across the Blood-Brain Barrier Model In Vitro. *Cell Mol Bioeng* **9**, 509-529 (2016).